ERDC TR-22-17

US Army Corps of Engineers®
Engineer Research and Development Center

ERDC
ENGINEER RESEARCH & DEVELOPMENT CENTER

Engineering with Nature and USACE Flood and Coastal Systems R&D Program

Wave Attenuation of Coastal Mangroves at a Near-Prototype Scale

Mary Anderson Bryant, Duncan B. Bryant, Leigh A. Provost, Nia Hurst, Maya McHugh, Anna Wargula, and Tori Tomiczek

September 2022

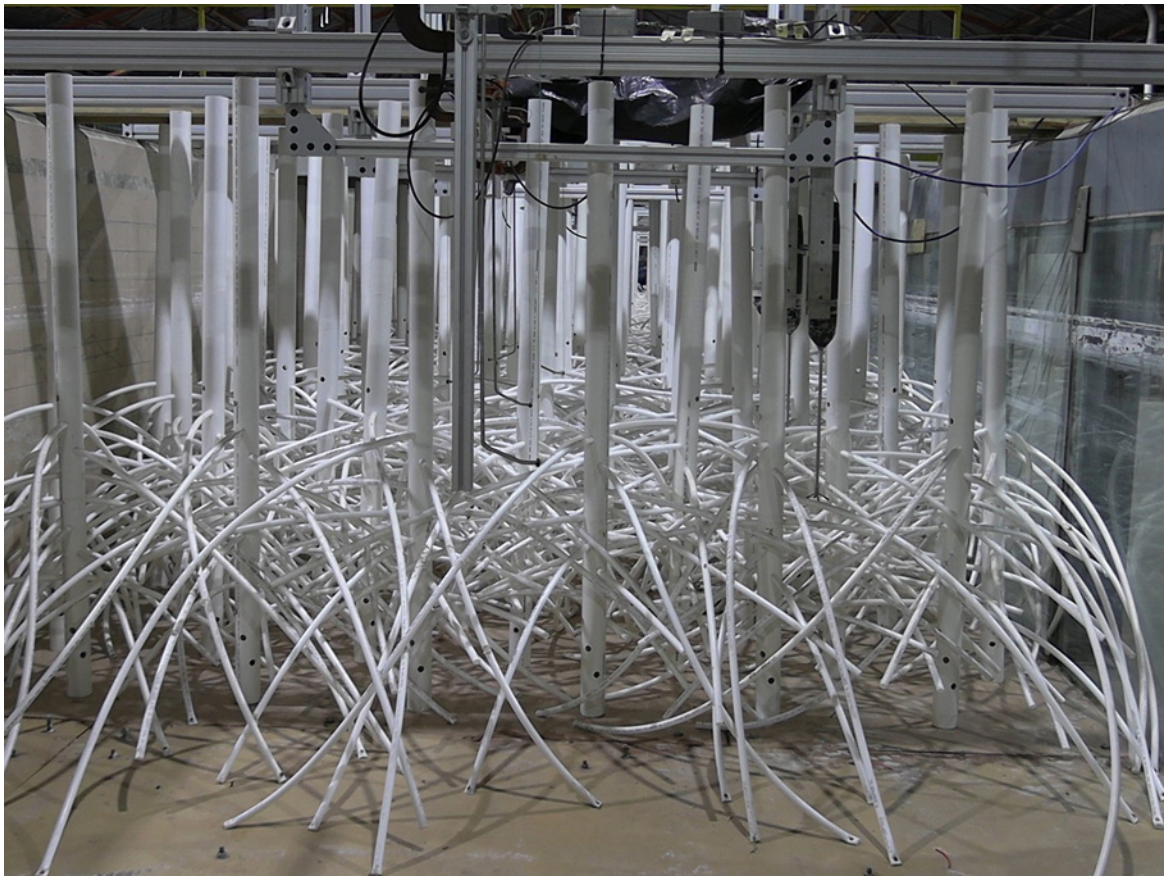

Engineer Research and Development Center

The US Army Engineer Research and Development Center (ERDC) solves the nation's toughest engineering and environmental challenges. ERDC develops innovative solutions in civil and military engineering, geospatial sciences, water resources, and environmental sciences for the Army, the Department of Defense, civilian agencies, and our nation's public good. Find out more at www.erdc.usace.army.mil.

To search for other technical reports published by ERDC, visit the ERDC online library at https://erdclibrary.on.worldcat.org/discovery.

Engineering with Nature and USACE Flood
and Coastal Systems R&D Program

ERDC TR-22-17
September 2022

Wave Attenuation of Coastal Mangroves at a Near-Prototype Scale

Mary Anderson Bryant, Duncan B. Bryant, and Leigh A. Provost

US Army Engineer Research and Development Center (ERDC)
Coastal and Hydraulics Laboratory (CHL)
3909 Halls Ferry Road
Vicksburg, MS 39180-6199

Nia Hurst

US Army Engineer Research and Development Center (ERDC)
Environmental Laboratory (EL)
3909 Halls Ferry Road
Vicksburg, MS 39180-6199

Maya McHugh

Princeton University
Princeton, NJ 08544

Anna Wargula and Tori Tomiczek

United States Naval Academy
121 Blake Road
Annapolis, MD 21402

Technical Report (TR)

Prepared for US Army Corps of Engineers
Washington, DC 20314-1000

Under Project 20-05 and 19-04, "Wave Attenuation of Coastal Mangroves during Extreme Water Levels at Near-Prototype Scales," funding account U4381627, AMSCO code 089500.

Abstract

A physical model study investigating the dissipation of wave energy by a 1:2.1 scale North American red mangrove forest was performed in a large-scale flume. The objectives were to measure the amount of wave attenuation afforded by mangroves, identify key hydrodynamic parameters influencing wave attenuation, and provide methodologies for application. Seventy-two hydrodynamic conditions, comprising irregular and regular waves, were tested. The analysis related the dissipation to three formulations that can provide estimates of wave attenuation for flood risk management projects considering mangroves: damping coefficient β, drag coefficient C_D, and Manning's roughness coefficient n.

The attenuation of the incident wave height through the 15.12 m long, 1:2.1 scale mangrove forest was exponential in form and varied from 13%–77%. Water depth and incident wave height strongly influenced the amount of wave attenuation. Accounting for differences in water depth using the submerged volume fraction resulted in a common fit of the damping coefficient as a function of relative wave height and wave steepness. The drag coefficient demonstrated a stronger relationship with the Keulegan–Carpenter number than the Reynolds number. The linear relationship between relative depth and Manning's n was stronger than that between Manning's n and either relative wave height or wave steepness.

Contents

Figures and Tables

Figures

Tables

Preface

This study was conducted for Engineering with Nature and USACE Flood and Coastal Systems R&D Programs under Project Numbers 20-05 (EWN) and 19-04 (FCS), "Wave Attenuation of Coastal Mangroves during Extreme Water Levels at Near-Prototype Scales," funding account U4381627, AMSCO 089500. The program manager for Engineering with Nature was Dr. Jeffrey King, and the program manager for Flood and Coastal Systems was Dr. Brandon Boyd.

The work was performed by the Coastal Processes Branch of the Flood and Storm Protection Division, US Army Engineer Research and Development Center, Coastal and Hydraulics Laboratory (ERDC-CHL). At the time of publication, Mr. Victor Gonzalez was chief, Coastal Processes Branch; Dr. Cary A. Talbot was chief, Flood and Storm Protection Division; Dr. Todd Bridges was the technical director for Engineering with Nature; and Dr. Julie Rosati was the technical director for USACE Flood and Coastal Systems R&D. The deputy director of ERDC-CHL was Mr. Keith W. Flowers, and the director was Dr. Ty V. Wamsley.

Additional work was performed by the Wetlands and Coastal Ecology Branch of the Ecosystem Evaluation and Engineering Division, ERDC Environmental Laboratory (EL). At the time of publication, Ms. Patricia M. Tolley was chief, Wetlands and Coastal Ecology Branch; and Mr. Mark D. Farr was division chief, Ecosystem Evaluation and Engineering Division. The deputy director of ERDC-EL was Dr. Brandon Lafferty, and the director was Dr. Edmond Russo.

COL Christian Patterson was the commander of ERDC, and Dr. David W. Pittman was the director.

This page intentionally left blank.

1 Introduction

1.1 Background

Given the intensifying risk of coastal flooding, communities are challenged to implement sustainable, adaptable solutions that reduce coastal flood risk. To that end, Congress directed the US Army Corps of Engineers (USACE) to consider natural and nature-based features (NNBFs), alone or in conjunction with traditional measures, in their feasibility reports on flood risk reduction across the national project portfolio (USACE 2017). NNBF solutions are expected to enhance resilience and mitigate the effects of coastal storm surge, wave attack, and erosion, all of which may be exacerbated by climate and sea-level change and population growth. Although consideration has been required since 2016, examples of NNBF implementation in USACE projects remain limited due to institutional guidance and experience that is less developed than those for traditional measures (e.g., unknowns as far as engineering design, performance, construction, environmental impacts and benefits, benefit quantification, lifecycle performance and asset management, and climate change adaptability; Carter and Lipiec 2020; personal communication with USACE Jacksonville District).

To date, most publications investigating NNBF to reduce flood risk have focused on wetlands, dunes, and beaches. However, there is growing interest in the application of mangroves to contribute to flood risk reduction (Tomiczek et al. 2021). Observations and hindcast modeling of mangrove forests suggest they offer significant protection during tsunami and shorter-duration surge events by restricting the flow of water (Kathiresan and Rajendran 2005; Krauss et al. 2009; Montgomery et al. 2019), and field observations have highlighted their capacity to attenuate wave energy under low-energy conditions (Horstman et al. 2014). However, the systematic assessment of wave attenuation by mangroves in controlled settings has been limited to small scale (e.g., 1:6 or smaller) laboratory studies; therefore, evaluation at near-prototype scales is critical for characterizing the contribution of effects such as friction for appropriate application to real-world systems.

1.2 Objectives

The objectives of this study were to (1) determine the physical attributes and (2) quantify the wave attenuation potential of mangrove forests, specifically North American red mangroves (*Rhizophora mangle*), at a near-prototype scale. The measured dissipation was then related to three different formulations for implementing mangrove systems into flood risk reduction applications: damping coefficient β, drag coefficient C_D, and Manning's roughness coefficient n*.

1.3 Approach

A 1:2.1 scale mangrove forest, constructed in the Coastal and Hydraulics Laboratory's 3 m flume, was used to evaluate the wave attenuation provided by North American red mangroves under a range of hydrodynamic conditions. Based on field measurements of red mangroves along the Florida Gulf Coast by Novitzky (2010) and the morphological model of the *Rhizophora* spp. by Ohira et al. (2013), a scaled, single representative tree model was constructed and duplicated to create a 15.12 m long mangrove forest. Sixteen wave gauges and six acoustic Doppler velocimeters (ADVs) captured changes in water surface elevation and velocity along the model. A total of 72 different hydrodynamic conditions, including both regular and irregular waves, were simulated to measure the hydrodynamics, determine the factors driving wave attenuation, and develop formulations that provide estimates of wave attenuation for flood risk management project planning.

* For a full list of the spelled-out forms of the units of measure used in this document and their conversions, please refer to *U.S. Government Publishing Office Style Manual*, 31st ed. (Washington, DC: US Government Publishing Office, 2016), 245–252, https://www.govinfo.gov/content/pkg/GPO-STYLEMANUAL-2016/pdf/GPO-STYLEMANUAL-2016.pdf.

2 Description of Experiments

2.1 Physical model setup

The experiments were performed at the US Army Engineer Research and Development Center in Vicksburg, Mississippi, in a 63.4 m long, 3.0 m wide, and 1.5 m deep concrete flume equipped with an electrohydraulic piston wave generator. The wave generator sits in a deeper section of the flume, which is 5.4 m long and connects to the 1.5 m deep flat testing area by a 19.5 m long, 1:44 slope. The flat testing area is 38.5 m long, with 12.2 m consisting of viewing glass. A dissipative, sloping beach that reduces wave reflection accounts for 9.0 m of the back end of the flume. The scaled mangrove model started 39.3 m from the wave generator and measured 15.12 m long. Figure 1 provides a cross-sectional view of the mangrove physical model setup.

Figure 1. Cross section of mangrove physical model (not drawn to scale). Measurements are in meters.

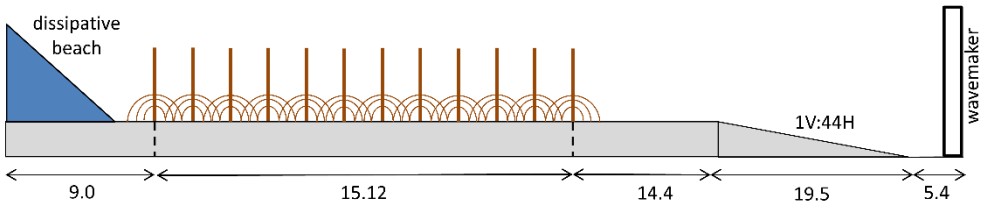

2.2 Mangrove forest model

As in other physical model studies of mangroves (Strusińska-Correia et al. 2013; Maza et al. 2017, 2019; Chang et al. 2019), a significant effort was made to develop a single representative tree model with hydraulic resistance that was similar to the selected mangrove tree species. The structural and biomechanical properties critical to hydraulic drag include tree density (N); tree spacing (Δs); bending stiffness (EI); prop root structure, including total number of primary roots (e.g., those originating from the trunk, N_R); root height above the ground (H_R); root length (L_R); and root diameter (D_R). Appendix A: Mangrove Field Methods contains an overview of common mangrove field measurements and techniques. The target species used to develop the model was the North American red mangrove (*Rhizophora mangle* [*R. mangle*]), a native species found in Florida (Tomiczek et al. 2021).

To develop the representative tree model, the tree structure was broken into three general parts: the canopy, the trunk, and the root system. The canopy only contributes to wave attenuation for very large inundation depths that were not considered in this effort and, thus, was neglected. However, other studies have suggested the wave attenuation of canopies is significant at high water levels (Mazda et al. 2006; He et al. 2019; Zhang et al. 2020). A simple cylinder represented the mangrove trunk. Ohira et al.'s (2013) stilt root morphology model, which relates the main trunk's diameter at breast height (DBH) to the root parameters, described the complex and dense root morphology of *R. mangle*. Applying Ohira et al.'s morphological model with an average *DBH* of 0.1274 m, which was reported for an *R. mangle*–dominated forest in Rookery Bay, Florida (Novitzky 2010), the calculated highest root height (H_{R_max}) was 1.41 m, and the total number of primary roots was N_R = 14 for the tree model. The diameters (D_R) of the primary roots ranged from 0.033 to 0.035 m.

Previous studies of flow and wave attenuation through mangroves have generally been performed at small geometric scale (e.g., Hashim and Catherine 2013; Strusińska-Correia et al. 2013; Maza et al. 2017, 2019; Wang et al. 2022). However, the scale effects associated with these studies are unknown, and further testing at near-prototype scales is crucial to evaluating the storm-risk benefits derived from mangroves during extreme weather events. A 1:2.1 scale was chosen scale for this experiment to allow multiple mangroves to span the flume width and simulate a forest, with scaling according to Froude similitude law (Chakrabarti 1994).

The scaled tree models were constructed using PVC and cross-linked polyethylene (PEX) pipe. Scaling the *DBH* of 0.1274 m resulted in 2 in. nominal diameter (0.0603 m) PVC pipe serving as the trunk. In addition to being relatively inexpensive, based on a structural analysis of *R. mangle* in Key West, Florida (Tomiczek et al. 2019; T. Tomiczek, personal communication), 2 in. diameter PVC pipe also has a bending stiffness (*EI*) that is similar to that of *R. mangle*. Scaling the root diameter yielded the closest match to 5/8 in. (0.016 m) flexible PEX pipe. These primary roots were threaded through the 2 in. PVC trunk in seven pairs and distributed about the trunk at eight different angles (i.e., at 45 degrees to each other) to project three-dimensional structure. Beginning with the lowest root pair (1) and proceeding to the highest root pair (7), the root pair elevations in meters along the trunk for the scaled model were 0.227, 0.291, 0.354, 0.418, 0.545, 0.608, and 0.672. A parabolic curve assumption like that proposed

by Ohira et al. (2013) described the curvature of the root pairs, where the curve shape and, thus, the root spread distance from the trunk were dependent on the root height. The root spread distances from the center of the trunk, beginning with lowest root pair (1) and proceeding to the highest root pair (7), were 0.579, 0.640, 0.792, 0.853, 0.914, and 0.975 m. Figure 2 contains a single scaled mangrove model.

Figure 2. Scaled (1:2.1) red mangrove tree model.

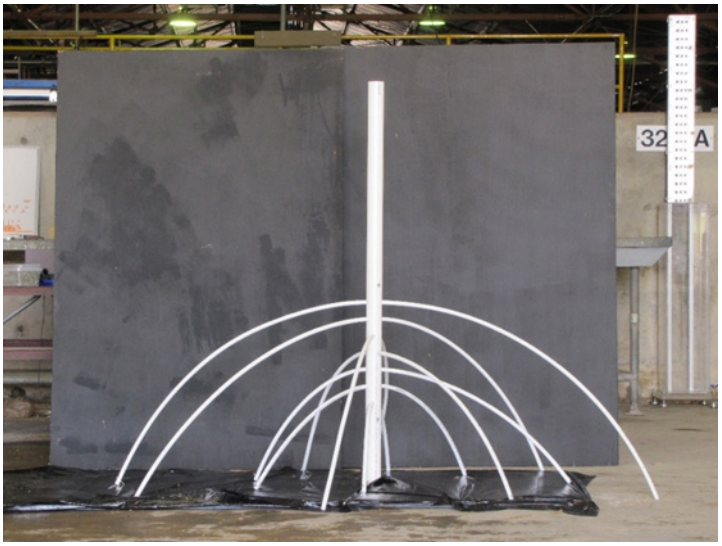

In contrast to Maza et al. (2015) and Kelty et al. (2022), who reported similar wave attenuation regardless of uniform or random arrangements, both Reimann et al. (2009) and Hashim and Catherine (2013) reported a lower wave attenuation in model mangroves arranged in tandem, rather than in a staggered arrangement. In addition, the staggered arrangement is a better simplification of the random spacing between mangroves found in nature and is easily implemented in restoration projects. Consequently, the staggered arrangement from Ozeren et al. (2014) served as the layout design, where vegetation density (N) related to the spacing (Δs) in this way:

$$N = \frac{2}{\sqrt{3}} \Delta s^{-2}. \quad (1)$$

Using N = 1.42 trees/m², as reported by Novitzky (2010), yielded a prototype in which Δs = 0.902 m. This spacing was then scaled according to the Froude similitude law, resulting in a model in which Δs = 0.427 m or N = 6.3 trees/m². Figure 3 provides a diagram of the model layout and a photo of the model installation in the flume. The rotation of the installed mangrove models was random.

Figure 3. Spacing layout for scaled mangrove model.

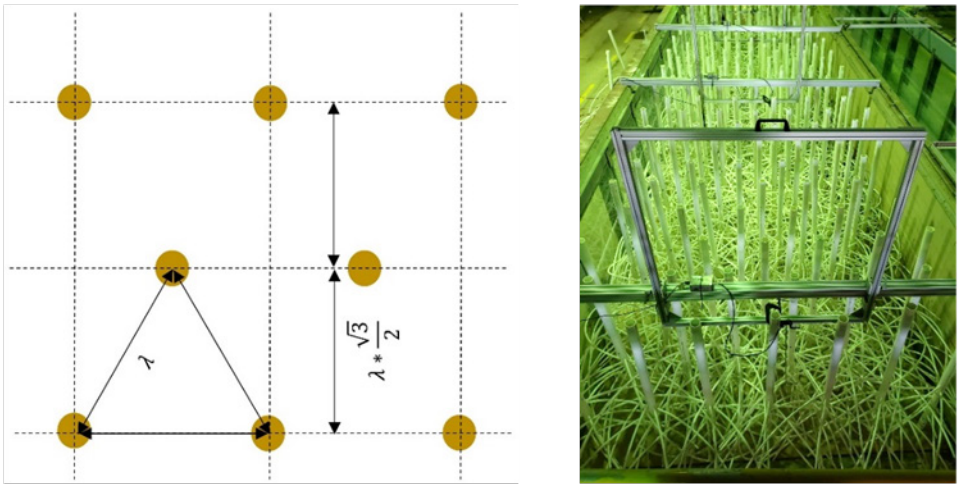

2.3 Instrumentation

A combination of capacitance wave gauges and ADVs collected water surface elevations and water velocity data at multiple locations within the mangrove model.

2.3.1 Water surface elevations

Sixteen single-wire Akamina AWP-24-3 capacitance wave gauges (WGs) measured water surface elevations along the length of the flume. The gauges had a wave-staff length of 60 cm. WGs were identified numerically in sequence, with WG 16 being most offshore (i.e., closest to the wave paddle) and WG 1 located at the leeward end of the mangrove forest. WGs 14–16 were positioned in a Goda array (Goda and Suzuki 1976) to determine wave reflection. WG 12 measured the conditions incident to the mangrove forest, with WGs 1–11 arranged in an exponential decay along the length of the mangrove forest. The sampling rate of the WGs was 50 Hz.

Prior to installation, the WGs were calibrated. A total of nine points, which related a voltage to a degree of submergence of the probe, calibrated each WG. Appendix B: Wave Gauge Calibration Data provides the results of the WG calibration. More information regarding WG calibration can be found in the *AWP-24-3 Wave Height Gauge User's Guide* (Akamina Technologies 2018).

2.3.2 Velocity measurements

Fixed-stem Nortek Vectrino ADVs measured water particle velocities at six locations along the length of the mangrove forest. These ADVs were paired with WGs 2, 4, 6, 8, 10, and 12 and were installed at approximately half the water depth (i.e., the height of the ADVs were adjusted for changes in water level). The orientation of the ADVs was such that the *x*-axis was aligned with the direction of wave propagation. The sampling rate of the ADVs was 25 Hz.

Figure 4 displays the instrumentation locations in the flume, where x = 0 at WG 12 and coincides with the beginning of the mangrove forest. In Figure 4, each black staff represents the location of a WG, and each red staff represents the location of a WG paired with an ADV.

Figure 4. Location of instrumentation, where x = 0 at WG 12. Measurements are in meters. Each *black staff* represents the location of a wave gauge (WG), and each *red staff* represents the location of a WG paired with an acoustic Doppler velocimeter (ADV).

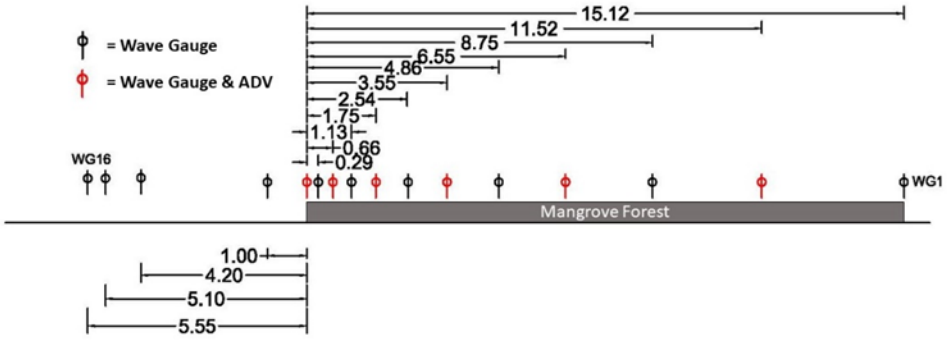

2.4 Hydrodynamic conditions

To quantify the wave dissipation afforded by mangrove systems, the experiments simulated a wide range of hydrodynamic conditions. The hydrodynamics applied the same Froude similarity scale as the model, with the scaling relationships for wave height and wave period as follows:

$$\text{Wave height} \qquad H_P: \lambda H_M, \tag{2}$$

$$\text{Wave period} \qquad T_P: \sqrt{\lambda} T_M, \tag{3}$$

where

P = prototype,

M = model, and
λ = geometric scale ratio, taken as 2.1 for this study.

Given the heterogeneous vertical structure of mangroves, four water levels were selected to subject the mangrove forest to various degrees of inundation. The 0.35 and 0.50 m water levels were at the prop root level (i.e., everyday water levels), whereas the 0.70 and 1.0 m water levels submerged the root systems (i.e., elevated water levels). These water levels correspond to prototype water levels equal to 0.74, 1.05, 1.47, and 2.10 m, respectively.

Testing included both irregular and regular waves, resulting in 72 total wave conditions (Table 1). Irregular waves were generated using a Texel, Marson, and Arsole (TMA) shallow-water spectral form with a peak enhancement factor of γ = 3.3 (see Hughes 1984 for a more detailed discussion). Wave periods tested for the regular (T) and irregular (T_p) waves were 2.0, 2.5, 3.0, and 4.0 sec at model scale, corresponding to prototype values of 2.9, 3.6, 4.3 and 5.8 sec, respectively. Incident wave heights ranged from 0.073 to 0.291 m at model scale (0.17 to 0.61 m at prototype scale) for the irregular waves (H_{moi}) and from 0.106 to 0.381 m at model scale (0.22 to 0.80 m at prototype scale) for the regular waves (H_i). By varying a single parameter of interest (e.g., wave height) while holding the other hydrodynamics (e.g., wave period and water depth) constant, the effect of water depth (h), incident wave height, and wave period on wave attenuation through the mangrove forest could be assessed. Incident conditions are those imminent to the mangrove forest and were measured by WG 12. Each irregular and regular wave signal was 20 min long. This signal length ensured the sampling of at least 300 waves when considering the longest period. The flume stilled for 15 min between wave signals.

Table 1. Incident wave conditions (measured at WG 12).

Irregular Waves			Regular Waves		
h [m]	H_{m0i} [cm]	T_P [sec]	h [m]	H_i [cm]	T [sec]
0.35	7.9	2.0	0.35	12.3	2.0
0.35	9.5	2.5	0.35	20.1	2.5
0.35	9.6	3.0	0.35	16.6	3.0
0.35	9.6	4.0	0.35	21.1	4.0
0.35	11.1	2.0	0.50	10.6	2.0
0.35	13.8	2.5	0.50	16.0	2.5
0.35	13.8	3.0	0.50	15.0	3.0

Table 1 (cont.). Incident wave conditions (measured at WG 12).

Irregular Waves			Regular Waves		
h [m]	H_{m0i} [cm]	T_P [sec]	h [m]	H_i [cm]	T [sec]
0.35	13.7	4.0	0.50	15.4	4.0
0.50	7.3	2.0	0.50	28.2	2.0
0.50	9.3	2.5	0.50	35.2	2.5
0.50	9.2	3.0	0.50	33.2	3.0
0.50	9.1	4.0	0.50	28.5	4.0
0.50	11.1	2.0	0.70	11.6	2.0
0.50	14.1	2.5	0.70	15.0	2.5
0.50	14.1	3.0	0.70	14.0	3.0
0.50	13.9	4.0	0.70	17.3	4.0
0.50	14.6	2.0	0.70	31.4	2.0
0.50	18.5	2.5	0.70	33.8	2.5
0.50	24.3	3.0	0.70	32.1	3.0
0.50	24.5	4.0	0.70	38.1	4.0
0.70	7.5	2.0	1.0	12.1	2.0
0.70	9.4	2.5	1.0	15.0	2.5
0.70	9.2	3.0	1.0	14.8	3.0
0.70	9.2	4.0	1.0	14.4	4.0
0.70	11.4	2.0	1.0	30.7	2.0
0.70	14.0	2.5	1.0	28.8	2.5
0.70	14.0	3.0	1.0	29.2	3.0
0.70	14.0	4.0	1.0	31.2	4.0
0.70	14.8	2.0			
0.70	18.7	2.5			
0.70	26.8	3.0			
0.70	27.7	4.0			
1.0	8.2	2.0			
1.0	9.8	2.5			
1.0	9.3	3.0			
1.0	9.0	4.0			
1.0	12.0	2.0			
1.0	14.8	2.5			
1.0	14.3	3.0			
1.0	14.0	4.0			
1.0	15.6	2.0			
1.0	19.6	2.5			
1.0	28.8	3.0			
1.0	29.1	4.0			

3 Data Analysis

3.1 Preliminary analysis

3.1.1 Wave height analysis

The data analysis performed on each water surface elevation time series included a zero up-crossing analysis to obtain the regular wave height (H) and root-mean-square wave height (H_{rms}) and a spectral analysis to calculate the zero-moment wave height (H_{mo}).

Prior to computing the wave heights, the full time series was subsampled to eliminate still water measurements and unwanted water level fluctuations (e.g., during wave ramp up) from the analysis. A dynamic threshold, based on the desired incident wave height, identified the beginning of the subsampled time series. Specifically, this threshold was selected as the initial time when the water surface elevation exceeded 15% of the desired incident wave height. The length of subsampled time series was then 20 min from the identified start time. An example of the time series identification process for an irregular wave signal is shown in Figure 5, where black is the full measured time series, and red is the subsampled portion used for wave height analysis. Each subsampled time series was demeaned prior to computing the wave heights.

Figure 5. Detected waves (*red*) from full time series (*black*).

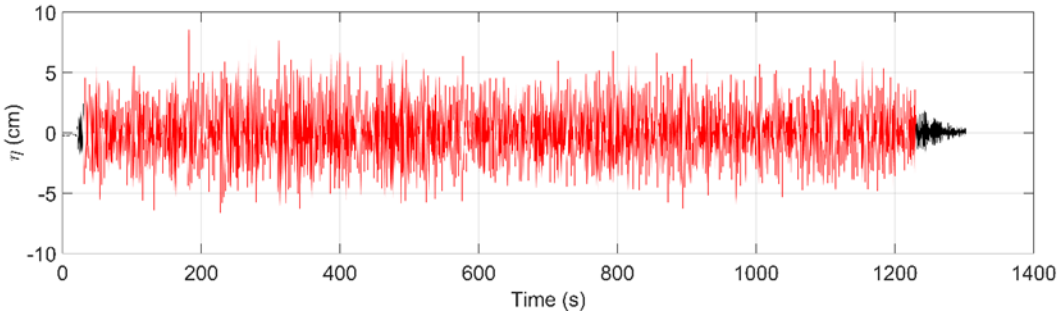

The regular wave height (H) and root-mean-square wave height (H_{rms}) were extracted from the regular and irregular time series, respectively, with the application of the zero up-crossing method. The zero up-crossing method is a standard method for dividing a time series into individual waves, from which statistical wave parameters are estimated. In this study, the regular wave height (H) is equivalent to the significant wave height,

defined as the mean wave height of the highest third of the waves. The calculation of the root-mean-square wave height (H_{rms}) was as follows:

$$H_{rms} = \sqrt{\frac{1}{n}\sum_{j=1}^{n} H_j^2}, \quad (4)$$

where

H_j = individual wave height and
n = total number of waves.

Additionally, a fast Fourier transformation (FFT) estimated the wave spectral energy density, *S(f)*, at each gauge for the irregular wave conditions. A filter removed all energy at frequencies lower than 0.05 Hz to eliminate low-frequency oscillations from the data. The zero-moment wave height, H_{mo}, was estimated from the wave spectra, *S(f)*, using the following relationship:

$$H_{m0} = 4.0\sqrt{\int S(f)df}, \quad (5)$$

where *df* is the frequency resolution.

The regular wave height (H) and the zero-moment wave height (H_{mo}) measured by WG 12 are the values for incident wave height provided in Table 1 for the regular and irregular conditions, respectively.

Note that the zero-moment wave height (H_{mo}), which is the statistical wave measurement most common in reporting and wave modeling, may be related to the H_{rms} by the following equation, assuming the waves follow a Rayleigh distribution (Sorensen 2006):

$$H_{m0} = \sqrt{2}H_{rms.} \quad (6)$$

The largest difference between H_{rms} computed directly from the irregular wave time series and that of Equation (6) was 1.49 cm, or 8.3%, considering WGs 1–12.

3.1.2 Linear dispersion relation

The wavelength of both the regular and irregular waves was computed using the linear dispersion relation:

$$\omega k = gk \tanh(kh), \tag{7}$$

where

$$\omega = \frac{2\pi}{T}, \tag{8}$$

$$k = \frac{2\pi}{L}, \tag{9}$$

and

ω = wave angular frequency,
k = wavenumber,
h = water depth,
T = wave period, and
L = wavelength.

Iteratively solving Equation (7) using the peak wave period (T_p) and monochromatic wave period (T) for the irregular and regular waves, respectively, yielded the peak wavenumber (k_p) and the monochromatic wavenumber (k). The peak wavelengths (L_p) for the random waves and the monochromatic wavelengths (L) for the regular waves were then computed using Equation (9).

3.2 Wave height attenuation

3.2.1 Damping coefficient

The wave height attenuation afforded by mangrove systems is of great interest in nature-based engineering applications because it relates to their ability to reduce coastal flood risk (Gijsman et al. 2021). A damping formulation created by Dalrymple et al. (1984), fitted to the normalized wave height evolution in the mangrove model (i.e., WGs 1–12), estimated the amount of attenuation:

$$\frac{H}{H_i} = \frac{1}{1 + \beta x}, \tag{10}$$

where

H = local wave height along the mangrove model,
H_i = incident wave height (e.g., x = 0 at WG 12),
β = damping coefficient, and
x = horizontal position along the forest referenced to x = 0.

The regular wave height, H, serves as the incident wave height in Equation (10) for regular waves, whereas Mendez and Losada (2004) suggest substituting H_{rms} for irregular waves:

$$\frac{H_{rms}}{H_{rmsi}} = \frac{1}{1 + \beta x}. \tag{11}$$

The damping coefficient (β) was fitted to each wave condition listed in Table 1 using the Gauss–Newton method of solving nonlinear least squares. Figure 6 shows two examples of fitted damping formulations: the top for an irregular wave condition, and the bottom for a regular wave condition. Red dots represent the normalized wave height evolution along the mangrove field (i.e., WGs 1–12), with the corresponding fitted damping formulation shown by the solid black line. The associated damping coefficient (β) and standard error of regression (s) are provided. The standard error has the same units as the dependent variable, in this case meters, and represents the average distance the observations fall from the regression line; smaller values are indicative of measurements lying closer to the fit.

Figure 6. Wave height decay along the mangrove forest for irregular (*top*) and regular (*bottom*) waves. Fitted damping coefficients (β) and the standard error of regression (s) are displayed.

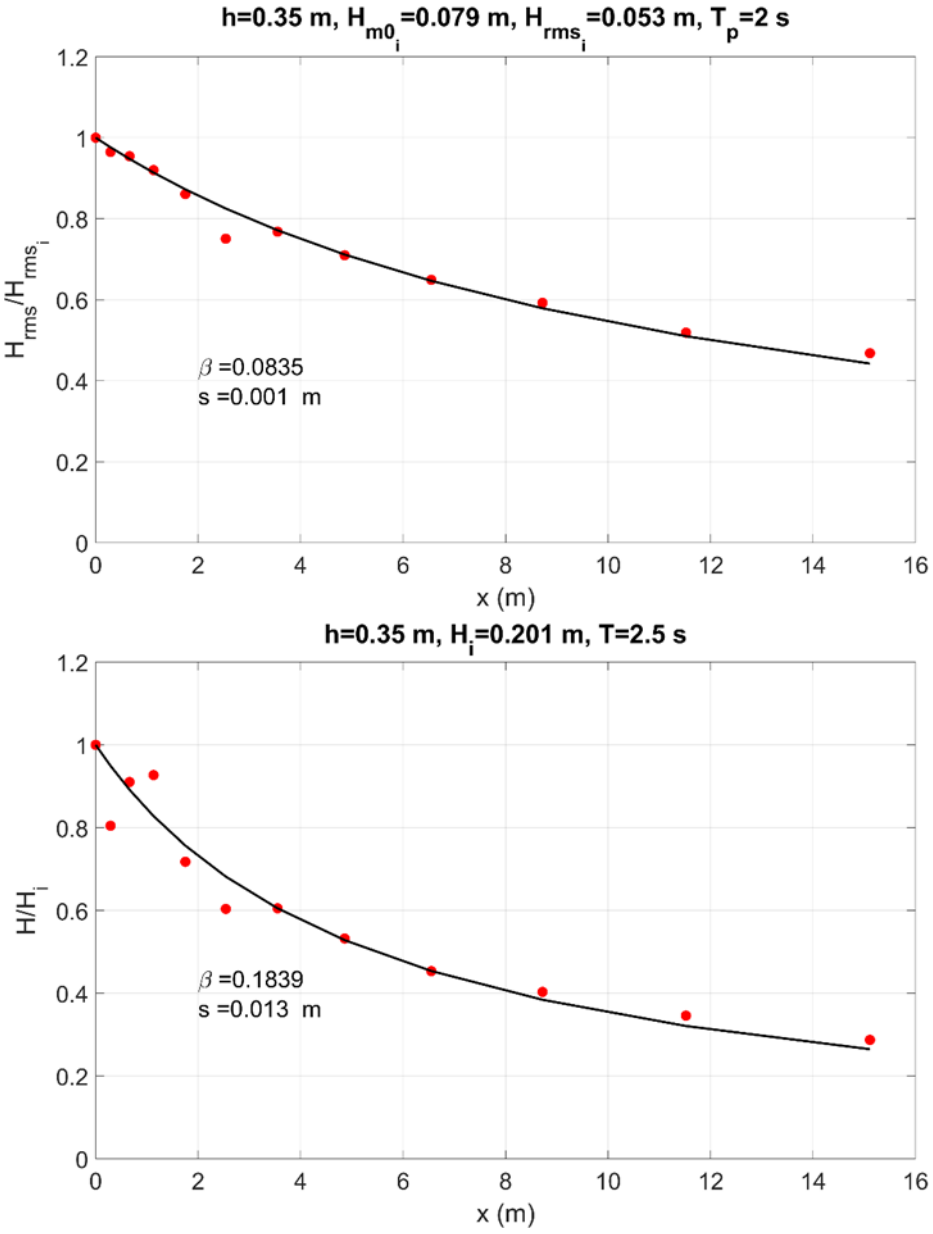

The wave height evolution fluctuated more for the regular waves than for the irregular waves, resulting in s values on the order of centimeters instead of millimeters. These modulations may have been due to increased wave reflection, wave–wave interaction, or standing wave generation within the mangrove model. Maza et al. (2019) also observed increased fluctuations in regular waves compared to irregular waves. Appendix C: Wave Damping Coefficients provides the normalized wave height evolution with fitted damping coefficients and standard errors for all tested

wave conditions. β values ranged from 0.017–0.125 per meter for irregular waves and 0.013–0.184 per meter for regular waves. The wave height decay after entering the mangroves was nonlinear for all hydrodynamic conditions.

3.2.2 Drag coefficient

Based on the conservation of wave energy, Dalrymple et al. (1984) formulated one of the earliest and most widely used models for wave dissipation by vegetation, where a Morison-type equation describes the wave-induced drag force, F_D (Morison et al. 1950):

$$F_D = \frac{1}{2}\rho C_D A_f u|u|, \tag{12}$$

where

ρ = water density,
C_D = drag coefficient,
A_f = reference area or cross-sectional area perpendicular to the flow, and
u = horizontal velocity due to the wave motion.

For application to vegetation fields, which are generally approximated as numerous circular cylinders, $A_f = d$, where d is the plant diameter, and the force is multiplied by the number of plants per square meter (N) to allow the total drag force to be a summation of the drag contributed by individual stems. This results in the equation that follows:

$$F_D = \frac{1}{2}\rho C_D N d u|u|. \tag{13}$$

Mendez and Losada (2004) extended the Dalrymple et al. (1984) formulation to irregular waves. This extension was implemented in the operational phase-averaged wave models of STWAVE (Anderson and Smith 2015), SWAN (Suzuki et al. 2012), WAVEWATCHIII (Abdolali et al. 2022), and the numerical storm-impact model XBEACH (van Rooijen et al. 2015). Detailed derivations of the Dalrymple et al. (1984) and Mendez and Losada (2004) formulations can be found in their respective manuscripts.

Using the formulations of Dalrymple et al. (1984) and Mendez and Losada (2004) for regular and irregular waves, respectively, the bulk drag coefficient (C_D) is obtained analytically as a function of β:

$$C_D = \frac{9\pi}{4NdH_i k}\frac{(\sinh 2kh + 2kh)\sinh kh}{\sinh^3 kl + 3\sinh kl}\beta, \tag{14}$$

$$C_D = \frac{3\sqrt{\pi}}{NdH_{rmsi}k_p}\frac{\left(\sinh 2k_p h + 2k_p h\right)\sinh k_p h}{\sinh^3 k_p l + 3\sinh k_p l}\beta, \tag{15}$$

where

d = plant diameter,
N = plant density per square meter,
k = monochromatic wavenumber for regular waves,
k_p = peak wavenumber for irregular waves,
h = water depth, and
l = vegetation height.

In this analysis, N = 6.3 trees/m² and $l = h$ because the mangroves are always emergent. In studies of wetland vegetation, such as that by Anderson and Smith (2014), the plant diameter (d) in Equations (14) and (15) is straightforward because a simple cylinder approximates plant geometry. In comparison, the frontal area of mangroves is complex and varies vertically, given the complex prop root geometry. To apply Equations (13) and (14) to mangroves, vertical integration of the mangrove frontal area over the water depth yields an equivalent diameter, d^*:

$$d^* = \frac{1}{h}\int_{-h}^{0} A(z)dz, \tag{16}$$

where $A(z)$ is the mangrove model frontal area.

To quantify $A(z)$, a single mangrove model was rotated on a base, and 25 photographs captured the three-dimensional variability of the root layout. Converting each photograph to a binary black and white image made it possible to relate pixels to centimeters, using the known diameter of the trunk as the basis (i.e., the number of pixels composing the trunk allowed for a pixels per centimeter conversion). Each pixel was 0.60302 mm. Applying this conversion identified the water depth on each of the black and white images, and the total frontal area was computed by summing the

number of pixels corresponding to the mangrove model below each water depth. The average projected area (A) for each water depth was 0.101, 0.141, 0.173, and 0.191 m² for water depth h = 0.35, 0.50, 0.70, and 1.0 m, respectively. After dividing by the corresponding water depth, the resultant d^* was equal to 0.290, 0.281, 0.247, and 0.191 m for h = 0.35, 0.50, 0.70, and 1.0 m, respectively. As shown in Figure 7, the prop roots contributed a major portion of the frontal area perpendicular to the flow, resulting in increasing d^* with shallower water. The values for d^* were substituted into Equations (14) and (15) for regular and irregular waves, respectively, to yield estimates of C_D.

Figure 7. Frontal area analysis. *Left* panel shows the superposition of 25 photos of the rotating mangrove model. *Right* panel shows the frontal area's vertical distribution.

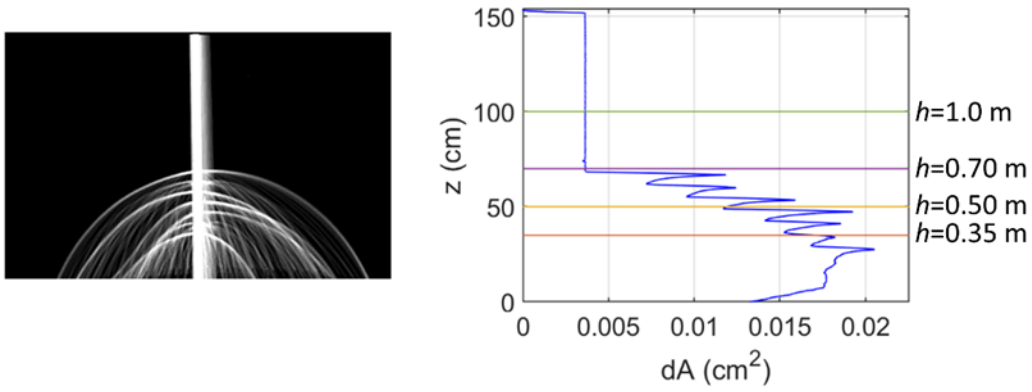

Figure 8 shows an example of the wave decay predicted by Equations (14) and (15) for a regular and an irregular wave condition compared to the measurements. The estimated drag coefficient (C_D) and standard error of regression (s) are given. Appendix D: Drag Coefficients provides the normalized wave height evolution with estimated drag coefficient (C_D) and standard error (s) for all tested wave conditions. C_D values ranged from 0.95–2.80 for irregular waves and from 0.52–1.85 for regular waves.

Figure 8. Wave height decay along the mangrove forest for irregular wave condition (*top*) and regular wave condition (*bottom*), with estimated drag coefficient (C_D) and standard of regression (s).

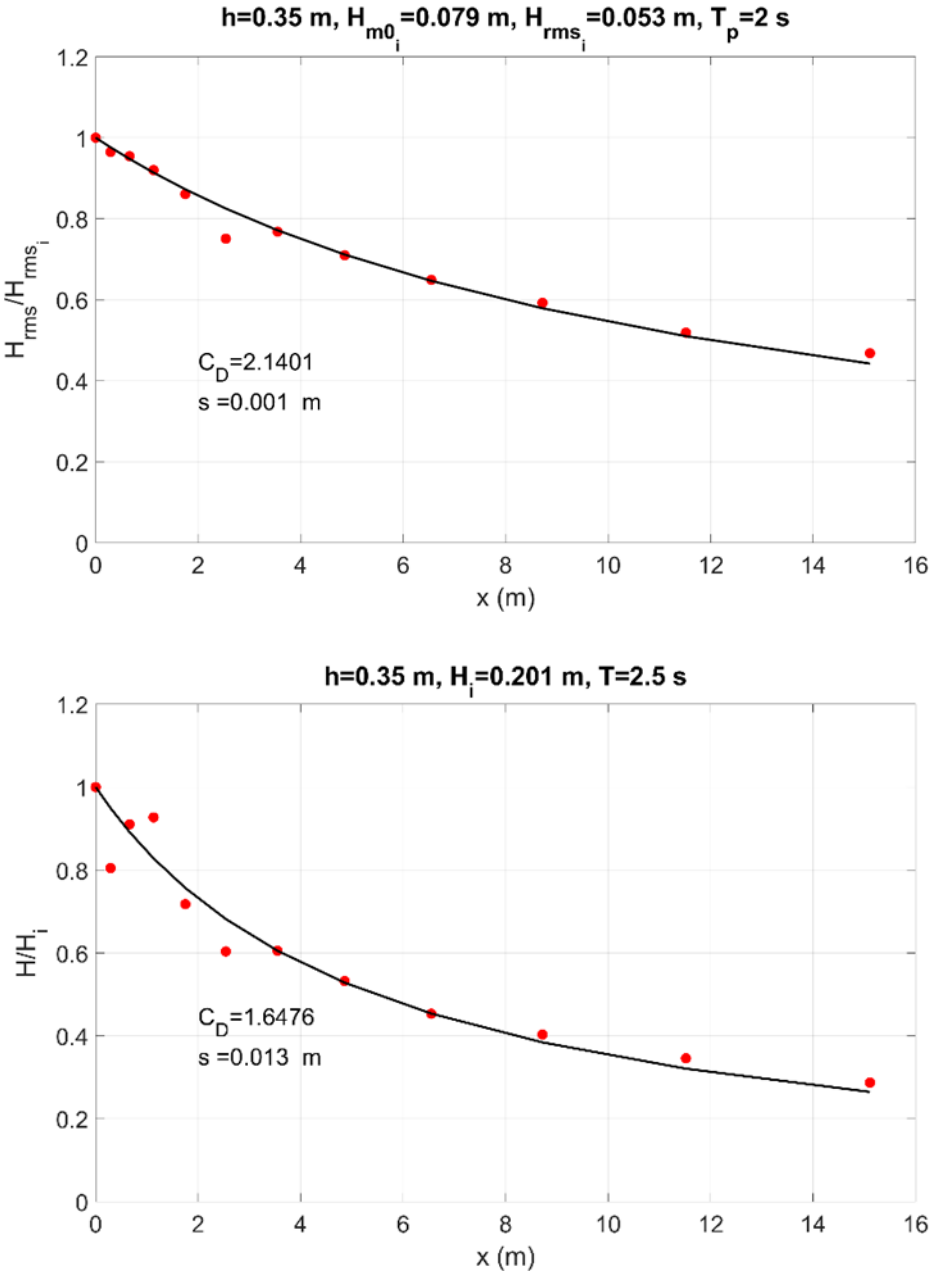

3.2.3 Manning's roughness coefficient *n*

While there is a growing consensus that the use of drag coefficients offers an improved, more accurate methodology for modeling wave dissipation through vegetation (Smith et al. 2016; Baron-Hyppolite et al. 2019), research into these drag coefficients is still in its infancy. Consequently, standard practice is to account for energy losses due to vegetation with

bottom friction sink terms. One of the formulations most often applied makes use of Manning's roughness coefficient n, which is generally associated with land cover databases (e.g., Bunya et al. 2010). Unlike applications of the JONSWAP bottom friction, which has historically varied between two values, one for swell conditions and another for wind sea conditions (Holthuijsen 2007), the Manning's n formulation allows for spatial variation tied to local terrain. The spectral wave models SWAN and STWAVE have both represented vegetation cover by Manning's n coefficients in numerous applications.

The STWAVE model, set up for the prototype, estimated the Manning's n coefficients for the irregular waves. Regular waves were omitted from this analysis because they are idealized and not representative of real-world conditions. The STWAVE model consisted of a domain measuring 31.75 m long by 84.0 m wide; the domain was widened to eliminate lateral boundary effects. The cell resolution was 0.42 m, resulting in 76 cells in the I-direction (i.e., the direction of wave propagation) and 200 cells in the J-direction. Monitoring locations, defined at x = 0, 0.609, 1.386, 2.373, 3.675, 5.334, 7.455, 10.206, 13.755, 18.375, 24.192, and 31.752 m, matched those of the WG locations scaled to prototype. The initial water depth of the domain was h_P = 0.735 m (h_M = 0.305 m), where constant water level adjustments of 0.315, 0.735, and 1.365 m increased the water level to h_P = 1.05, 1.47, and 2.1 m (h_M = 0.5, 0.7, and 1.0 m, respectively). The computational spectral grids spanned the range of $0.5f_p$ to $2f_p$ (where f_p is the peak frequency of the prototype), with a frequency resolution of 0.02 Hz. The spectral forcing was constructed using a TMA spectrum with the H_{mo} and T_p measured by WG 12 scaled to prototype, and the peak enhancement (γ) and directional spreading factors defined as 3.3 and 100, respectively. The model was executed iteratively until the percent difference between the STWAVE solution and the prototype-scaled wave heights was less than 3%. Figure 9 shows the STWAVE results compared to prototype-scaled measurements for Manning's n = 0.38. Appendix E: Manning's n provides comparisons of STWAVE results with prototype-scaled measurements, the estimated Manning's n, and the standard error (s) for all tested irregular wave conditions. The greatest standard error was 0.016 m, and Manning's n coefficients ranged from 0.25 to 0.97.

Figure 9. STWAVE calibration of Manning's *n* for wave dissipation through mangroves using prototype-scaled measurements of wave height.

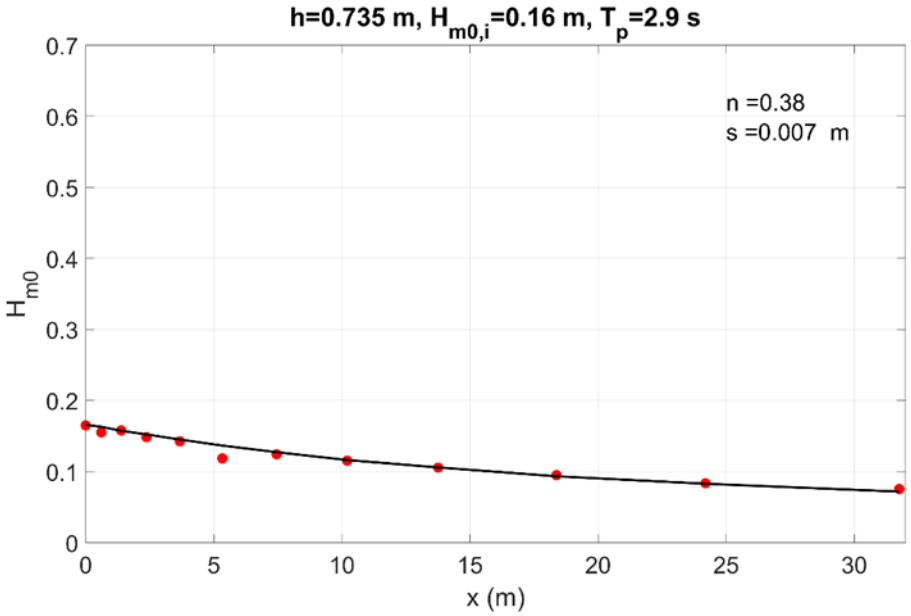

4 Results

4.1 Wave height attenuation

The attenuation of the incident wave height through the 15.12 m mangrove forest varied from 13% to 77% over all conditions, depending on the incident hydrodynamic conditions. The wave attenuation through the 15.12 m forest for the irregular and regular waves ranged from 14% to 65% and from 13% to 77%, respectively. Focusing on the irregular wave conditions, the wave attenuation range at each water depth (h) was as follows: 48%–63% at h = 0.35 m, 38%–65% at h = 0.50 m, 26%–53% at h = 0.70 m, and 14%–38% at h = 1.0 m.

4.1.1 Damping coefficient

To determine the influence of water depth, wave height, and wave period on wave dissipation, the damping coefficient (β) was related to key nondimensional parameters of relative wave height (H/h), wave steepness (H/L), and relative depth (kh). Larger H/L values are indicative of steeper waves, and kh <<1 are shallow water waves or long waves. As opposed to deep water waves (i.e., kh>>1) that do not interact with the bottom, the wave-induced velocity field of shallow water waves extends all the way from the top to the bottom of the water column such that their behavior or transformation is influenced by the bed. The experimental conditions herein ranged from near-shallow to near-deep water waves.

Figure 10 displays the relationship between β and relative wave height (H/h), wave steepness (H/L), and relative depth (kh) for all tested wave conditions. The incident zero-moment wave height (H_{moi}), peak wavelength (L_p), and peak wavenumber (k_p) defined the nondimensional parameters for the irregular waves. The incident regular wave height (H_i) and the monochromatic wavelength (L) and wavenumber (k) corresponding with the monochromatic wave period (T) defined the nondimensional parameters for the regular waves. β displayed a positive linear relationship with H/h and H/L, increasing with larger values of both parameters across all water depths. The greater attenuation found with larger wave heights, when considering the same depth, agrees with Gijsman et al.'s (2021) review. The positive linear relationship between β and kh was weaker, showing only marginal increases of β with larger values of kh. This preferential dissipation of shorter period waves is supported by Maza et al. (2019) and

Gijsman et al. (2021). These relationships reveal that, for the wave regimes tested in this experiment, wave height, rather than wave period, is a key variable driving wave attenuation in mangroves. Maza et al. (2019) reported similar findings.

All three nondimensional parameters depend on water depth; the highest β was obtained for the shallower water depths, for which the frontal area of the mangroves was the largest. This dependence on water depth was most obvious when considering H/L, although it was apparent for H/h and kh to lesser degrees. As in Maza et al. (2019), the difference in the frontal projected area at each water depth was accounted for by calculating the submerged volume fraction (*SVF*):

$$SVF = \frac{\text{Solid volume}}{\text{Water volume}} = \frac{\pi \left(\frac{d^*}{2}\right)^2 h * N}{A_h * h}, \quad (17)$$

where A_h is the horizontal unit area.

In other words, the *SVF* defines the percent of the water volume occupied by the mangroves model per unit meter squared. As expected, the *SVF* increased with shallower water depths. The calculated *SVF*s were 0.4145, 0.3913, 0.3029, and 0.1811 per square meter for h=0.35, 0.50, 0.70, and 1.0 m, respectively. The panels on the right side of Figure 10 show the relationship between the nondimensional parameters with the inclusion of the *SVF*. The dependence of β on water depth is captured for both H/h and H/L as the data collapse to a common fit. The linear regression for H/h yields a higher coefficient of determination (R^2 = 0.89) than H/L (R^2 = 0.77). A common fit is not found for β as a function of kh*SVF, resulting in a poor R^2 value of 0.094.

Figure 10. Damping coefficient (β) as a function of relative wave height (H/h), wave steepness (H/L), and relative depth (kh) for all wave conditions. The *right* panels display results when nondimensional parameters were multiplied by the submerged volume fraction (*SVF*) at each water depth. Irregular wave conditions are represented by *circles*, and regular wave conditions are represented by *triangles*.

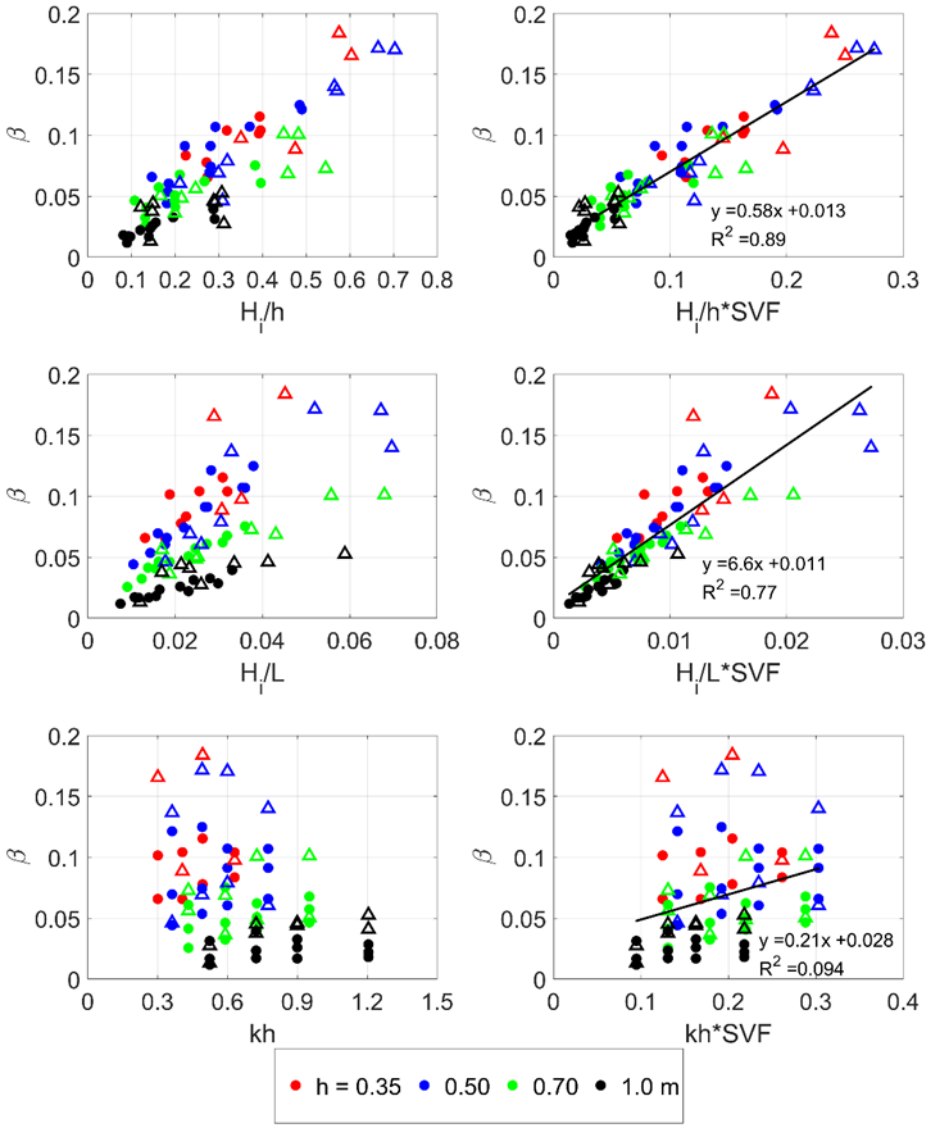

The same analysis was repeated for only the irregular wave conditions because these waves are representative of real nearshore environments. Again, the incident zero-moment wave height (H_{moi}), peak wavelength (L_p), and peak wavenumber (k_p) defined the nondimensional parameters for the irregular waves. Figure 11 displays the relationship between β and H/h, H/L, and kh for all irregular wave conditions. Again, positive relationships between β and H/h and β and H/L are seen, whereas there is a weak linear relationship between β and kh. Unlike the regular waves, which had similar scatter in both parameters, the linear relationship with

H/L is slightly stronger than the one for *H/h* but is clearly also dependent on water depth. Multiplying the nondimensional parameters by the *SVF* of each water depth collapsed β for both *H/h* and *H/L*, yielding linear regressions with identical R^2 values of 0.88. Again, the linear regression of *kh* accounting for the *SVF* is poor, with R^2 = 0.14, indicating that wave height, rather than wave period, is the dominant driver of wave attenuation.

Figure 11. Damping coefficient (β) as a function of relative wave height (*H/h*), wave steepness (*H/L*), and relative depth (*kh*) for all irregular wave conditions. The *right* panels display results when nondimensional parameters were multiplied by the SVF at each water depth.

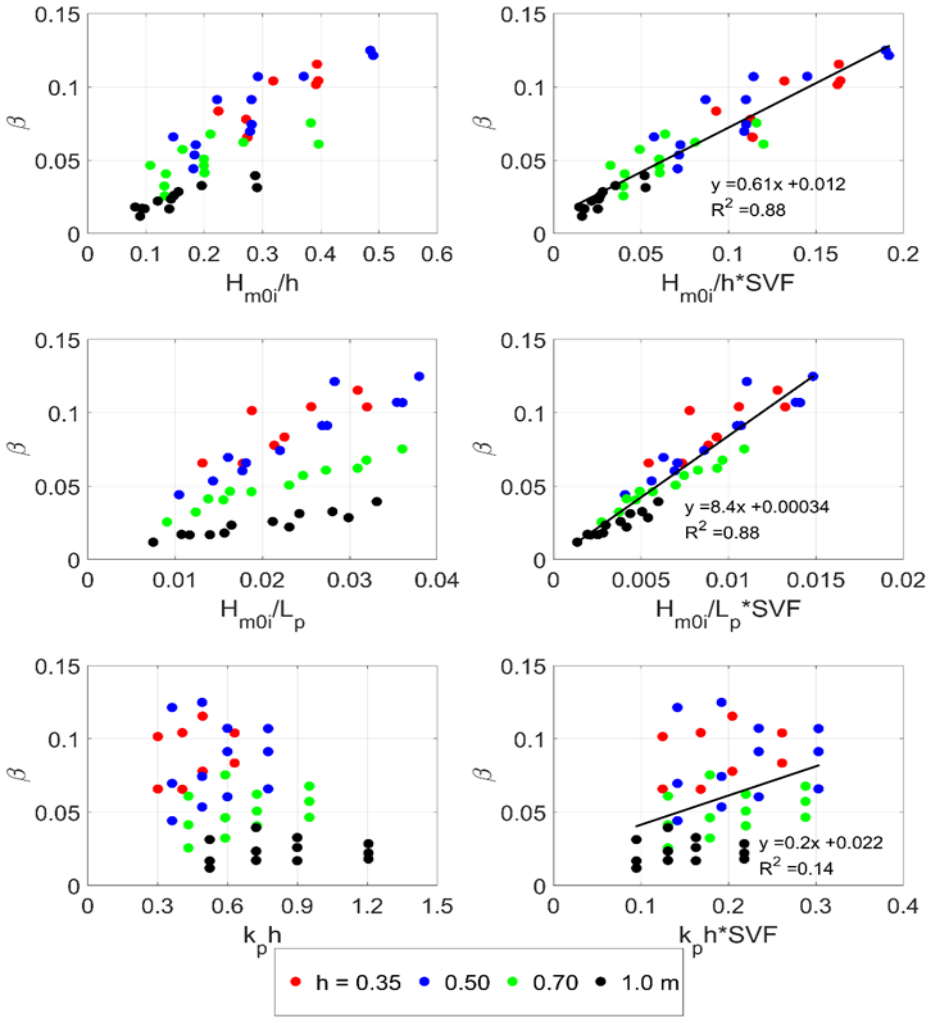

4.1.2 Drag coefficient

The capability of the Dalrymple et al. (1984) and Mendez and Losada (2004) formulations to successfully predict wave attenuation through vegetation is directly related to the value of the drag coefficient (C_D), which is

the only unknown and is specific to the vegetation. C_D is a function of both the hydrodynamic and biomechanical properties of the vegetation, and thus, its value should be determined by calibration using measurements at the project site. However, as measurements are not always available, it is common to relate C_D to nondimensional flow parameters like the Reynolds number (*Re*) or the Keulegan–Carpenter number (*KC*) to expand its prediction via empirical parameterizations (e.g., Kelty et al. 2022; Anderson and Smith 2014).

The Reynolds number (*Re*) and Keulegan–Carpenter number (*KC*) were defined as follows:

$$Re = \frac{U d^*}{\nu}, \tag{18}$$

$$KC = \frac{UT}{d^*}, \tag{19}$$

where

U = depth-averaged horizontal velocity,
ν = kinematic viscosity (10^{-6} m²/s), and
T = peak wave period (T_p) for irregular waves and the monochromatic wave period (T) for the regular waves.

The depth-averaged velocity (U) was computed as follows:

$$U = \frac{1}{h}\int_{-h}^{0} \frac{H}{2}\omega \frac{\cosh k(h+z)}{\sinh kh}\, dz, \tag{20}$$

where

ω = wave angular frequency and
z = 0 at the still water line and $-h$ at the bottom.

The depth-averaged velocity (U) was computed using the incident root-mean-square wave height (H_{rmsi}), peak wave period (T_p), and peak wave-number (k_p) for the irregular wave conditions and using the incident wave height (H_i), monochromatic wave period (T), and monochromatic wave-number (k) for the regular waves. The dz value was 0.01 m.

Figure 12 shows the drag coefficient (C_D) as a function of *Re* and *KC* for all wave conditions using a form common in literature (Kobayashi et al. 1993; Kelty et al. 2022). C_D decreases with larger values of both nondimensional numbers, a behavior that was observed in many recent studies of wave attenuation through mangroves (Kelty et al. 2022; Wang et al. 2022; Chang et al. 2019) and other wave–vegetation literature (e.g., Anderson and Smith 2014). However, this trend was not observed in Maza et al. (2019), albeit the range of *Re* was much smaller and narrower. C_D demonstrated a better fit with *KC* (R^2 = 0.60) than *Re* (R^2 = 0.21). Unlike β, C_D did not show significant differences between water depths. This may, in part, be due to the equivalent diameter (d^*) serving as the length scales in both the Reynolds and Keulegan–Carpenter number.

Figure 12. Drag coefficient (C_D) as a function of Reynolds number (*Re*; *top panel*) and Keulegan–Carpenter number (*KC*; *bottom panel*), along with associated fits and R^2 values for all wave conditions. The *dotted red line* is the drag coefficient associated with a single cylinder (C_D = 1.0). Irregular wave conditions are represented by *circles*, and regular wave conditions are represented by *triangles*.

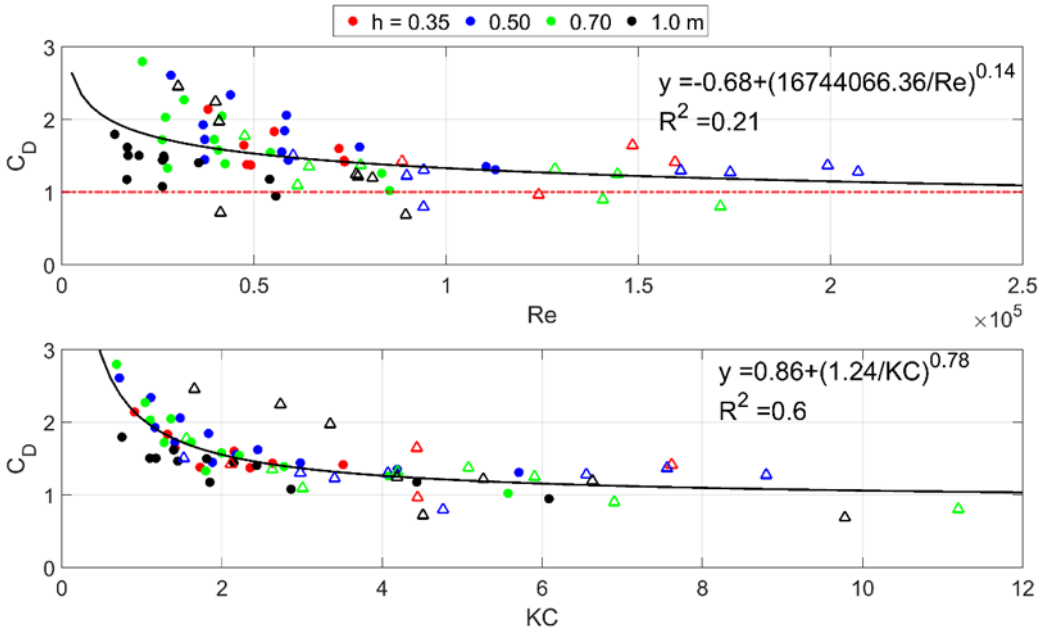

Like with β, the same analysis was repeated for only the irregular waves. Figure 13 shows C_D as a function of *Re* and *KC*, fitted for only the irregular waves. There is still significant scatter for C_D as a function of *Re* (R^2 = 0.07) compared to *KC* (R^2 = 0.70). Removing the regular waves slightly improved the fit with respect to *KC*, likely because the increased fluctuation in the wave evolution (Figure 8) ultimately affected the calibration of the C_D values.

Figure 13. Drag coefficient (C_D) as a function of Reynolds number (*Re*; *top panel*) and Keulegan–Carpenter number (*KC*; *bottom panel*), along with associated fits and R^2 values for only irregular wave conditions. *The dotted red line* is the drag coefficient associated with a single cylinder (C_D = 1.0).

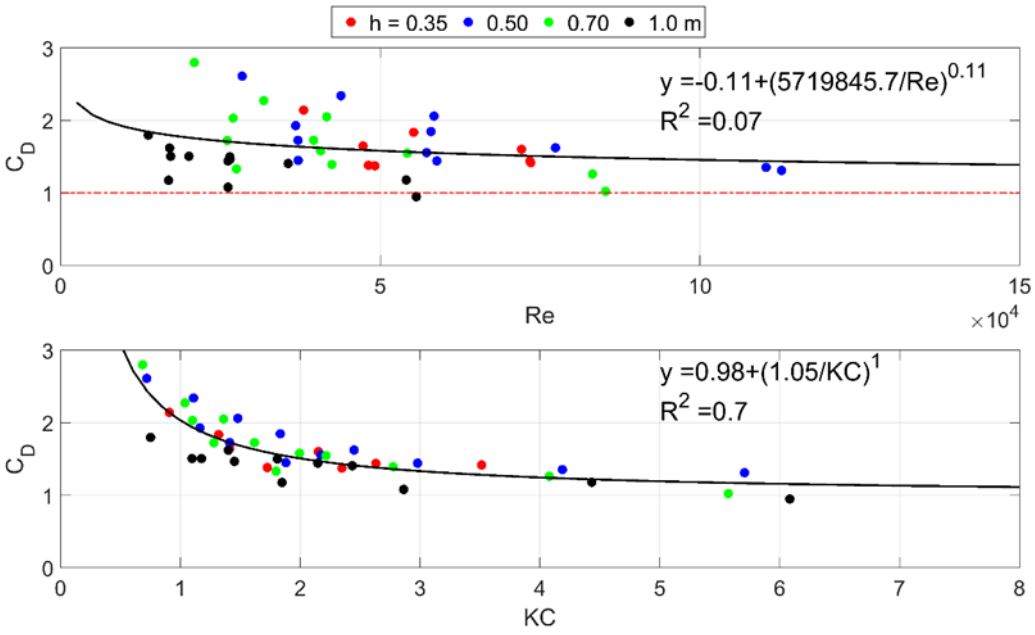

Traditionally, drag coefficients for flow around cylinders and other bodies are parameterized by the Reynolds number. However, this study found a greater degree of agreement between C_D and *KC*. Existing literature, which is largely focused on small-diameter wetland and submerged vegetation, shared this conflicting finding, with some reporting better parameterizations with *Re* (Bradley and Houser 2009; Anderson and Smith 2014; Hu et al. 2014; Wu and Cox 2015) and some with *KC* (Ozeren et al. 2014; Jadhav et al. 2013). Future parameterizations of C_D should report both nondimensional parameters to draw connections between the statistically higher fit and underlying physics. Furthermore, the assumption that inertia effects can be ignored may be incorrect because mangroves may be large enough that inertia effects are nonnegligible (i.e., inertia forces dominate for $KC < 5$, and both drag and inertia dominate for $5 < KC < 25$; Chang et al. 2019). Ultimately, neglecting inertial effects could result in overestimations of C_D at smaller *KC* when inertial effects dominate or are comparable to drag.

4.1.3 Manning's roughness coefficient *n*

Manning's *n* coefficients calibrated using the STWAVE model ranged from 0.25–0.97; these were significantly higher than the Manning's *n* values typically associated with standard hydraulic literature (Chow 1959) and

applied for nearshore hydrodynamic modeling based on land cover (Bunya et al. 2010). The Manning's n coefficient assigned to mangroves for flow and storm surge inundation is approximately 0.14–0.20 for most studies (Wolanski 1992; Zhang et al. 2012; Liu et al. 2013; McIvor et al. 2015).

To better understand how this wide range of Manning's n affects wave attenuation, a single wave condition (H_{mo} = 0.5 m, T_p = 5.0 s) was transformed with different Manning's n coefficients for three water depths, h = 1.0, 2.0, and 3.0 m, using STWAVE (Figure 14). The Manning's n coefficients considered for mangroves were n = 0.15, 0.40, and 0.90 over a propagation distance of 5,000 m (approximately 3.1 mi). The model resolution was 25 m. The computational spectral grids spanned the range of $0.5f_p$ to $2f_p$, with a frequency resolution of 0.015 Hz. The spectral forcing was a TMA spectrum with the peak enhancement and directional spreading factors defined as 3.3 and 4.0, respectively.

The Manning's n coefficient required to obtain a similar degree of dissipation also depends on the peak enhancement factor (γ), which controls the magnitude of the peak wave energy and modifies the peakedness of the spectral shape. The peak enhancement factor (γ) is commonly assigned a value of 3.3, with a lower and upper limit generally regarded as 1 to 10. As γ increases, the spectra shape becomes narrower and more peaked, with energy focused near the spectral peak (i.e., the total energy is distributed amongst a narrower band of frequencies, so the peak magnitude is larger). These narrower spectra require a smaller Manning's n to obtain the same amount of attenuation as compared to those with larger γ values.

The largest differences in wave height occurred at the beginning of the mangrove transect. This was especially evident for h = 2.0 m and h = 3.0 m. For h = 2.0 m, the wave height reduction at x = 175 m was 26% for n = 0.15, 72% for n = 0.40, and 93% for n = 0.9. For h= 3.0 m, the wave height reduction was 10%, 44%, and 78% for n = 0.15, 0.4, and 0.9, respectively. The reduction in wave height was similar for h = 1.0 m because the wave height is quickly dissipated for all Manning's n values. The wave height reduction becomes increasingly similar as the propagation distance increases. At x = 5,000 m, the wave height reduction for n = 0.15, 0.40, and 0.90 was 90%, 98%, and 99% for h = 2.0 m and was 74%, 90%, and 94% for h = 3.0 m. These results show that the amount of wave dissipation over increasingly long distances is not directly

proportional to the Manning's *n* coefficient (i.e., doubling the value does not double the dissipation).

Figure 14. Sensitivity of wave dissipation to Manning's *n* for three different water depths. The water depths are as follows: (*top left*) *h* = 1.0 m, (*top right*) *h* = 2.0 m, and (*bottom*) *h* = 3.0 m.

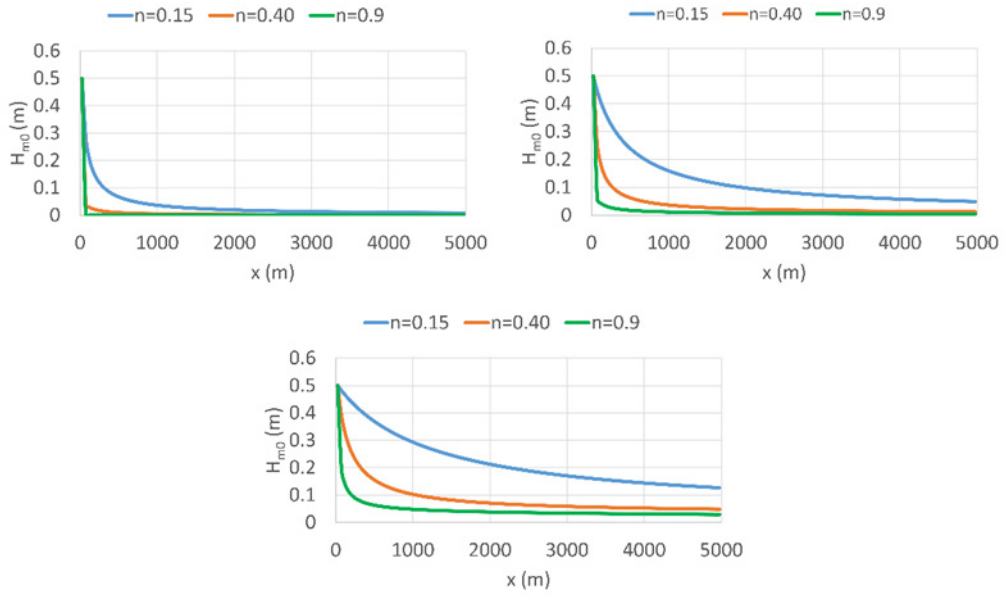

An analysis similar to that for the damping coefficient (β) was repeated to determine the relationships between Manning's *n* for the mangrove prototype and the nondimensional parameters of relative wave height (H/h), wave steepness (H/L), and relative depth (kh; Figure 15). Again, the incident zero-moment wave height (H_{moi}), peak wavelength (L_p), and peak wavenumber (k_p) defined these nondimensional parameters. The calibrated Manning's *n* displayed a negative relationship with H/h (R^2 = 0.45), with Manning's *n* generally decreasing with larger H/h. There was no apparent correlation between Manning's *n* and H/L. The strongest linear relationship was found for Manning's *n* and kh (R^2 = 0.91). This was not surprising given that Manning's *n* formulation has an inverse dependence on water depth and given that the degree of interaction of waves with the bottom is determined by kh.

Figure 15. Manning's *n* as a function of relative wave height (*H/h*), wave steepness (*H/L*), and relative depth (*kh*) for all irregular wave conditions, scaled to prototype.

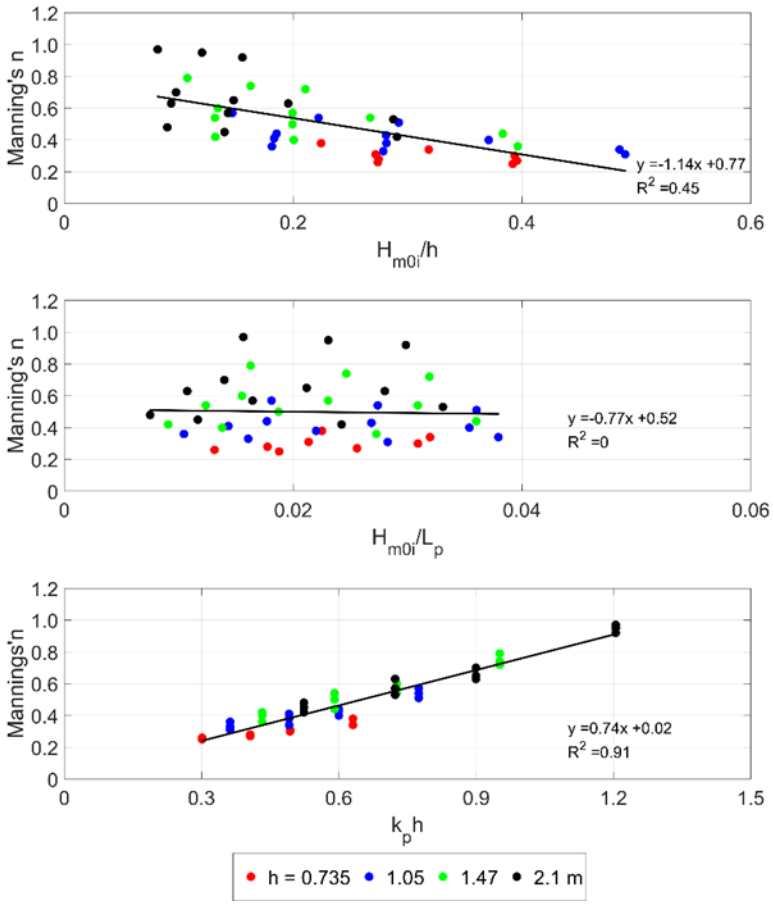

5 Conclusions

5.1 Review of findings

This report quantified the wave attenuation afforded by a 1:2.1 scale North American red mangrove forest. The representative tree model, constructed from PVC and PEX tubing, mimicked the trunk and complex prop root system of this mangrove species. These tree models were installed with a random rotation in a staggered arrangement to create a 15.12 m long forest. The conclusions that follow may be drawn from this study:

- The modeled mangrove forests were effective at reducing wave energy for all tested wave conditions. Wave attenuation through the 15.12 m long forest varied from a minimum of 13% to a maximum of 77%, depending on the hydrodynamic conditions. Wave attenuation increased with shallower water depths.
- The nonlinear damping formulation proposed by Dalrymple (1984) and extended to random waves by Mendez and Losada (2004) captures the wave evolution through the mangrove forest well.
- The damping coefficient (β) showed a strong positive relationship with relative wave height (H/h) and wave steepness (H/L), but it showed a weaker correlation with relative depth (kh). A common fit with H/h and H/L was achieved by using the SVF to account for the additional dependence of β on water depth.
- Wave height has more influence on the degree of wave attenuation than wavelength.
- The drag coefficient (C_D) demonstrated a better fit with the Keulegan–Carpenter number than the Reynolds number. Although ignored in most previous and existing works, including this one, inertia effects may dominate (KC < 5) or be comparable to drag effects (5 < KC < 25), and both should be considered for mangroves in future research.
- Calibrated Manning's n coefficients for mangroves were significantly higher than those reported in standard hydraulic literature and implemented in storm surge modeling.
- A sensitivity study of Manning's n showed the greatest difference in wave attenuation occurs at the beginning of the mangrove forest, with differences decreasing with longer propagating distances. Ultimately, the amount of wave dissipation over increasingly longer distances is not directly proportional to the Manning's n coefficient (i.e., doubling the value does not double the dissipation).

- Manning's n coefficients displayed a negative relationship with relative wave height (H/h). There was no apparent relationship between Manning's n and wave steepness (H/L). The strongest linear relationship was found for Manning's n and relative depth (kh).

5.2 Implications for using mangroves as part of coastal storm risk management solutions

The measured wave attenuation of mangroves was related to three different formulations: damping coefficient (β), drag coefficient (C_D), and Manning's roughness coefficient (n). Suggested applications for each of these follow.

The simplest application of the three, the damping coefficient (β), may be used for fast estimates of wave dissipation across a one-dimensional transect of mangrove forests where other wave transformation physics, such as wave growth, shoaling, and breaking, are neglected and plant properties are unknown.

The application of the drag coefficient (C_D) is limited to instances in which measurements of plant density, stem length, and stem diameter are known. Although operational wave models support its use, research into C_D for mangroves in wave environments is ongoing, so its practical application remains limited and largely theoretical or exploratory. Applications of these sophisticated drag formulations for predicting wave attenuation across marshes are now gaining traction, even though there are growing concerns regarding C_D and its assumptions and derivation (Tempest et al. 2015; Garzon et al. 2019).

Standard practice in nearshore wave modeling is to account for energy losses due to vegetation using bottom friction source terms, like Manning's roughness coefficient, n. These models, like STWAVE and SWAN, can replicate waves through vegetation fields over large spatial scales. However, more research is needed into the discrepancy between the Manning's n coefficients calibrated herein and those presently applied in nearshore modeling based on hydraulic literature and land cover.

The mangrove characteristics and hydrodynamics tested herein were extremely limited given the natural environment, and the presented formulations are likely specific to North American red mangrove populations with properties (i.e., stem density, size, frontal area, forest heterogeneity,

and survivability) similar to those tested. Thus, these formulations should serve as first estimates of wave attenuation, with calibration to data from the area of interest serving as the primary methodology. If measured data are unavailable, engineering judgment should be exercised when applying these formulations to extrapolated hydrodynamic and mangrove conditions.

References

Abdolali, A., T. J. Hesser, M. A. Bryant, A. Roland, A. Khalid, J. M. Smith, C. Ferreira, A. Mehra, and M. D. Sikiric. 2022. "Wave Attenuation by Vegetation: Model Implementation and Validation Study." *Frontiers in Built Environment* 8: 891612. https://doi.org/10.3389/fbuil.2022.891612.

Akamina Technologies. 2018. *AWP-24-3 Wave Height Gauge User's Guide*. College Station, TX: Akamina Technologies. http://www.akamina.com/Documents/AWP-24-3_Users_Guide.pdf.

Anderson, M. E., and J. M. Smith. 2014. "Wave Attenuation by Flexible, Idealized Salt Marsh Vegetation." *Coastal Engineering* 83: 82–92. https://doi.org/10.1016/j.coastaleng.2013.10.004.

Anderson, M. E., and J. M. Smith. 2015. *Implementation of Wave Dissipation by Vegetation in STWAVE*. ERDC/CHL CHETN-I-85. Vicksburg, MS: US Army Engineer Research and Development Center.

Baron-Hyppolite, C., C. H. Lashley, J. Garzon, T. Miesse, C. Ferreira, and J. D. Bricker. 2019. "Comparison of Implicit and Explicit Vegetation Representations in SWAN Hindcasting Wave Dissipation by Coastal Wetlands in Chesapeake Bay." *Geosciences* 9 (1): 8. https://doi.org/10.3390/geosciences9010008.

Bradley, K., and C. Houser. 2009. "Relative Velocity of Seagrass Blades: Implications for Wave Attenuation in Low-Energy Environments." *Journal of Geophysical Research: Earth Surface* 114 (F1). https://doi.org/10.1029/2007JF000951.

Bunya, S., J. C. Dietrich, J. J. Westerink, B. A. Ebersole, J. M. Smith, J. H. Atkinson, R. Jensen, et al. 2010. "A High-Resolution Coupled Riverine Flow, Tide, Wind, Wind Wave, and Storm Surge Model for Southern Louisiana and Mississippi. Part 1: Model Development and Validation." *Monthly Weather Review* 138 (2): 345–377. https://doi.org/10.1175/2009MWR2906.1.

Burger, B. 2005. "Wave Attenuation in Mangrove Forests." MA thesis, Delft University of Technology. http://resolver.tudelft.nl/uuid:0e4c6450-fe5d-4693-9ca9-58da343448b7.

Carter, N. T., and E. Lipiec. 2020. *Flood Risk Reduction from Natural and Nature-Based Features: Army Corps of Engineers Authorities*. CRS Report R46328. Washington, DC: Congressional Research Service. https://crsreports.congress.gov/product/pdf/R/R46328.

Chakrabarti, S. K. 1994. *Offshore Structure Modeling*. Singapore: World Scientific.

Chang, C-W., N. Mori, N. Tsuruta, and K. Suzuki. 2019. "Estimation of Wave Force Coefficients on Mangrove Models." *Journal of Japan Society of Civil Engineers, Ser. B2 (Coastal Engineering)* 75 (2): I_1105–I_1110. https://doi.org/10.2208/kaigan.75.I_1105.

Chave, J., C. Andalo, S. Brown, M. A. Cairns, J. Q. Chambers, D. Eamus, H. Fölster, et al. 2005. "Tree Allometry and Improved Estimation of Carbon Stocks and Balance in Tropical Forests." *Oecologia* 145 (1): 87–99. https://doi.org/10.1007/s00442-005-0100-x.

Chow, V. T. 1959. *Open-Channel Hydraulics*. New York: McGraw-Hill.

Dalrymple, R. A., J. T. Kirby, and P. Hwang. 1984. "Wave Diffraction Due to Areas of Energy Dissipation." *Journal of Waterway, Port, Coastal, and Ocean Engineering* 110 (1): 67–79. https://doi.org/10.1061/(ASCE)0733-950X(1984)110:1(67).

DES (Department of Environment and Science). 2018. *Monitoring and Sampling Manual: Environmental Protection (Water) Policy 2009*. Brisbane: State of Queensland. https://environment.des.qld.gov.au/__data/assets/pdf_file/0031/89914/monitoring-sampling-manual-2018.pdf.

Ellison, A. M., and E. J. Farnsworth. 1997. "Simulated Sea Level Change Alters Anatomy, Physiology, Growth, and Reproduction of Red Mangrove (*Rhizophora mangle* L.)." *Oecologia* 112: 435–446. https://doi.org/10.1007/s004420050330.

Fourqurean, J. W., B. Johnson, J. B. Kauffman, H. Kennedy, C. Lovelock, D. M. Alongi, M. Cifuentes, et al. 2014. "Field Sampling of Vegetation Carbon Pools in Coastal Ecosystems." In *Coastal Blue Carbon: Methods for Assessing Carbon Stocks and Emissions Factors in Mangroves, Tidal Salt Marshes and Seagrass Meadows*, edited by J. Howard, S. Hoyt, K. Isensee, E. Pidgeon, and M. Telszewski, 39–66. Arlington, VA: Conservation International, Intergovernmental Oceanographic Commission of UNESCO, International Union for Conservation of Nature.

Garzon, J. L., T. Miesse, and C. M. Ferreira. 2019. "Field-Based Numerical Model Investigation of Wave Propagation across Marshes in the Chesapeake Bay under Storm Conditions." *Coastal Engineering* 146: 32–46. https://doi.org/10.1016/j.coastaleng.2018.11.001.

Gijsman, R., E. M. Horstman, D. van der Wal, D. A. Friess, A. Swales, and K. M. Wijnberg. 2021. "Nature-Based Engineering: A Review on Reducing Coastal Flood Risk with Mangroves." *Frontiers in Marine Science* 8: 702412. https://doi.org/10.3389/fmars.2021.702412.

Goda, Y., and T. Suzuki. 1976. "Estimation of Incident and Reflected Waves in Random Wave Experiments." *Coastal Engineering Proceedings* 1 (15): 47. https://doi.org/10.9753/icce.v15.47.

Hashim, A. M., and S. M. P. Catherine. 2013. "A Laboratory Study on Wave Reduction by Mangrove Forests." *APCBEE Procedia* 5: 27–32. https://doi.org/10.1016/j.apcbee.2013.05.006.

He, F., J. Chen, and C. Jiang. 2019. "Surface Wave Attenuation by Vegetation with the Stem, Root, and Canopy." *Coastal Engineering* 152: 103509. https://doi.org/10.1016/j.coastaleng.2019.103509.

Holthuijsen, L. H. 2007. *Waves in Oceanic and Coastal Waters*. Cambridge: Cambridge University Press.

Horstman, E. M., C. M. Dohmen-Janssen, P. M. F. Narra, N. J. F. van den Berg, M. Siemerink, and S. J. M. H. Hulscher. 2014. "Wave Attenuation in Mangroves: A Quantitative Approach to Field Observations." *Coastal Engineering* 94: 47–62. https://doi.org/10.1016/j.coastaleng.2014.08.005.

Hu, Z., T. Suzuki, T. Zitman, W. Uittewaal, and M. Stive. 2014. "Laboratory Study on Wave Dissipation by Vegetation in Combined Current-Wave Flow." *Coastal Engineering* 88: 131–142. https://doi.org/10.1016/j.coastaleng.2014.02.009.

Hughes, S. A. 1984. *The TMA Shallow-Water Spectrum Description and Applications*. CERC-84-7. Vicksburg, MS: Coastal Engineering Research Center.

Jadhav, R. S., Q. Chen, and J. M. Smith. 2013. "Spectral Distribution of Wave Energy Dissipation by Salt Marsh Vegetation." *Coastal Engineering* 77: 99–107. https://doi.org/10.1016/j.coastaleng.2013.02.013.

Kathiresan, K., and N. Rajendran. 2015. "Coastal Mangrove Forests Mitigated Tsunami." *Estuarine, Coastal, and Shelf Science* 65 (3): 601–606. https://doi.org/10.1016/j.ecss.2005.06.022.

Kauffman, J. B., and D. C. Donato. 2012. *Protocols for the Measurement, Monitoring and Reporting of Structure, Biomass and Carbon Stocks in Mangrove Forests*. Working Paper 86. Bogor, Indonesia: Center for International Forestry Research. https://www.cifor.org/publications/pdf_files/WPapers/WP86CIFOR.pdf.

Kelty, K., T. Tomiczek, D. T. Cox, P. Lomonaco, and W. Mitchell. 2022. "Prototype-Scale Physical Model of Wave Attenuation through a Mangrove Forest of Moderate Cross-Shore Thickness: LiDAR-Based Characterization and Reynolds Scaling for Engineering with Nature." *Frontiers in Marine Science* 8: 780946. https://doi.org/10.3389/fmars.2021.780946.

Kobayashi, N., A. W. Raichle, and T. Asano. 1993. "Wave Attenuation by Vegetation." *Journal of Waterway, Port, Coastal, and Ocean Engineering* 119 (1): 30–48. https://doi.org/10.1061/(ASCE)0733-950X(1993)119:1(30).

Komiyama, A., J. E. Ong, and S. Poungparn. 2008. "Allometry, Biomass, and Productivity of Mangrove Forests: A Review." *Aquatic Botany* 89 (2): 128–137. https://doi.org/10.1016/j.aquabot.2007.12.006.

Krauss, K. W., T. W. Doyle, T. J. Doyle, C. M. Swarzenski, A. S. From, R. H. Day, and W. H. Conner. 2009. "Water Level Observations in Mangrove Swamps during Two Hurricanes in Florida." *Wetlands* 29 (142): 142–149. https://doi.org/10.1672/07-232.1.

Larjavaara, M., and H. C. Muller-Landau. 2013. "Measuring Tree Height: A Quantitative Comparison of Two Common Field Methods in a Moist Tropical Forest." *Methods in Ecology and Evolution* 4 (9): 793–801. https://doi.org/10.1111/2041-210X.12071.

Liu, H., K. Zhang, Y. Li, and L. Xie. 2013. "Numerical Study of the Sensitivity of Mangroves in Reducing Storm Surge and Flooding to Hurricane Characteristics in Southern Florida." *Continental Shelf Research* 64 (1): 51–65. https://doi.org/10.1016/j.csr.2013.05.015.

Maza, M., K. Adler, D. Ramos, A. M. Garcia, and H. Nepf. 2017. "Velocity and Drag Evolution from the Leading Edge of a Model Mangrove Forest." *Journal of Geophysical Research: Oceans* 122 (11): 9144–9159. https://doi.org/10.1002/2017JC012945.

Maza, M., J. L. Lara, and I. J. Losada. 2015. "Tsunami Wave Interaction with Mangrove Forests: A 3D Numerical Approach." *Coastal Engineering* 98: 33–54. https://doi.org/10.1016/j.coastaleng.2015.01.002.

Maza, M., J. L. Lara, and I. J. Losada. 2019. "Experimental Analysis of Wave Attenuation and Drag Forces in a Realistic Fringe *Rhizophora* Mangrove Forest." *Advances in Water Resources* 131: 103376. https://doi.org/10.1016/j.advwatres.2019.07.006.

Mazda, Y., M. Magi, Y. Ikeda, T. Kurokawa, and T. Asano. 2006. "Wave Reduction in a Mangrove Forest Dominated by *Sonneratia sp*." *Wetlands Ecology and Management* 14: 365–378. https://doi.org/10.1007/s11273-005-5388-0.

McIvor, A., I. Möller, T. Spencer, and M. Spalding. 2012. *Reduction of Wind and Swell Waves by Mangroves. Natural Coastal Protection Series: Report 1*. Cambridge Coastal Research Unit Working Paper 40. Arlington County, VA: The Nature Conservancy and Wetlands International.

McIvor, A., T. Spencer, M. Spalding, C. Lacambra, and I. Möller. 2015. "Mangroves, Tropical Cyclones, and Coastal Hazard Risk Reduction." In *Coastal and Maine Hazards, Risks, and Disasters*, edited by J. F. Shroder, J. T. Ellis, and D. J. Sherman, 402–429. Waltham, MA: Elsevier. https://doi.org/10.1016/B978-0-12-396483-0.00014-5.

Mendez, F. J., and I. J. Losada. 2004. "An Empirical Model to Estimate the Propagation of Random Breaking and Nonbreaking Waves over Vegetation Fields." *Coastal Engineering* 51 (2): 103–118. https://doi.org/10.1016/j.coastaleng.2003.11.003.

Montgomery, J. M., K. R. Bryan, J. C. Mullarney, and E. M. Horstman. 2019. "Attenuation of Storm Surges by Coastal Mangroves." *Geophysical Research Letters* 46 (5): 2680–2689. https://doi.org/10.1029/2018GL081636.

Mori, N., C.-W. Chang, T. Inoue, Y. Akaji, K. Hinokidani, S. Baba, M. Takagi, et al. 2022. "Parameterization of Mangrove Root Structure of *Rhizophora stylosa* in Coastal Hydrodynamic Model." *Frontiers in Built Environment* 7: 782219. https://doi.org/10.3389/fbuil.2021.782219.

Morison, J. R., M. P. O'Brien, J. W. Johnson, and S. A. Schaaf. 1950. "The Force Exerted by Surface Waves on Piles." *Petroleum Transactions* 189: 149–154. https://doi.org/10.2118/950149-G.

Novitzky, P. 2010. "Analysis of Mangrove Structure and Latitudinal Relationships on the Gulf Coast Peninsular Florida." MA thesis, University of South Florida. https://digitalcommons.usf.edu/etd/1726.

Ohira, W., K. Honda, M. Nagai, and A. Ratanasuwan. 2013. "Mangrove Stilt Root Morphology Modeling for Estimating Hydraulic Drag in Tsunami Inundation Simulation." *Trees* 27 (1): 141–148.

Ozeren, Y., D. G. Wren, and W. Wu. 2014. "Experimental Investigation of Wave Attenuation through Model and Live Vegetation." *Journal of Waterway, Port, Coastal, and Ocean Engineering* 140 (5): 04014019. https://doi.org/10.1061/(ASCE)WW.1943-5460.0000251.

Reimann, S., S. Husrin, A Strusińska, and H. Oumeraci. 2009. *Damping Tsunami and Storm Waves by Coastal Forests—Parameterisation and Hydraulic Model Tests*. Hannover, Germany: Coastal Research Centre. https://www.fzk.uni-hannover.de/fileadmin/fzk/publications/1_02_Reimann_et_al.pdf.

Smith, J. M., M. A. Bryant, and T. V. Wamsley. 2016. "Wetland Buffers: Numerical Modeling of Wave Dissipation by Vegetation." *Earth Surface Processes and Landforms* 41(6): 847–854. https://doi.org/10.1002/esp.3904.

Smith, T. J., and K. R. T. Whelan. 2006. "Development of Allometric Relations for Three Mangrove Species in South Florida for Use in the Greater Everglades Ecosystem Restoration." *Wetlands Ecology and Management* 14 (5): 409–419. https://doi.org/10.1007/s11273-005-6243-z.

Sorensen, R. M. 2006. *Basic Coastal Engineering*. New York: Springer.

Strusińska-Correia, A., S. Husrin, and H. Oumeraci. 2013. "Tsunami Damping by Mangrove Forest: A Laboratory Study Using Parameterized Trees." *Natural Hazards and Earth System Sciences* 13: 483–503. https://doi.org/10.5194/nhess-13-483-2013.

Suwa, R., R. Rollon, S. Sharma, M. Yoshikai, G. M. Albano, K. Ono, N. S. Adi, et al. 2021. "Mangrove Biomass Estimation Using Canopy Height and Wood Density in the South East and East Asian Regions." *Estuarine, Coastal and Shelf Science* 248: 106937. https://doi.org/10.1016/j.ecss.2020.106937.

Suzuki, T., M. Zijlema, B. B. Burger, M. C. Meijer, and S. Narayan. 2012. "Wave Dissipation by Vegetation with Layer Schematization in SWAN." *Coastal Engineering* 59 (1): 64–71. https://doi.org/10.1016/j.coastaleng.2011.07.006.

Tempest, J., I. Möller, and T. Spencer. 2015. "A Review of Plant-Flow Interactions on Salt Marshes: The Importance of Vegetation Structure and Plant Mechanical Characteristics." *Wiley Interdisciplinary Reviews: Water* 2 (6): 669–681. https://doi.org/10.1002/wat2.1103.

Tomiczek, T., A. Wargula, N. R. Hurst, D. B. Bryant, and L. A. Provost. 2021. *Engineering with Nature: The Role of Mangroves in Coastal Protection*. ERDC/TN EWN-21-1. Vicksburg, MS: US Army Engineer Research and Development Center. http://dx.doi.org/10.21079/11681/42420.

Tomiczek, T., A. Wargula, M. Jendrysik, S. Goodwin, A. B. Kennedy, P. Lynett, P. Lomonaco, and D. T. Cox. 2019. "Physical Model Investigation of Parcel-Scale Effects of Mangroves on Wave Transformation and Force Reduction in the Built Environment." In *Proceedings of Coastal Structures Conference*, ASCE, October 2019, Hannover, Germany. http://dx.doi.org/10.18451/978-3-939230-64-9_100.

Tomiczek, T., A. Wargula, P. Lomónaco, S. Goodwin, D. Cox, A. Kennedy, and P. Lynett. 2020. "Physical Model Investigation of Mid-Scale Mangrove Effects on Flow Hydrodynamics and Pressures and Loads in the Built Environment." *Coastal Engineering* 162: 103791. https://doi.org/10.1016/j.coastaleng.2020.103791.

USACE (US Army Corps of Engineers). 2017. *Implementation Guidance for Section 1184 of the Water Resources Development Act of 2016 (WRDA 2016), Consideration of Measures*. Memorandum for Commanders, Major Subordinate Commands, 28 September 2017. Washington, DC: Department of the Army, US Army Corps of Engineers. https://usace.contentdm.oclc.org/digital/collection/p16021coll5/id/1200/.

van Rooijen, A. A., J. van Thiel de Vries, R. T. McCall, A. van Dongeren, D. J. A. Roelvink, and A. Reniers. 2015. "Modeling of Wave Attenuation by Vegetation with XBEACH." In *E-proceedings, 36th IAHR World Congress, IAHR*, June 2015, The Hague, Netherlands.

Wang, Y., Z. Yin, and Y. Liu. 2022. "Experimental Investigation of Wave Attenuation and Bulk Drag Coefficient in Mangrove Forest with Complex Root Morphology." *Applied Ocean Research* 118: 102974. https://doi.org/10.1016/j.apor.2021.102974.

Wolanski, E. 1992. "Hydrodynamics of Mangrove Swamps and Their Coastal Waters." *Hydrobiologia* 247: 141–161. https://doi.org/10.1007/BF00008214.

Wu, W.-C., and D. T. Cox. 2015. "Effects of Wave Steepness and Relative Water Depth on Wave Attenuation by Emergent Vegetation." *Estuarine, Coastal, and Shelf Science* 164: 443–450. https://doi.org/10.1016/j.ecss.2015.08.009.

Wu, W.-C., and D. T. Cox. 2016. "Effects of Vertical Variation in Vegetation Density on Wave Attenuation." *Journal of Waterway, Port, Coastal, and Ocean Engineering* 142(2): 04015020. https://doi.org/10.1061/(ASCE)WW.1943-5460.0000326.

Zhang, K., H. Liu, Y. Li, H. Xu, J. Shen, J. Rhome, and T. J. Smith, III. 2012. "The Role of Mangroves in Attenuation Storm Surges." *Estuarine, Coastal, and Shelf Science* 102: 11–23. https://doi.org/10.1016/j.ecss.2012.02.021.

Zhang, Y., Y. Yang, K. Yang, X. Tan, X. Sun, B. Leng, C. Zhou, and B. Zhu. 2020. "Non-linear Wave Attenuation Quantification Model Improves the Estimation of Wave Attenuation Efficiency of Mangroves." *Estuarine, Coastal, and Shelf Science* 245: 106927. https://doi.org/10.1016/j.ecss.2020.106927.

Appendix A: Mangrove Field Methods

There are several important vegetative characteristic measurements that can be included in engineering models to help assess the potential for wave attenuation by mangrove forests. The entire mangrove plant, from its complex aerial root system to its well-developed trunk and canopy, is involved in the deflection of wave energy and should be included in models evaluating the effect of mangrove forests on coastal protection (Wu and Cox 2016). The specific mangrove species and their density, coverage, and biomass all influence the coastal protection abilities of a mangrove forest. Because the ability to mitigate wave impacts depends on where the wave interacts with mangrove vegetation characteristics, field measurements are often divided into three categories, as defined by Suzuki et al. (2012): the roots, trunk, and canopy. The subsections that follow describe the best monitoring practices to measure mangrove components that can affect their potential for wave attenuation.

A.1 Mangrove forest vegetative characteristics

A.1.1 Mangrove study plots

Before initiating a field study, sampling plots should be established for the assessment of mangrove characteristics. Establishing plots perpendicular to the shoreline along the length of the intertidal zone, study site, or area of influence will help describe the representative mangrove community used to study wave attenuation. Plot size can vary based on the needs of the investigation, and several studies describe the considerations needed to successfully establish forest plots (Kauffman and Donato 2012; Horstman et al. 2014).

A.1.2 Species dominance

Documentation of the correct mangrove species in each plot is imperative for assessing the mangrove vegetative community and ensuring the correct allometric equation for biomass is utilized (Section A.2.5) for each species.

A.2 Trunk and canopy

A.2.1 Tree diameter at breast height (DBH)

DBH measurements assess the biomass of individual trees and are necessary for estimating mangrove basal area and aboveground biomass. DBH measurements are collected using diameter tape (i.e., fabric measuring tape) at 1.3 m above the soil surface (Tomiczek et al. 2020; Mori et al. 2022; Figure A-1). If recording the diameter of smaller trees and shrubs, calipers can be used. In the case of mangroves with aerial roots or buttressing, DBH is typically measured immediately above the highest prop root or at the point where the tree buttressing ends (Kauffman and Donato 2012). Some studies have measured DBH at 0.3–0.5 m above the tallest prop root (Stringer et al. 2015; DES 2018). Either method is sufficient if the measurements are consistent throughout the study. Several studies provide detailed guidance on DBH measurements for irregular trees (e.g., trees with forked stems or exceedingly high prop roots; Fourqurean et al. 2014; DES 2018). The DBH is calculated as follows:

$$DBH = \frac{c}{\pi}, \tag{A-1}$$

where c is the trunk circumference.

Figure A-1. Example of tree diameter at breast height (DBH) measurements. (Photo by Daniel Murdiyarso, Center for International Forestry Research; https://flic.kr/p/WKu6fY.)

A.2.2 Tree density (individual trees/square meter)

Tree density measures the number of trees per square meter in a mangrove stand. Tree density is calculated by counting the number of individual trees in a plot and dividing by plot area. The density of trees in a mangrove forest has a significant influence on wave attenuation models (Novitzky 2010; Ohira et al. 2013; Tomiczek et al. 2021). Tree density (N) is calculated as follows:

$$N = \frac{\text{\# of trees}}{\text{plot area}}. \tag{A-2}$$

A.2.3 Stand Basal Area (square meter/hectare)

Basal area describes stand density and measures the size of the mangrove community by determining the average amount of land occupied by mangroves within a known area, usually a hectare. To calculate stand basal area, the basal area (BA) of individual trees within the area must first be calculated. The basal area (in square meters) for an individual tree is calculated as follows:

$$BA = \pi r^2, \tag{A-3}$$

where r is the tree radius (i.e., half of DBH).

Basal area for a mangrove stand (in square meters/hectare) is calculated as the sum of the basal areas of all trees in a known area divided by that area:

$$stand\ BA = \frac{\sum BA}{plot\ area}, \tag{A-4}$$

where ΣBA is the sum of all tree basal areas in a plot.

A.2.4 Tree height (meters)

The height of mangrove trees is measured to document the relation of mangrove component characteristics as they relate to the wave height. Tree height is also used in allometric equations to estimate tree biomass. Tree height is divided into three segments for evaluation: (1) total tree height, which measures from the soil surface to the top of the canopy

crown; (2) trunk height, which measures the trunk from the top of the tallest prop root (if applicable) or the soil surface to the bottom of the tree canopy; and (3) root layer height, which measures from the soil surface to the tallest prop root (if applicable; Figure A-2). Canopy height, which accounts for the length of the canopy from the lowest branch to the apex of the main stem, can also be derived from these measurements. There are several options available for measuring tree height. Altimeters and laser range finders both use trigonometry to calculate tree height and are especially useful for large trees (Larjavaara and Muller-Landau 2013). Depending on the height of the tree, the simplest method for measuring tree height is to use a height pole, meter stick, or measuring tape (DES 2018).

Figure A-2. Schematic of tree height measurements where (*1*) total height measures the entire length of the tree from the soil surface to the top of the canopy, (*2*) the trunk layer measures the length of the tree from the tallest prop root (if applicable) or the soil surface to the bottom of the tree canopy, and (*3*) the aerial root layer (if applicable) is measured from the soil surface to the top of the tallest prop root. (Unannotated photo by Big Cypress National Preserve; https://flic.kr/p/P9dnST.)

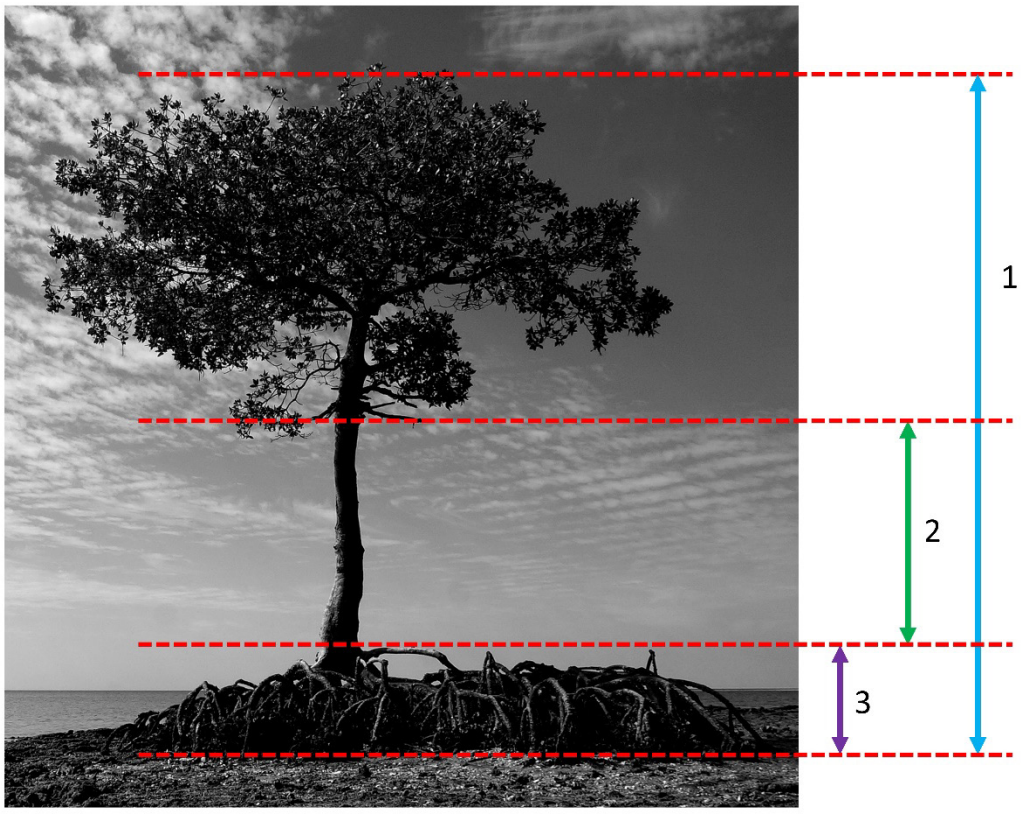

A.2.5 Aboveground biomass (kilogram/square meter)

Aboveground biomass calculates the total density of mangrove stems, roots, and canopies in a mangrove forest (Ellison and Farnsworth 1997). Measuring biomass can be an intensive field effort, but allometric equations are often used to estimate biomass using only tree height and DBH measurements. Allometric equations must be calibrated by ground-truthing field efforts and should be regional or site specific. Several studies have developed allometric equations for biomass calculations (Chave et al. 2005; Smith and Whelan 2006; Komiyama et al. 2008; Novitzky 2010; Suwa et al. 2021).

The stilt roots of *Rhizophora* spp. are usually included in the allometric equations that estimate mangrove biomass, whereas the pneumatophores of *Avicennia* spp. generally are not. If biomass estimates are desired for pneumatophores, destructive sampling of roots would be required (Kauffman and Donato 2012).

A.3 Roots

Ohira et al. (2013) provide an example of regional allometric equation development to estimate root number, height, diameter, and spread distance for trees using only DBH measurements, which can be useful when field measurements are not feasible.

A.3.1 Root density (roots/square meter)

Root density measures the total number of roots in a known area, usually within a square meter or larger quadrat plot (Figure A-3). The number of roots per individual tree can also be recorded.

Figure A-3. An example of pneumatophore (root) density counting measurements for an *Avicennia* spp. within a quadrat. (Photo by Boone Kauffman and reproduced from Fourqurean et al. 2014, 85.)

A.3.2 Root height (centimeter)

For stilt roots, root height is determined by the height of the tallest primary root on each tree (Ohira et al. 2013; Horstman et al. 2014). For other aerial roots, such as pneumatophores, the heights of individual roots are measured and averaged across the plot (Figure A-4). Root height is often measured using a measuring tape or a meter stick.

Figure A-4. Root height measurement of an *Avicennia* spp. pneumatophore. (Photo by Boone Kauffman and reproduced from Fourqurean et al. 2014, 85).

A.3.3 Root Diameter (centimeter)

Root diameter is measured to the nearest centimeter using calipers at a predetermined height or distance from the mangrove tree trunk (Ohira et al. 2013; Horstman et al. 2014; Mori et al. 2022; Figure A-5). Although it can vary for a specific project and research goals, previous studies have measured root diameter at a height of 20 cm (Mori et al. 2022) or at a distance of 15 cm away from the trunk (Ohira et al. 2013).

Figure A-5. Root diameter measurements using a caliper. (Photo by Tori Tomiczek and reproduced from Tomiczek et al. 2019, 1000.).

A.3.4 Root spread distance (meters)

Root spread distance measures the distance from the base of the tree trunk to the edge of outermost primary root, which can be measured using a measuring tape, a ruler, or a meter stick (Ohira et al. 2013; Mori et al. 2022; Figure A-6).

Figure A-6. A schematic of a *Rhizophora mangle* trunk and root structure and associated measurements. (Image reproduced from Tomiczek et al. 2021, 10.)

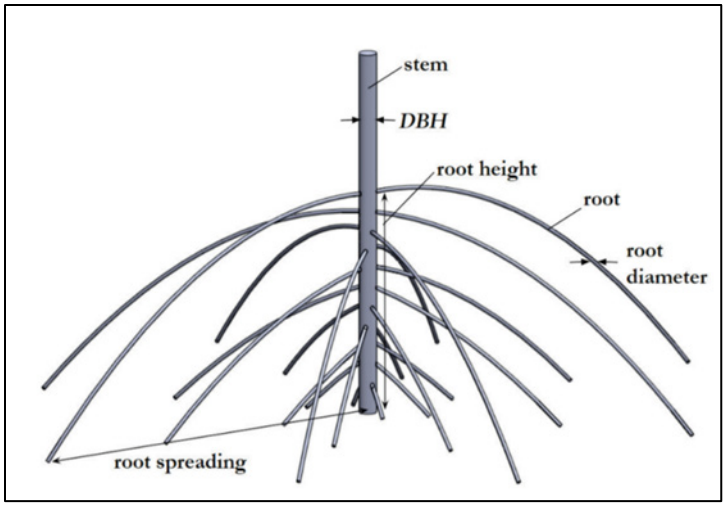

Appendix B: Wave Gauge Calibration Data

Table B-1. Detailed calibration information for WGs 1–16.

Gauge 1		Gauge 2		Gauge 3		Gauge 4	
Position (cm)	Voltage (V)	Position (cm)	Voltage (V)	Position (cm)	Voltage (V)	Position (cm)	Voltage (V)
0	−4.552	0	−4.534	0	−4.543	0	−4.539
15	−1.818	15	−1.813	15	−1.802	15	−1.814
30	0.925	30	0.923	30	0.929	30	0.91
45	3.654	45	3.636	45	3.656	45	3.632
50	4.56	50	4.545	50	4.579	50	4.535
45	3.661	45	3.639	45	3.654	45	3.632
30	0.925	30	0.927	30	0.929	30	0.908
15	−1.814	15	−1.807	15	−1.804	15	−1.814
0	−4.551	0	−4.534	0	−4.539	0	−4.541
Slope cm/V	5.484	Slope cm/V	5.506	Slope cm/V	5.488	Slope cm/V	5.508
Intercept	24.952	Intercept	24.95	Intercept	24.91	Intercept	25.00
R^2	1.00	R^2	1.00	R^2	1.00	R^2	1.00
Gauge 5		**Gauge 6**		**Gauge 7**		**Gauge 8**	
Position	Voltage	Position	Voltage	Position	Voltage	Position	Voltage
0	−4.551	0	−4.574	0	−4.55	0	−4.564
15	−1.794	15	−1.848	15	−1.82	15	−1.836
30	0.921	30	0.903	30	0.91	30	0.909
45	3.654	45	3.676	45	3.639	45	3.667
50	4.578	50	4.582	50	4.555	50	4.571
45	3.663	45	3.681	45	3.641	45	3.664
30	0.939	30	0.921	30	0.915	30	0.909
15	−1.779	15	−1.832	15	−1.821	15	−1.835
0	−4.532	0	−4.567	0	−4.548	0	−4.572
Slope cm/V	5.490	Slope cm/V	5.456	Slope cm/V	5.493	Slope cm/V	5.466
Intercept	24.89	Intercept	24.98	Intercept	24.99	Intercept	25.00
R^2	1.00	R^2	1.00	R^2	1.00	R^2	1.00

Table B-1 (cont.). Detailed calibration information for WGs 1–16.

Gauge 9		Gauge 10		Gauge 11		Gauge 12	
Position (cm)	Voltage (V)	Position (cm)	Voltage (V)	Position (cm)	Voltage (V)	Position (cm)	Voltage (V)
0	−4.547	0	−4.589	0	−4.592	0	−4.549
15	−1.804	15	−1.863	15	−1.844	15	−1.807
30	0.954	30	0.892	30	0.889	30	0.922
45	3.66	45	3.654	45	3.588	45	3.652
50	4.567	50	4.579	50	4.513	50	4.547
45	3.669	45	3.653	45	3.289	45	3.651
30	0.954	30	0.895	30	0.851	30	0.924
15	−1.806	15	−1.858	15	−1.882	15	−1.808
0	−4.541	0	−4.602	0	−4.593	0	−4.552
Slope cm/V	5.483	Slope cm/V	5.451	Slope cm/V	5.553	Slope cm/V	5.492
Intercept	24.88	Intercept	25.09	Intercept	25.42	Intercept	24.96
R^2	1.00	R^2	1.00	R^2	1.00	R^2	1.00
Gauge 13		**Gauge 14**		**Gauge 15**		**Gauge 16**	
Position	Voltage	Position	Voltage	Position	Voltage	Position	Voltage
0	−4.583	0	−4.566	0	−4.57	0	−4.589
15	−1.845	15	−1.805	15	−1.827	15	−1.865
30	0.885	30	0.928	30	0.922	30	0.904
45	3.609	45	3.66	45	3.669	45	3.659
50	4.508	50	4.564	50	4.57	50	4.593
45	3.613	45	3.661	45	3.665	45	3.671
30	0.891	30	0.927	30	0.925	30	0.949
15	−1.831	15	−1.806	15	−1.828	15	−1.854
0	−4.554	0	−4.56	0	−4.567	0	−4.590
Slope cm/V	5.505	Slope cm/V	5.477	Slope cm/V	5.466	Slope cm/V	5.443
Intercept	25.132	Intercept	24.95	Intercept	24.97	Intercept	25.02
R^2	1.00	R^2	1.00	R^2	1.00	R^2	1.00

Appendix C: Wave Damping Coefficients

Appendix C: Wave Damping Coefficients shows the normalized wave height evolution with fitted damping coefficients (β) and standard error (s) for all tested wave conditions, both irregular (C.1) and regular (C.2). The label at the top of each figure corresponds with a wave condition in Table 1.

C.1 Irregular Waves

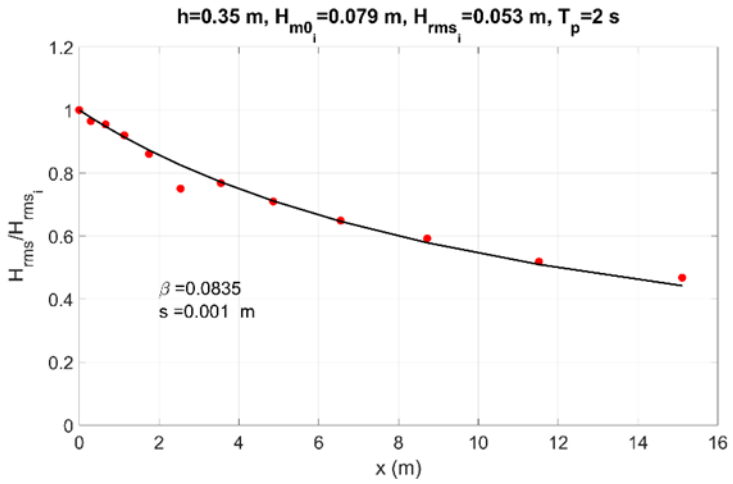

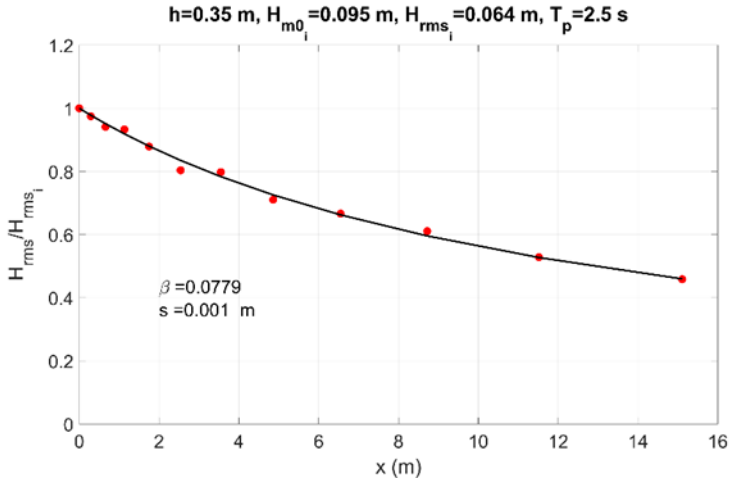

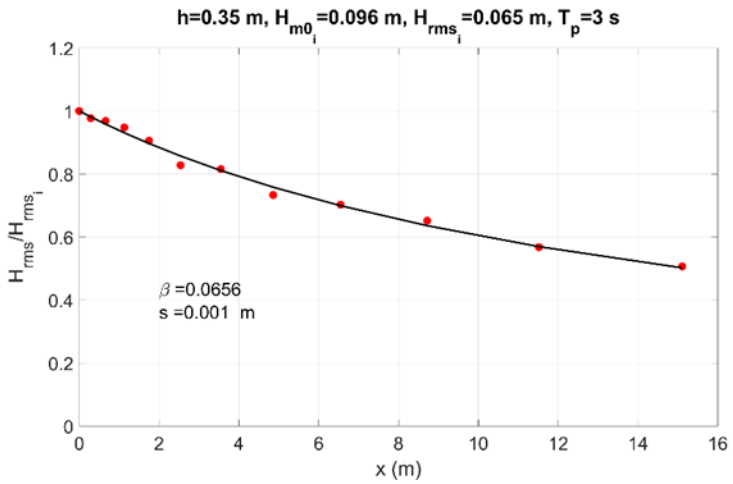
h=0.35 m, H$_{m0_i}$=0.096 m, H$_{rms_i}$=0.065 m, T$_p$=3 s
H$_{rms}$/H$_{rms_i}$
x (m)
β =0.0656
s =0.001 m

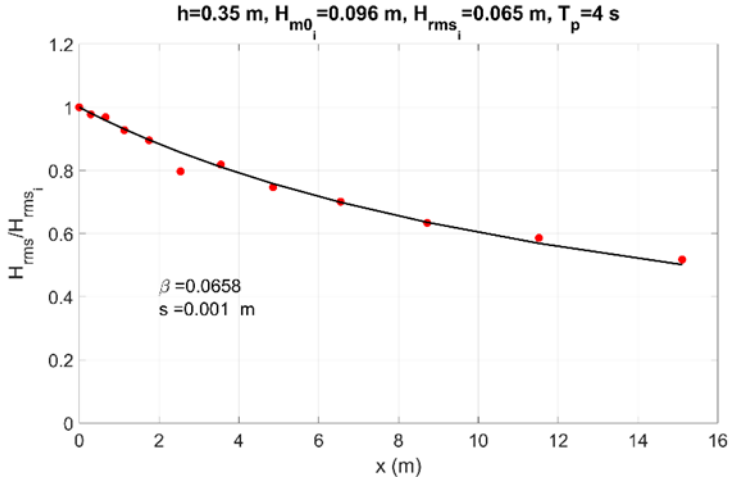
h=0.35 m, H$_{m0_i}$=0.096 m, H$_{rms_i}$=0.065 m, T$_p$=4 s
H$_{rms}$/H$_{rms_i}$
x (m)
β =0.0658
s =0.001 m

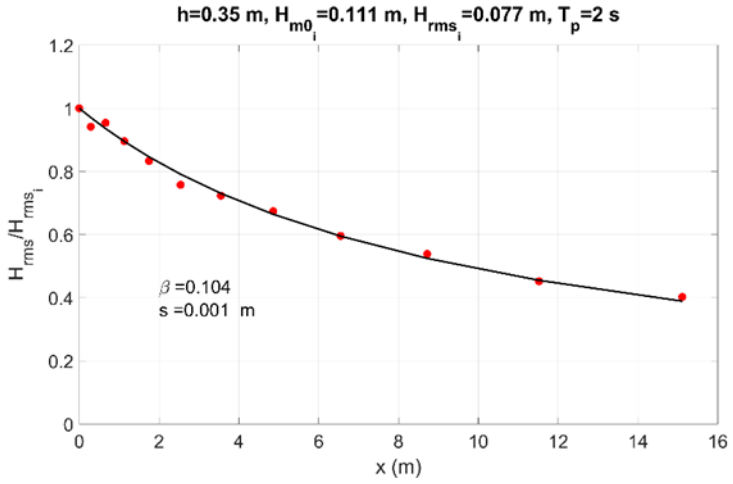
h=0.35 m, H$_{m0_i}$=0.111 m, H$_{rms_i}$=0.077 m, T$_p$=2 s
H$_{rms}$/H$_{rms_i}$
x (m)
β =0.104
s =0.001 m

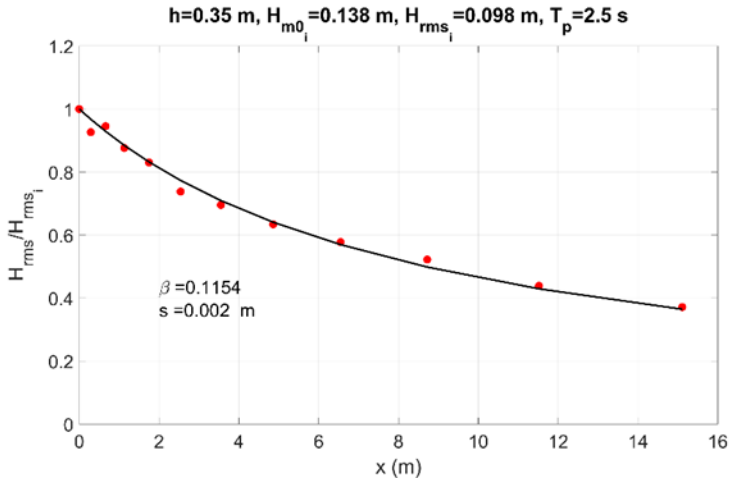
h=0.35 m, H$_{m0_i}$=0.138 m, H$_{rms_i}$=0.098 m, T$_p$=2.5 s
H$_{rms}$/H$_{rms_i}$
x (m)
β =0.1154
s =0.002 m

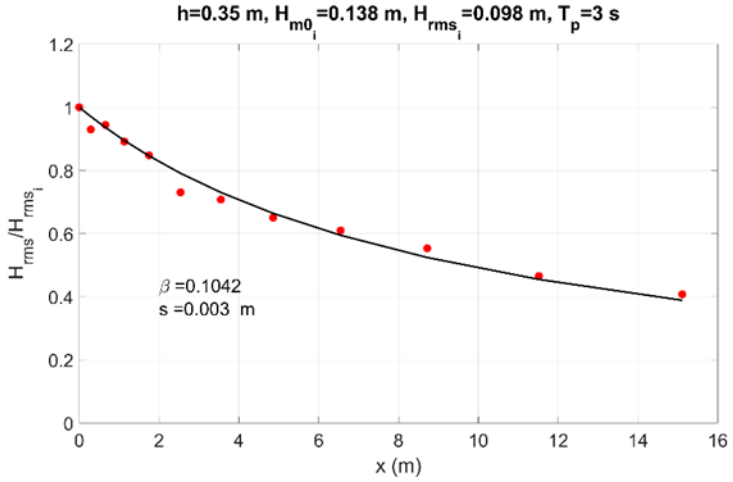
h=0.35 m, H$_{m0_i}$=0.138 m, H$_{rms_i}$=0.098 m, T$_p$=3 s
H$_{rms}$/H$_{rms_i}$
x (m)
β =0.1042
s =0.003 m

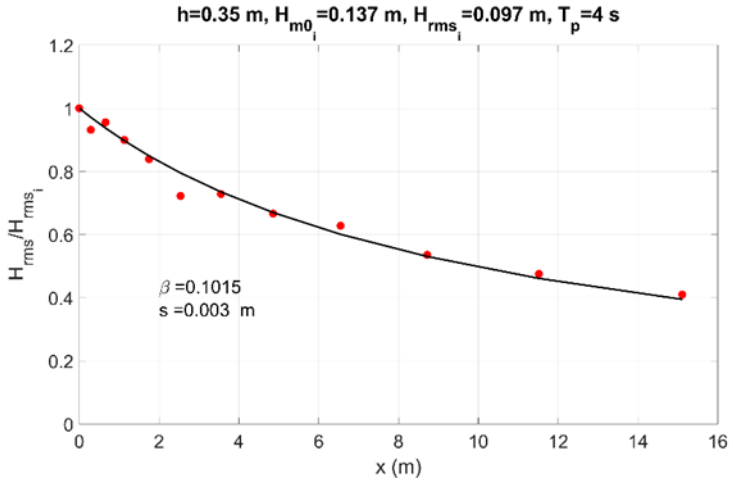
h=0.35 m, H$_{m0_i}$=0.137 m, H$_{rms_i}$=0.097 m, T$_p$=4 s
H$_{rms}$/H$_{rms_i}$
x (m)
β =0.1015
s =0.003 m

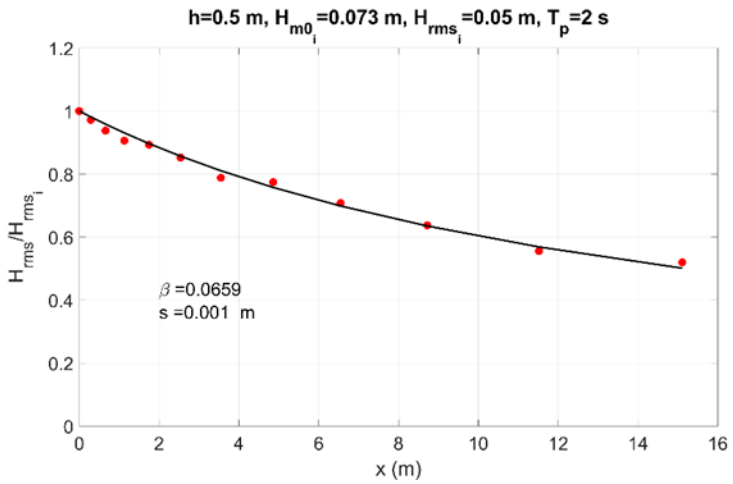
h=0.5 m, H$_{m0_i}$=0.073 m, H$_{rms_i}$=0.05 m, T$_p$=2 s
H$_{rms}$/H$_{rms_i}$
x (m)
β =0.0659
s =0.001 m

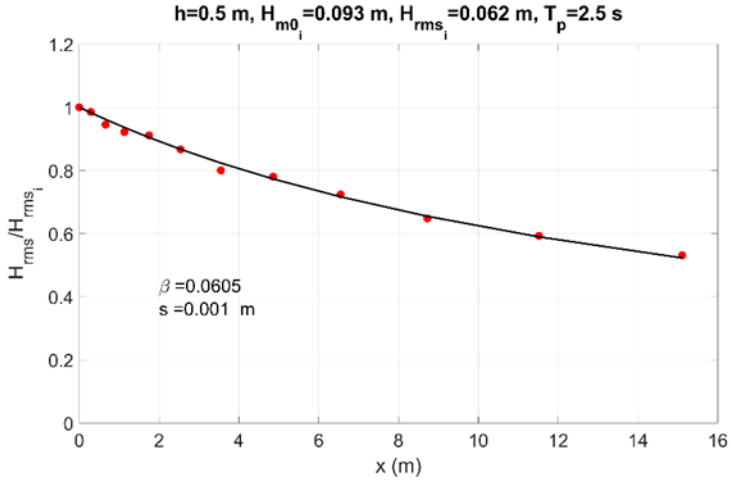
h=0.5 m, H$_{m0_i}$=0.093 m, H$_{rms_i}$=0.062 m, T$_p$=2.5 s
H$_{rms}$/H$_{rms_i}$
x (m)
β =0.0605
s =0.001 m

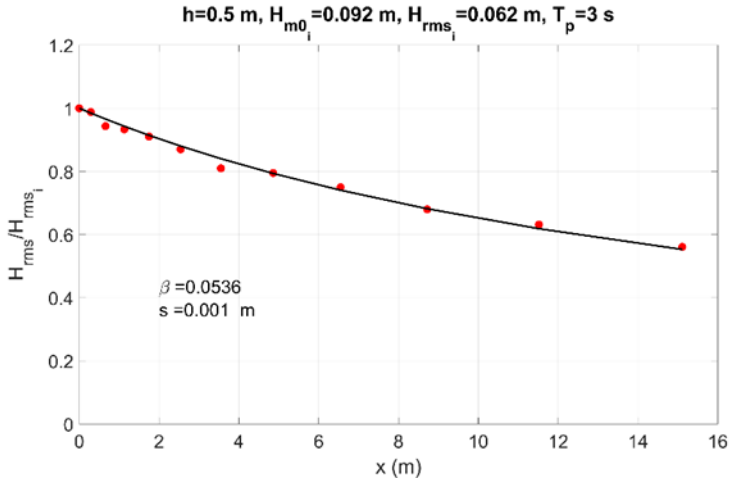
h=0.5 m, H$_{m0_i}$=0.092 m, H$_{rms_i}$=0.062 m, T$_p$=3 s
H$_{rms}$/H$_{rms_i}$
x (m)
β =0.0536
s =0.001 m

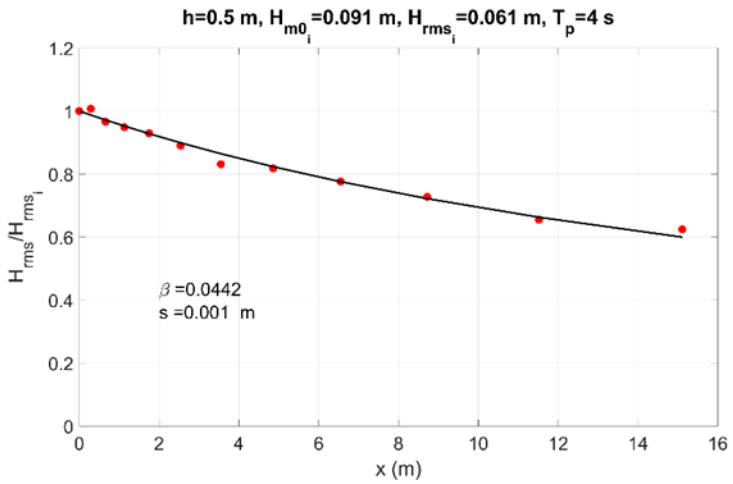
h=0.5 m, H$_{m0_i}$=0.091 m, H$_{rms_i}$=0.061 m, T$_p$=4 s
H$_{rms}$/H$_{rms_i}$
x (m)
β =0.0442
s =0.001 m

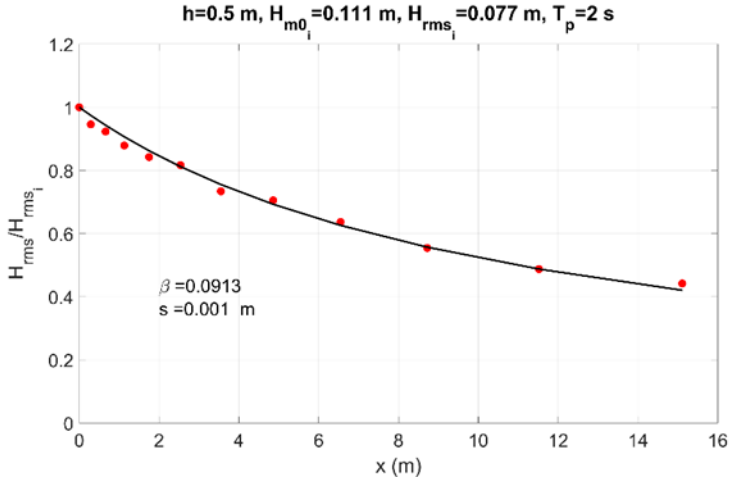
h=0.5 m, H$_{m0_i}$=0.111 m, H$_{rms_i}$=0.077 m, T$_p$=2 s
H$_{rms}$/H$_{rms_i}$
x (m)
β =0.0913
s =0.001 m

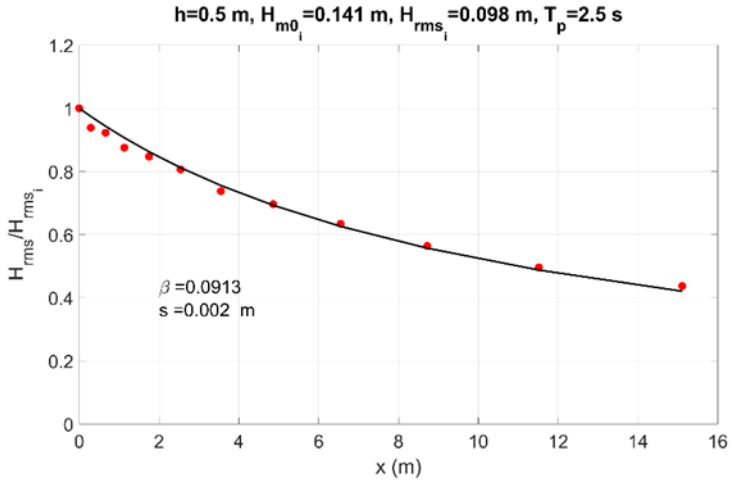
h=0.5 m, H$_{m0_i}$=0.141 m, H$_{rms_i}$=0.098 m, T$_p$=2.5 s
H$_{rms}$/H$_{rms_i}$
x (m)
β =0.0913
s =0.002 m

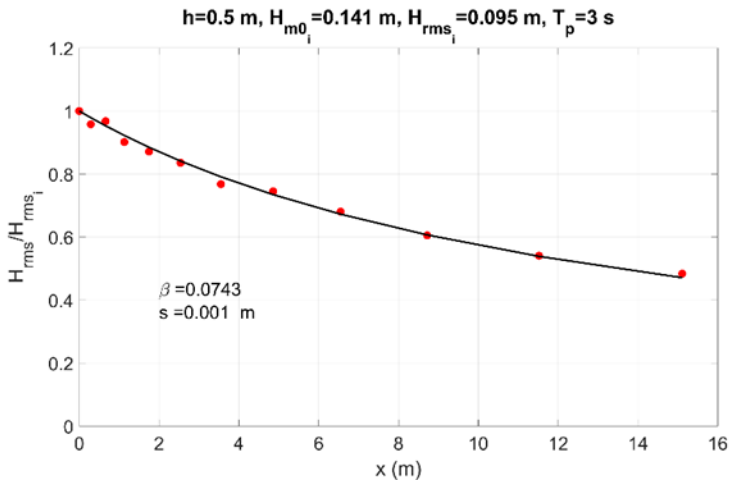
h=0.5 m, H$_{m0_i}$=0.141 m, H$_{rms_i}$=0.095 m, T$_p$=3 s
H$_{rms}$/H$_{rms_i}$
x (m)
β =0.0743
s =0.001 m

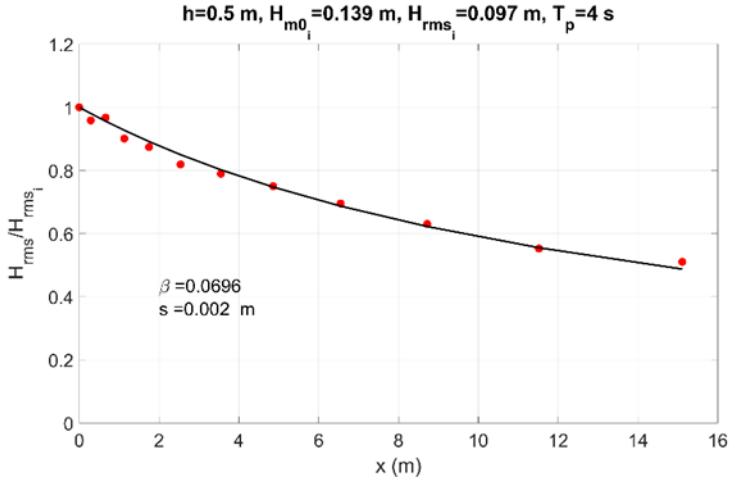
h=0.5 m, H$_{m0_i}$=0.139 m, H$_{rms_i}$=0.097 m, T$_p$=4 s
H$_{rms}$/H$_{rms_i}$
x (m)
β =0.0696
s =0.002 m

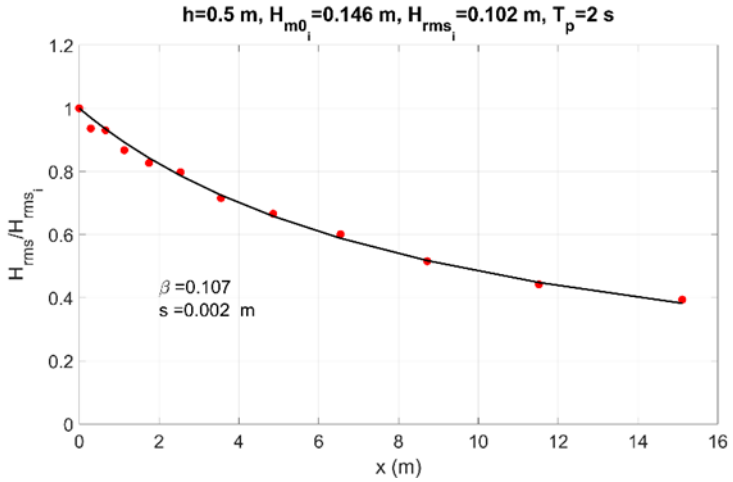
h=0.5 m, H$_{m0_i}$=0.146 m, H$_{rms_i}$=0.102 m, T$_p$=2 s
H$_{rms}$/H$_{rms_i}$
x (m)
β =0.107
s =0.002 m

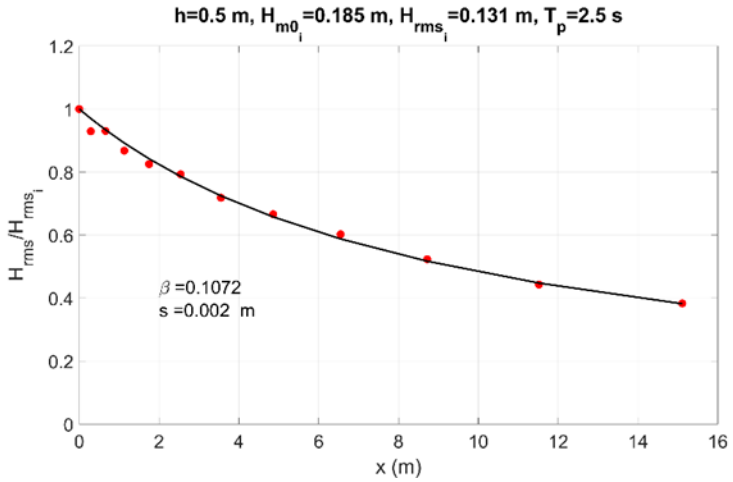
h=0.5 m, H$_{m0_i}$=0.185 m, H$_{rms_i}$=0.131 m, T$_p$=2.5 s
H$_{rms}$/H$_{rms_i}$
x (m)
β =0.1072
s =0.002 m

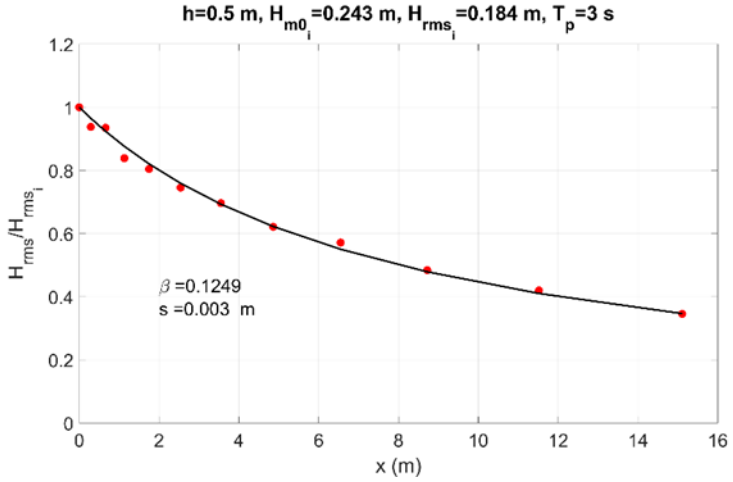
h=0.5 m, H$_{m0_i}$=0.243 m, H$_{rms_i}$=0.184 m, T$_p$=3 s
H$_{rms}$/H$_{rms_i}$
x (m)
β =0.1249
s =0.003 m

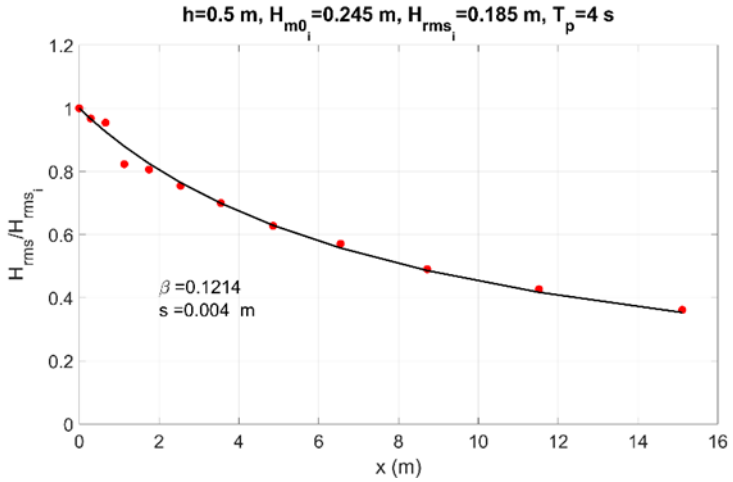
h=0.5 m, H$_{m0_i}$=0.245 m, H$_{rms_i}$=0.185 m, T$_p$=4 s
H$_{rms}$/H$_{rms_i}$
x (m)
β =0.1214
s =0.004 m

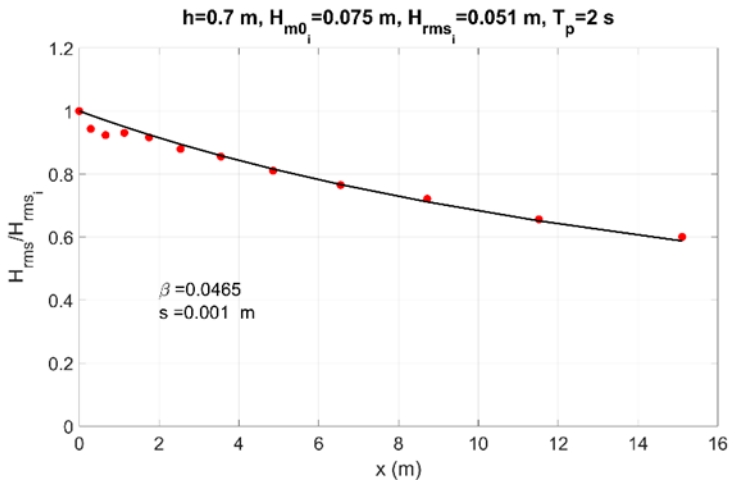
h=0.7 m, H$_{m0_i}$=0.075 m, H$_{rms_i}$=0.051 m, T$_p$=2 s
H$_{rms}$/H$_{rms_i}$
x (m)
β =0.0465
s =0.001 m

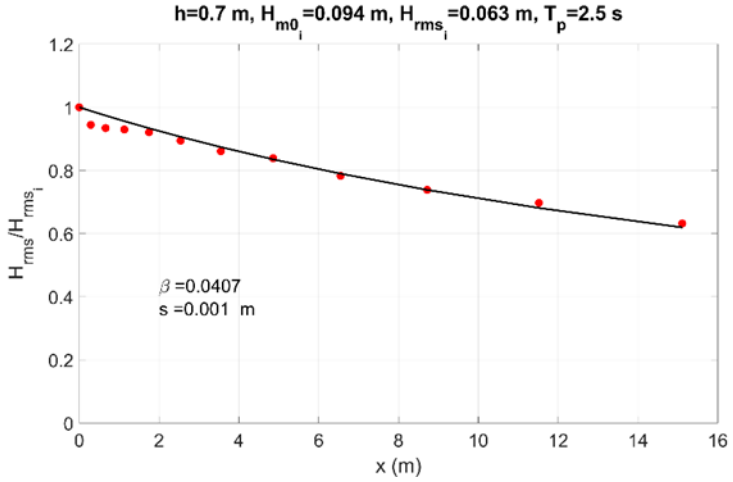
h=0.7 m, H$_{m0_i}$=0.094 m, H$_{rms_i}$=0.063 m, T$_p$=2.5 s
H$_{rms}$/H$_{rms_i}$
x (m)
β =0.0407
s =0.001 m

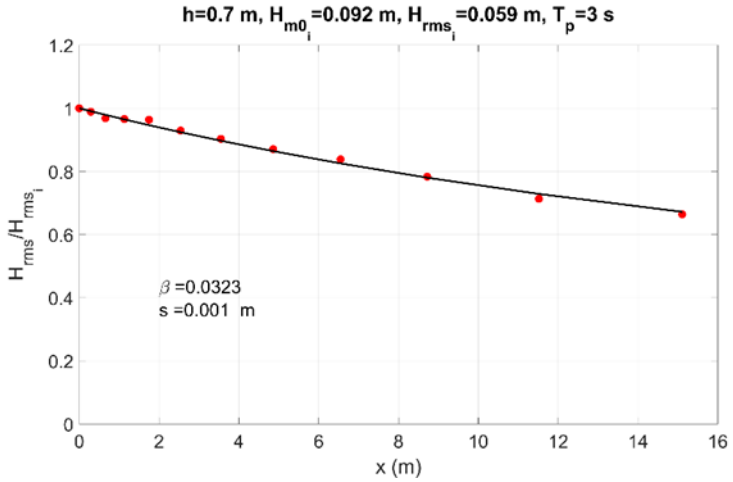
h=0.7 m, H$_{m0_i}$=0.092 m, H$_{rms_i}$=0.059 m, T$_p$=3 s
H$_{rms}$/H$_{rms_i}$
x (m)
β =0.0323
s =0.001 m

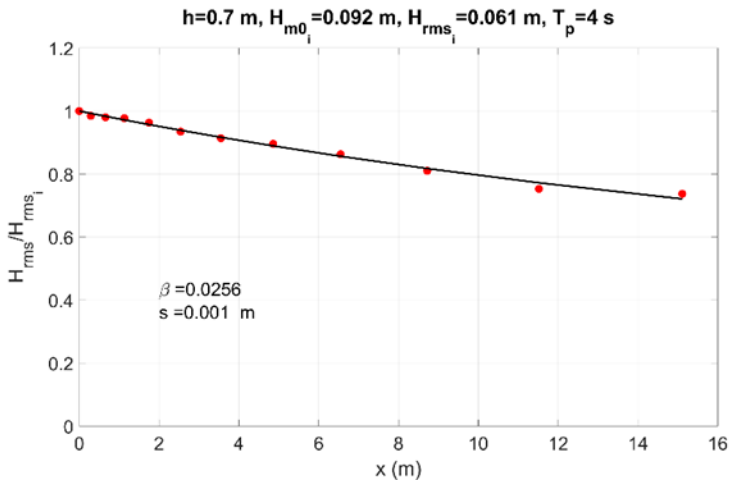
h=0.7 m, H$_{m0_i}$=0.092 m, H$_{rms_i}$=0.061 m, T$_p$=4 s
H$_{rms}$/H$_{rms_i}$
x (m)
β =0.0256
s =0.001 m

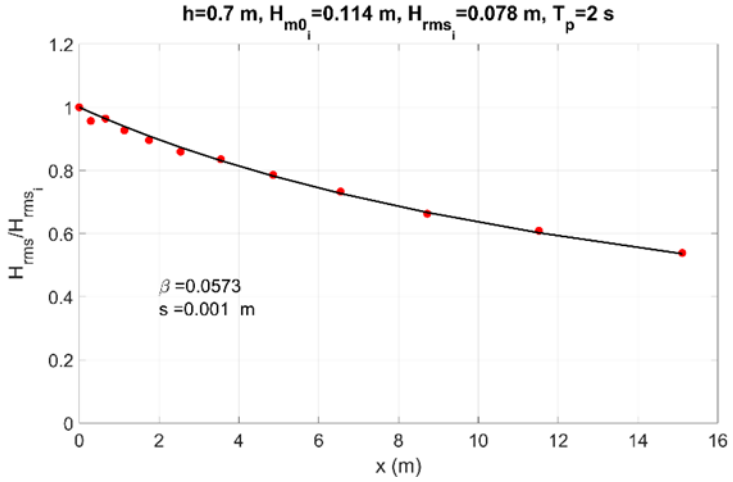
h=0.7 m, H$_{m0_i}$=0.114 m, H$_{rms_i}$=0.078 m, T$_p$=2 s
H$_{rms}$/H$_{rms_i}$
x (m)
β =0.0573
s =0.001 m

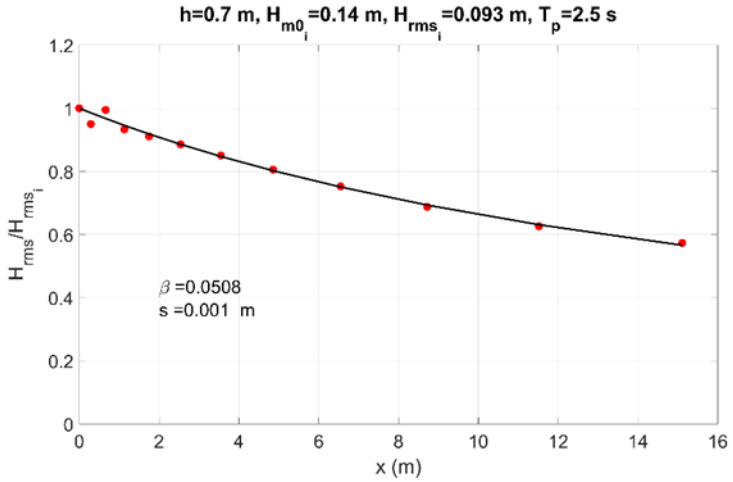
h=0.7 m, H$_{m0_i}$=0.14 m, H$_{rms_i}$=0.093 m, T$_p$=2.5 s
H$_{rms}$/H$_{rms_i}$
x (m)
β =0.0508
s =0.001 m

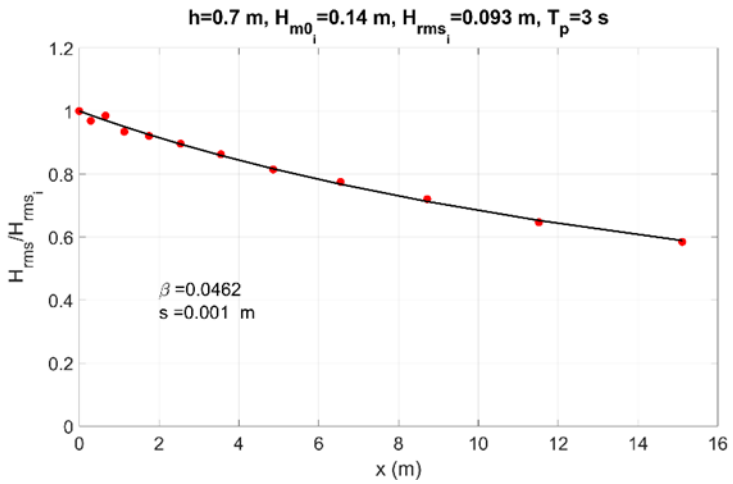
h=0.7 m, H$_{m0_i}$=0.14 m, H$_{rms_i}$=0.093 m, T$_p$=3 s
H$_{rms}$/H$_{rms_i}$
x (m)
β =0.0462
s =0.001 m

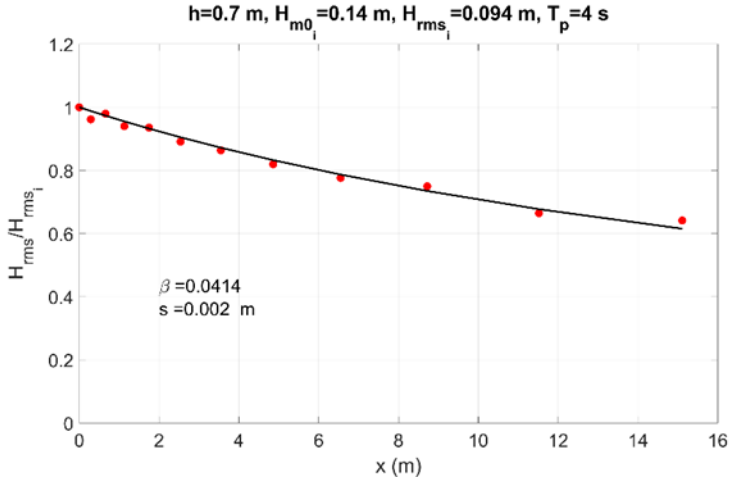
h=0.7 m, H$_{m0_i}$=0.14 m, H$_{rms_i}$=0.094 m, T$_p$=4 s
H$_{rms}$/H$_{rms_i}$
x (m)
β =0.0414
s =0.002 m

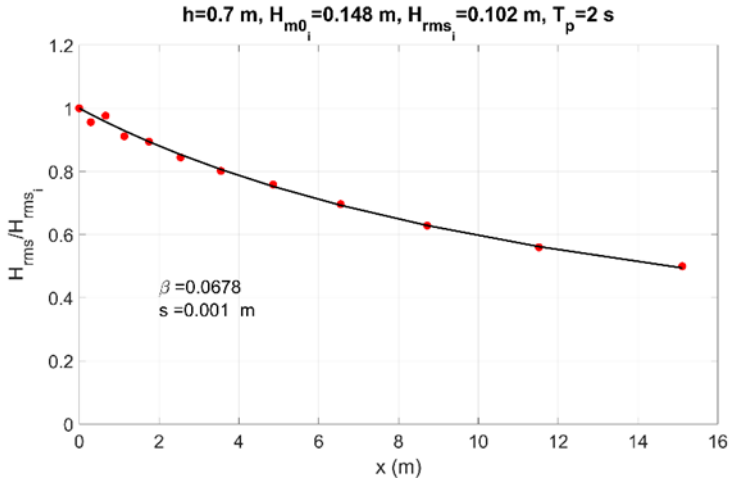
h=0.7 m, H$_{m0_i}$=0.148 m, H$_{rms_i}$=0.102 m, T$_p$=2 s
H$_{rms}$/H$_{rms_i}$
x (m)
β =0.0678
s =0.001 m

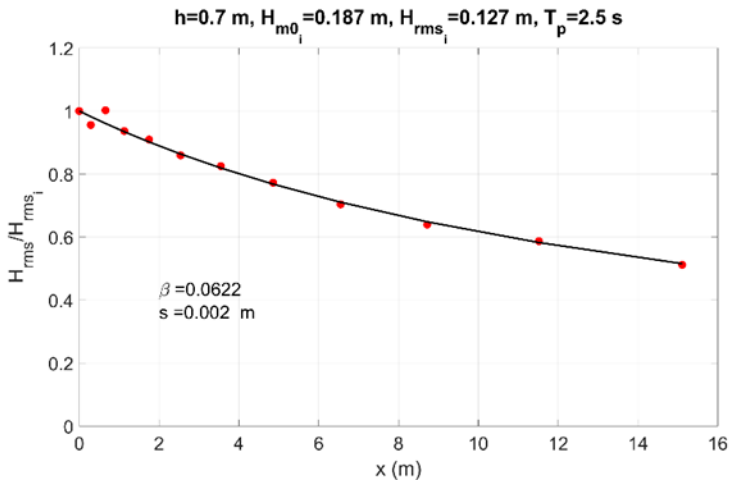
h=0.7 m, H$_{m0_i}$=0.187 m, H$_{rms_i}$=0.127 m, T$_p$=2.5 s
H$_{rms}$/H$_{rms_i}$
x (m)
β =0.0622
s =0.002 m

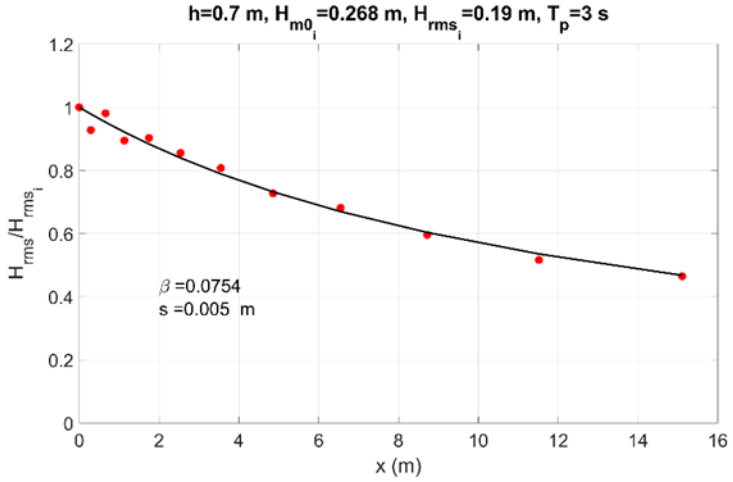
h=0.7 m, H$_{m0_i}$=0.268 m, H$_{rms_i}$=0.19 m, T$_p$=3 s
H$_{rms}$/H$_{rms_i}$
x (m)
β =0.0754
s =0.005 m

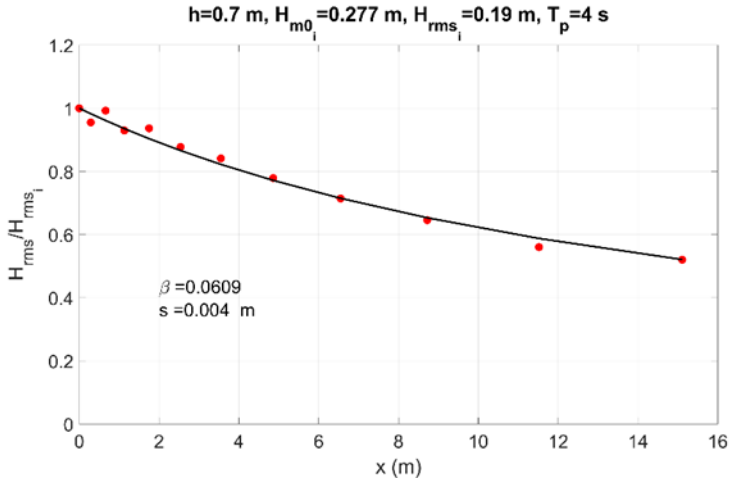
h=0.7 m, H$_{m0_i}$=0.277 m, H$_{rms_i}$=0.19 m, T$_p$=4 s
H$_{rms}$/H$_{rms_i}$
x (m)
β =0.0609
s =0.004 m

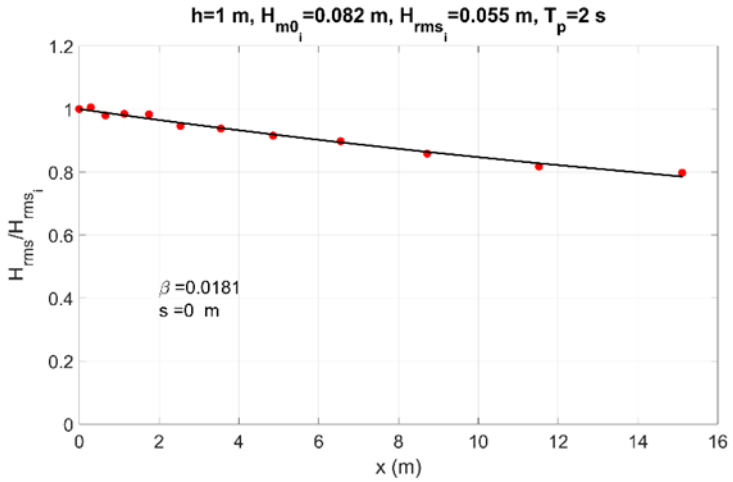
h=1 m, H$_{m0_i}$=0.082 m, H$_{rms_i}$=0.055 m, T$_p$=2 s
H$_{rms}$/H$_{rms_i}$
x (m)
β =0.0181
s =0 m

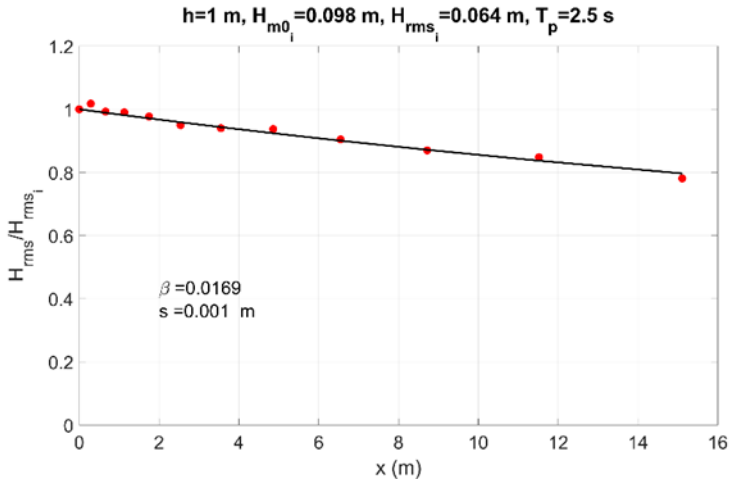
h=1 m, H$_{m0_i}$=0.098 m, H$_{rms_i}$=0.064 m, T$_p$=2.5 s
H$_{rms}$/H$_{rms_i}$
x (m)
β =0.0169
s =0.001 m

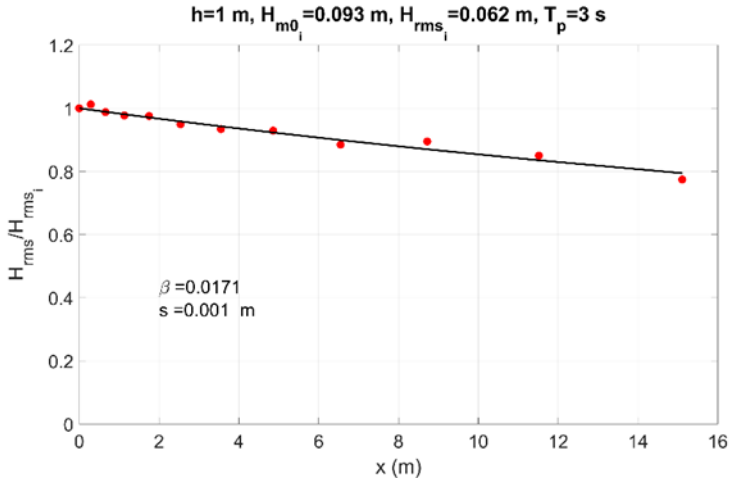
h=1 m, H$_{m0_i}$=0.093 m, H$_{rms_i}$=0.062 m, T$_p$=3 s
H$_{rms}$/H$_{rms_i}$
x (m)
β =0.0171
s =0.001 m

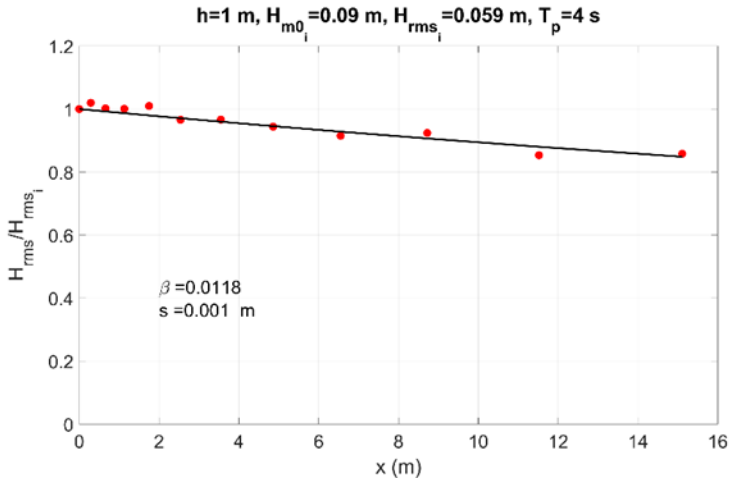
h=1 m, H$_{m0_i}$=0.09 m, H$_{rms_i}$=0.059 m, T$_p$=4 s
H$_{rms}$/H$_{rms_i}$
x (m)
β =0.0118
s =0.001 m

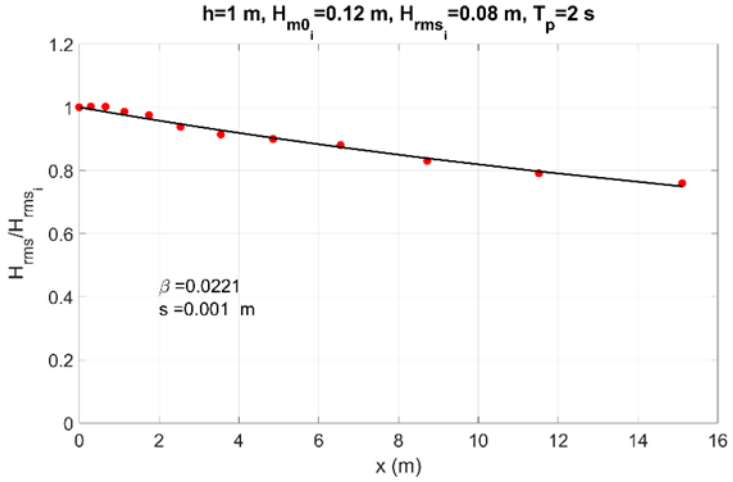
h=1 m, H$_{m0_i}$=0.12 m, H$_{rms_i}$=0.08 m, T$_p$=2 s
H$_{rms}$/H$_{rms_i}$
x (m)
β =0.0221
s =0.001 m

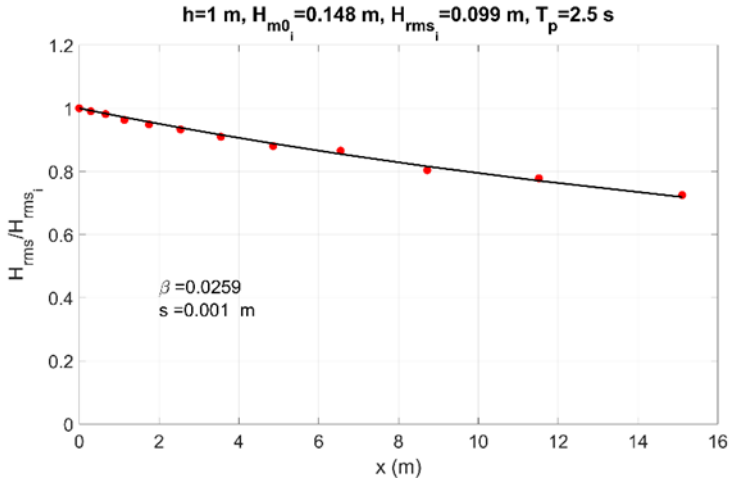
h=1 m, H$_{m0_i}$=0.148 m, H$_{rms_i}$=0.099 m, T$_p$=2.5 s
H$_{rms}$/H$_{rms_i}$
x (m)
β =0.0259
s =0.001 m

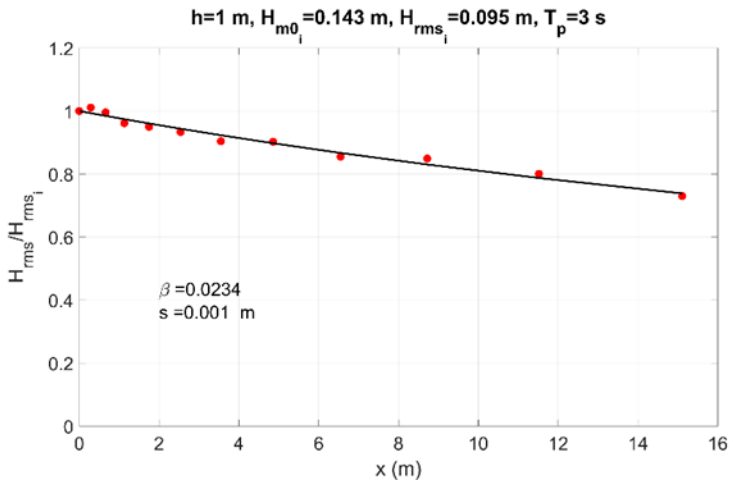
h=1 m, H$_{m0_i}$=0.143 m, H$_{rms_i}$=0.095 m, T$_p$=3 s
H$_{rms}$/H$_{rms_i}$
x (m)
β =0.0234
s =0.001 m

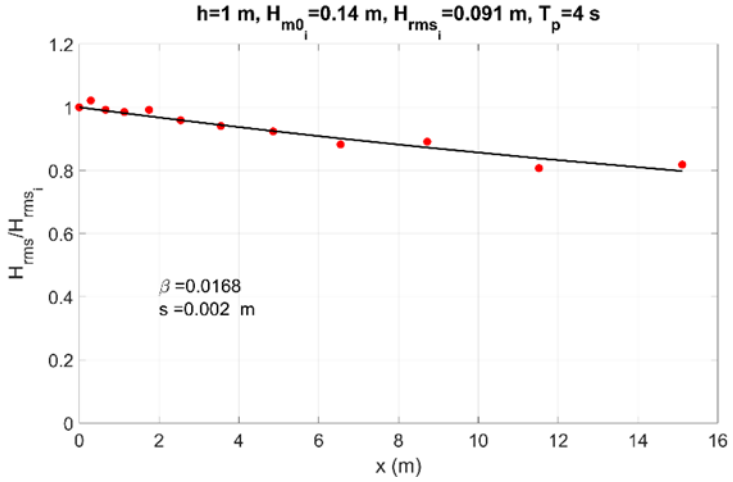
h=1 m, H$_{m0_i}$=0.14 m, H$_{rms_i}$=0.091 m, T$_p$=4 s
H$_{rms}$/H$_{rms_i}$
x (m)
β =0.0168
s =0.002 m

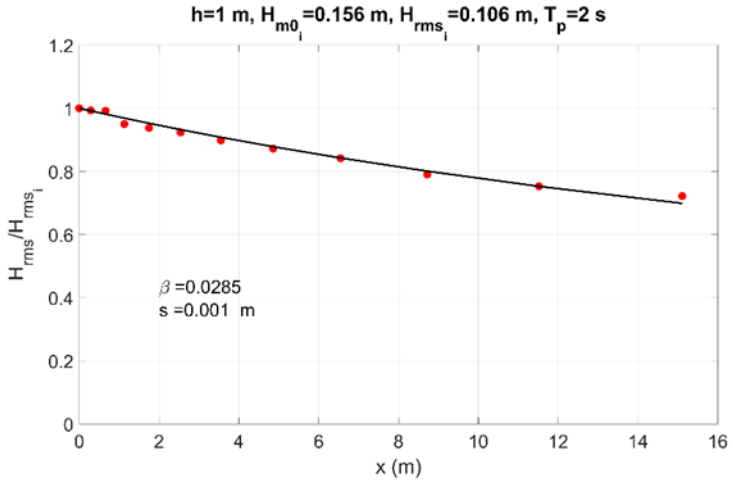
h=1 m, H$_{m0_i}$=0.156 m, H$_{rms_i}$=0.106 m, T$_p$=2 s
H$_{rms}$/H$_{rms_i}$
x (m)
β =0.0285
s =0.001 m

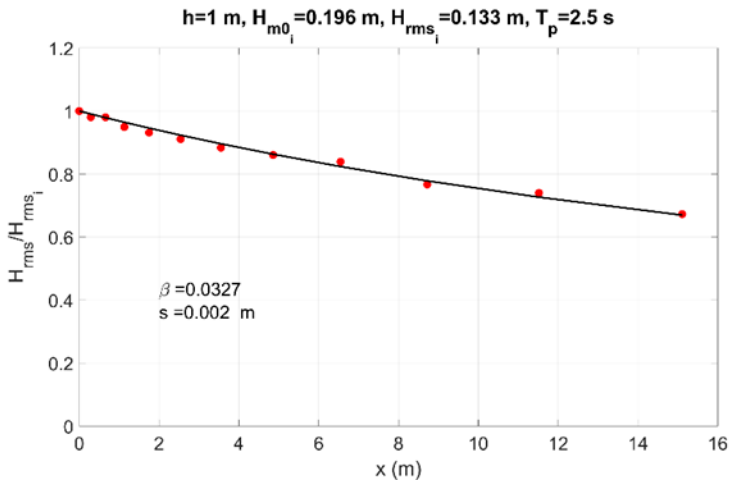
h=1 m, H$_{m0_i}$=0.196 m, H$_{rms_i}$=0.133 m, T$_p$=2.5 s
H$_{rms}$/H$_{rms_i}$
x (m)
β =0.0327
s =0.002 m

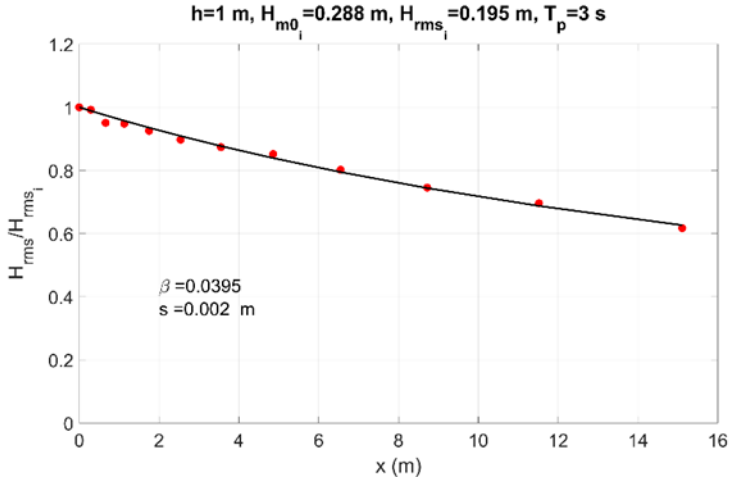
h=1 m, H$_{m0_i}$=0.288 m, H$_{rms_i}$=0.195 m, T$_p$=3 s
H$_{rms}$/H$_{rms_i}$
x (m)
β =0.0395
s =0.002 m

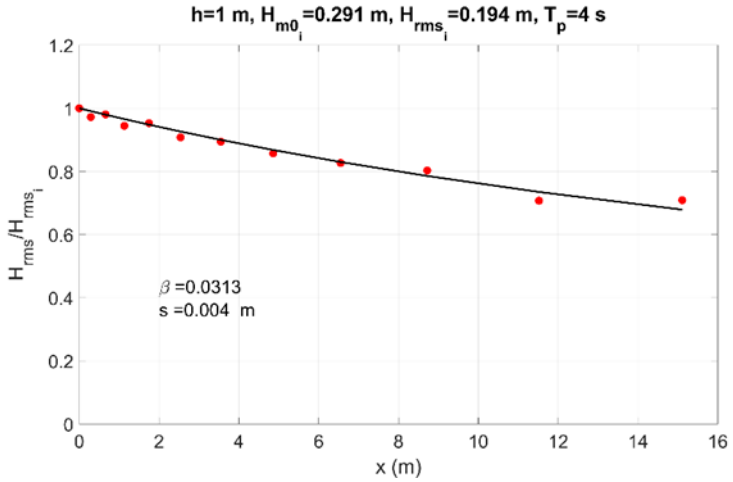
h=1 m, H$_{m0_i}$=0.291 m, H$_{rms_i}$=0.194 m, T$_p$=4 s
H$_{rms}$/H$_{rms_i}$
x (m)
β =0.0313
s =0.004 m

C.2 Regular waves

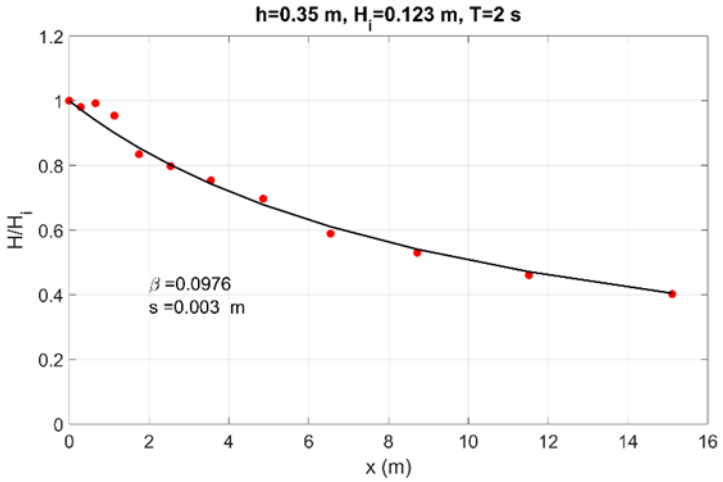

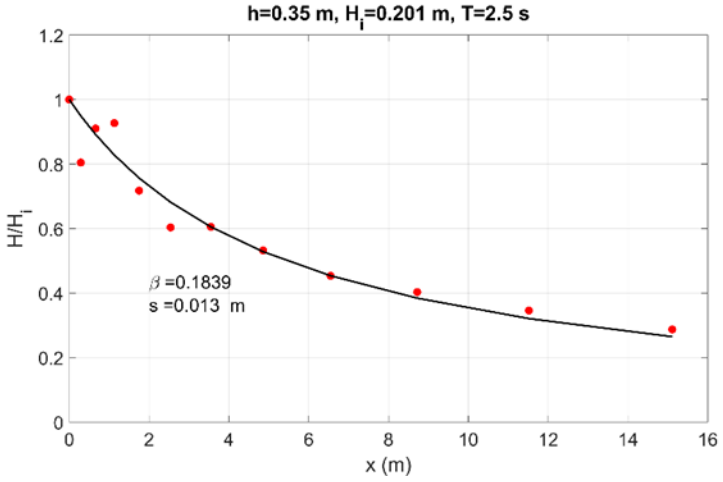

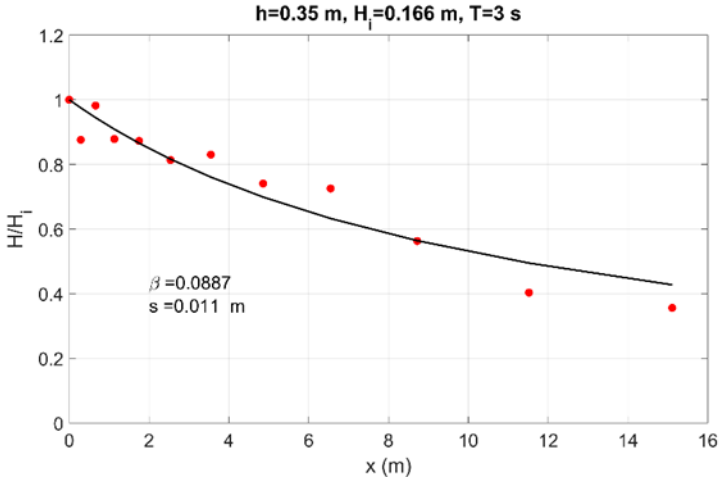

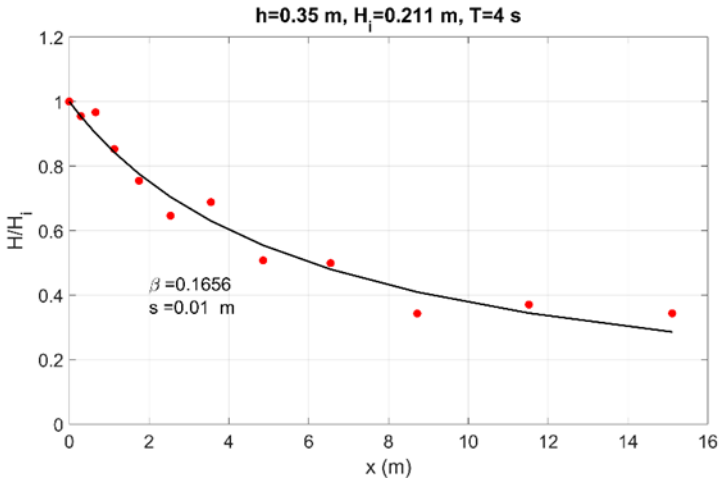
h=0.35 m, H$_i$=0.211 m, T=4 s
H/H$_i$
x (m)
β =0.1656
s =0.01 m

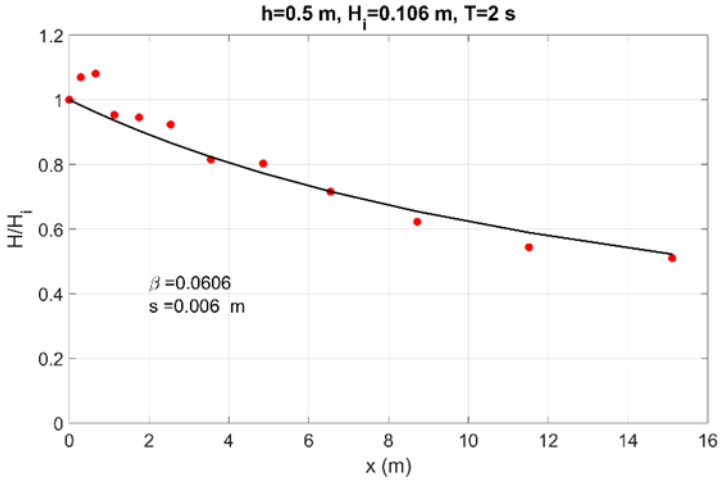
h=0.5 m, H$_i$=0.106 m, T=2 s
H/H$_i$
x (m)
β =0.0606
s =0.006 m

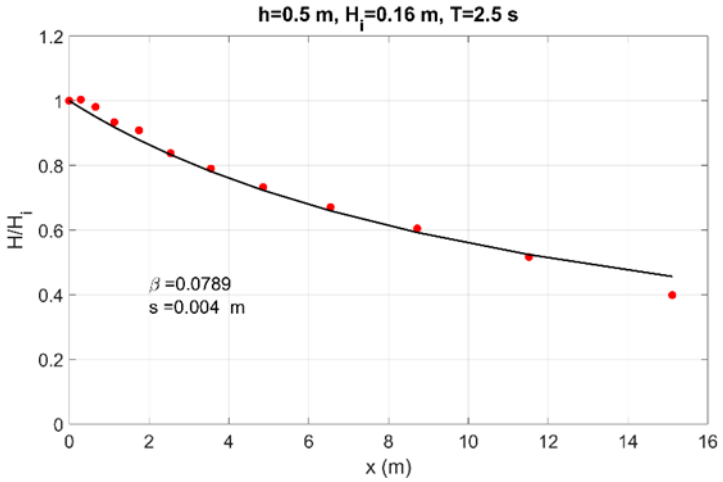
h=0.5 m, H$_i$=0.16 m, T=2.5 s
H/H$_i$
x (m)
β =0.0789
s =0.004 m

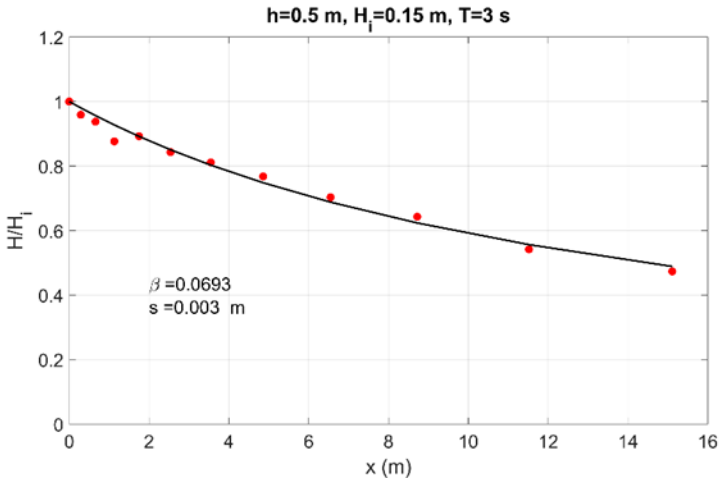
h=0.5 m, H$_i$=0.15 m, T=3 s
H/H$_i$
x (m)
β =0.0693
s =0.003 m

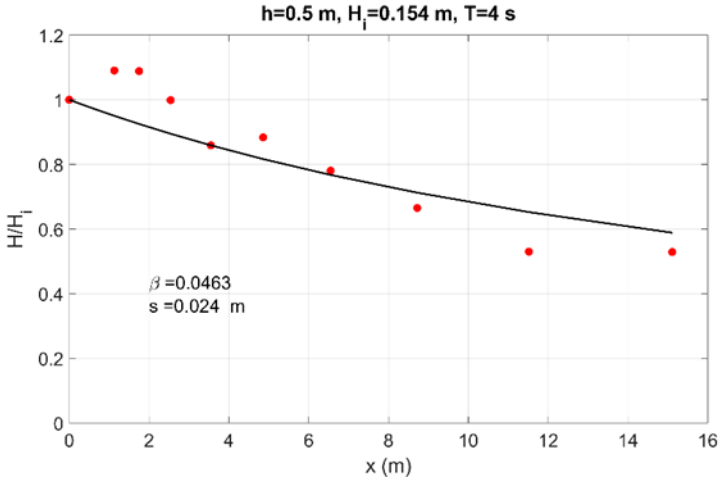
h=0.5 m, H$_i$=0.154 m, T=4 s
H/H$_i$
x (m)
β =0.0463
s =0.024 m

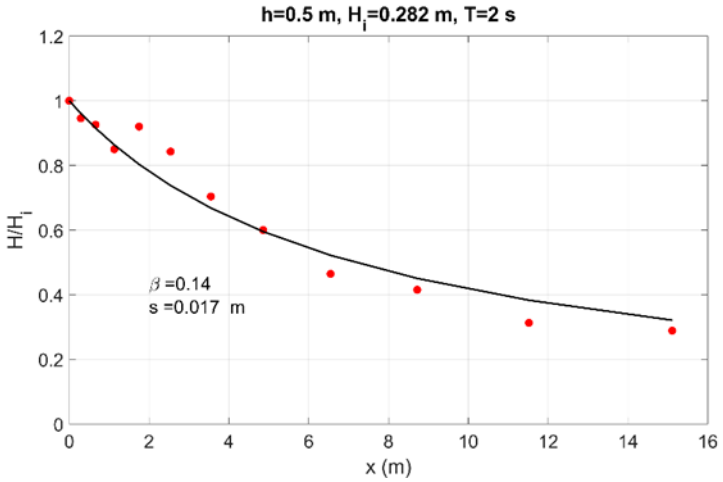
h=0.5 m, H$_i$=0.282 m, T=2 s
H/H$_i$
x (m)
β =0.14
s =0.017 m

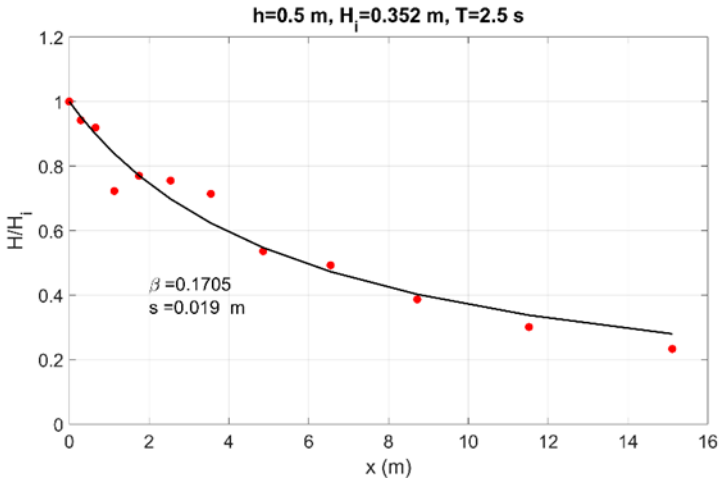
h=0.5 m, H$_i$=0.352 m, T=2.5 s
H/H$_i$
x (m)
β =0.1705
s =0.019 m

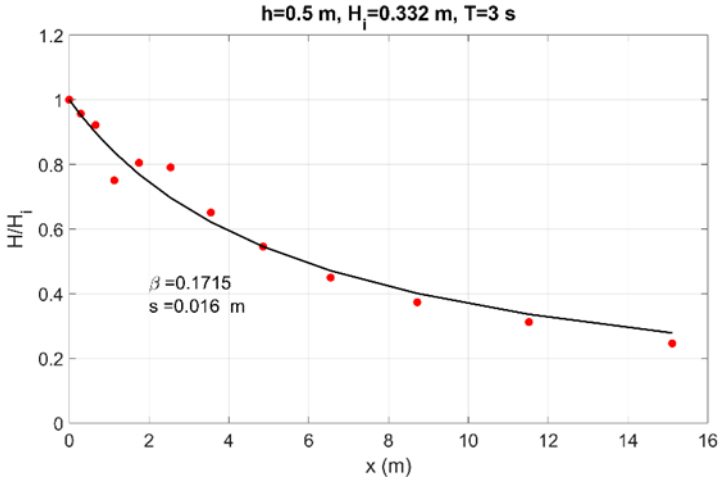
h=0.5 m, H$_i$=0.332 m, T=3 s
H/H$_i$
x (m)
β =0.1715
s =0.016 m

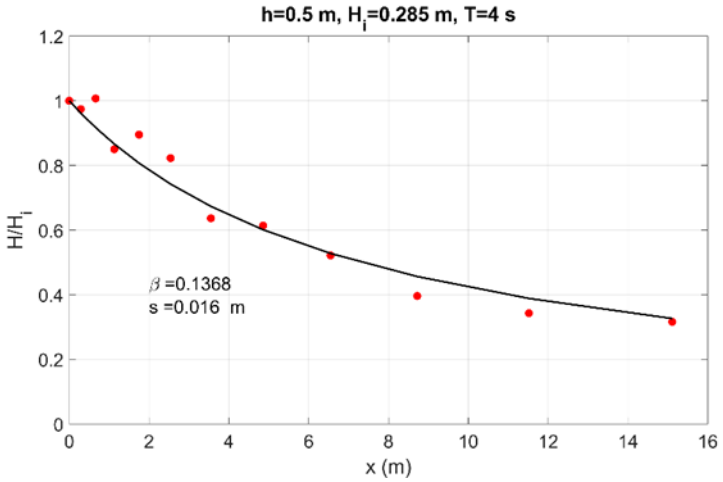
h=0.5 m, H$_i$=0.285 m, T=4 s
H/H$_i$
x (m)
β =0.1368
s =0.016 m

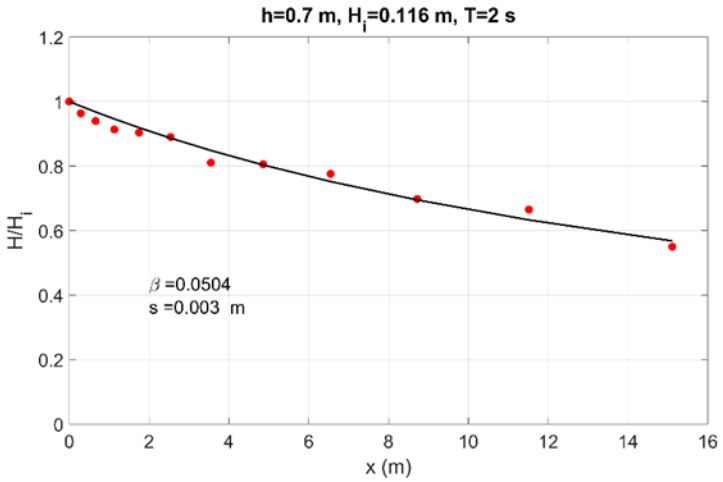
h=0.7 m, H$_i$=0.116 m, T=2 s
H/H$_i$
x (m)
β =0.0504
s =0.003 m

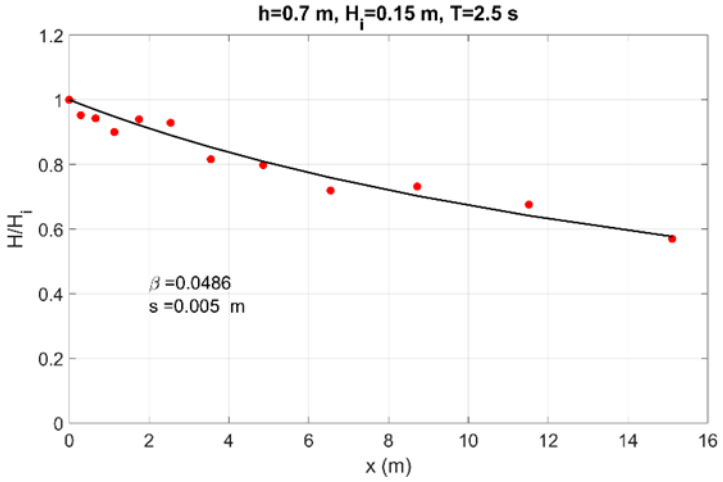
h=0.7 m, H$_i$=0.15 m, T=2.5 s
H/H$_i$
x (m)
β =0.0486
s =0.005 m

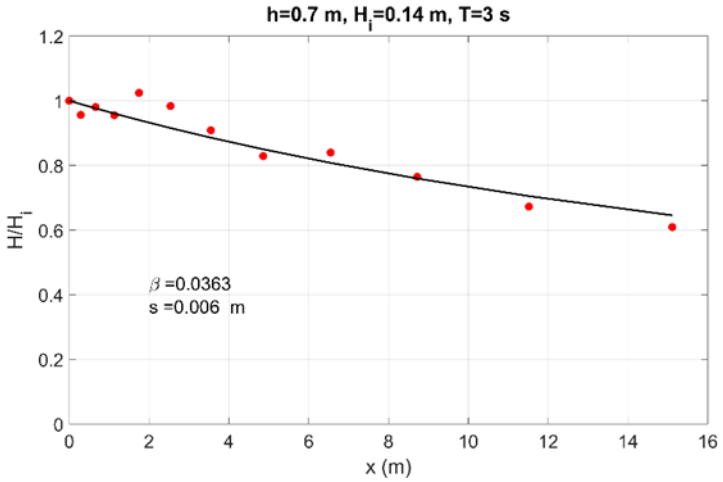
h=0.7 m, H$_i$=0.14 m, T=3 s
H/H$_i$
x (m)
β =0.0363
s =0.006 m

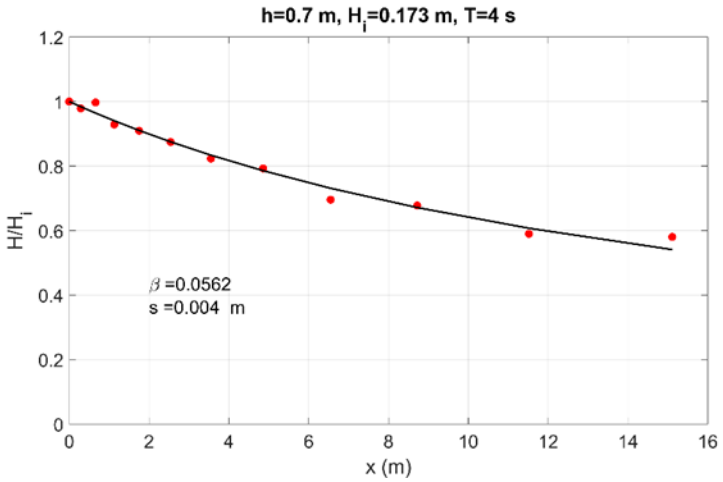
h=0.7 m, H$_i$=0.173 m, T=4 s
H/H$_i$
x (m)
β =0.0562
s =0.004 m

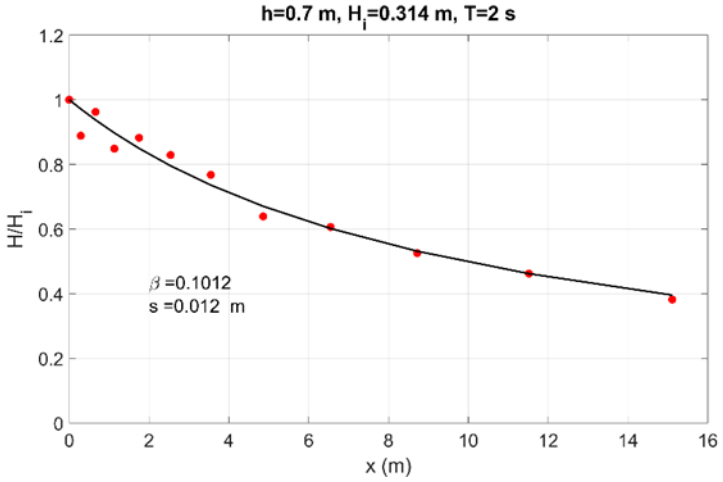
h=0.7 m, H$_i$=0.314 m, T=2 s
H/H$_i$
x (m)
β =0.1012
s =0.012 m

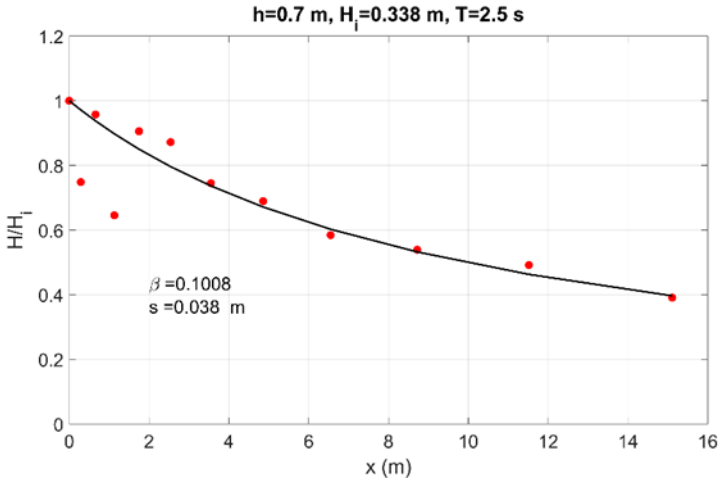
h=0.7 m, H$_i$=0.338 m, T=2.5 s
H/H$_i$
x (m)
β =0.1008
s =0.038 m

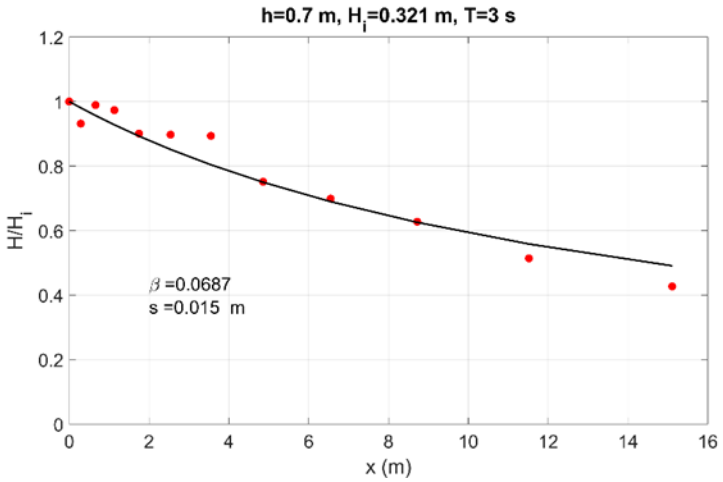
h=0.7 m, H$_i$=0.321 m, T=3 s
H/H$_i$
x (m)
β =0.0687
s =0.015 m

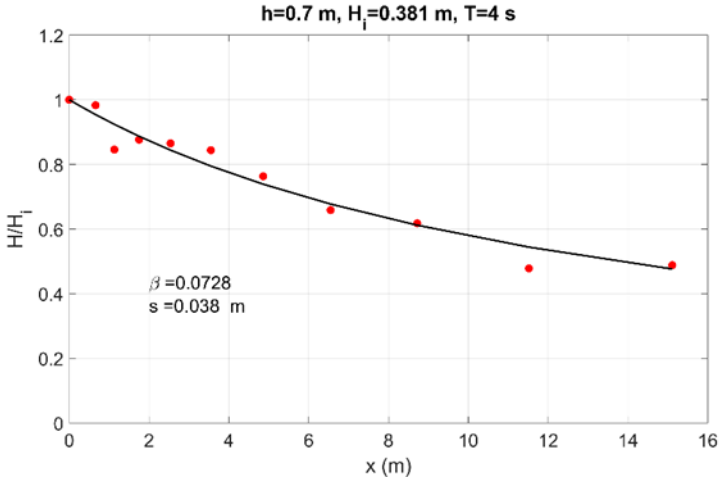
h=0.7 m, H$_i$=0.381 m, T=4 s
H/H$_i$
x (m)
β =0.0728
s =0.038 m

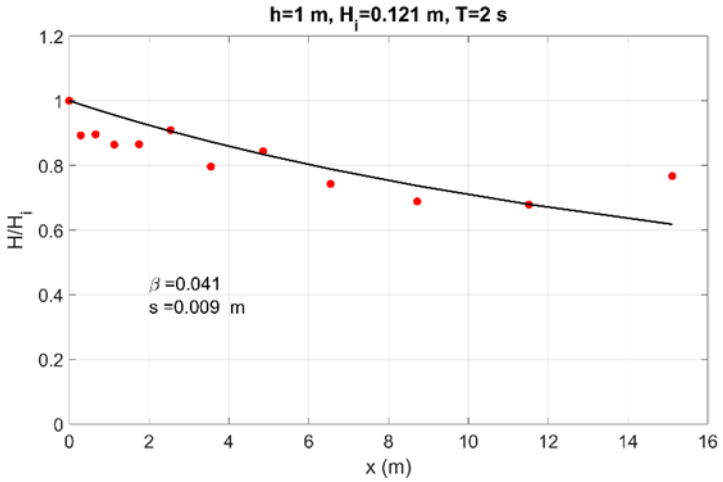
h=1 m, H$_i$=0.121 m, T=2 s
H/H$_i$
x (m)
β =0.041
s =0.009 m

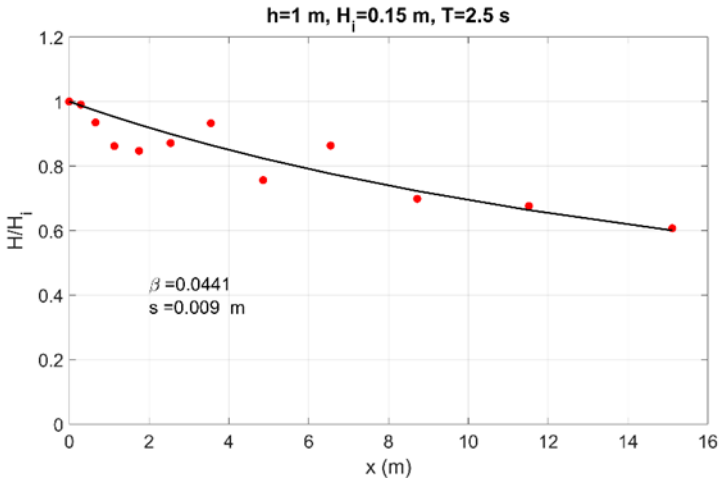
h=1 m, H$_i$=0.15 m, T=2.5 s
H/H$_i$
x (m)
β =0.0441
s =0.009 m

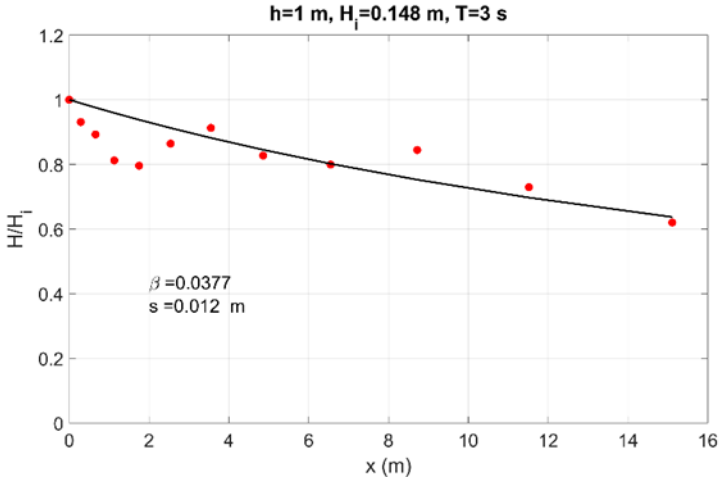
h=1 m, H$_i$=0.148 m, T=3 s
H/H$_i$
x (m)
β =0.0377
s =0.012 m

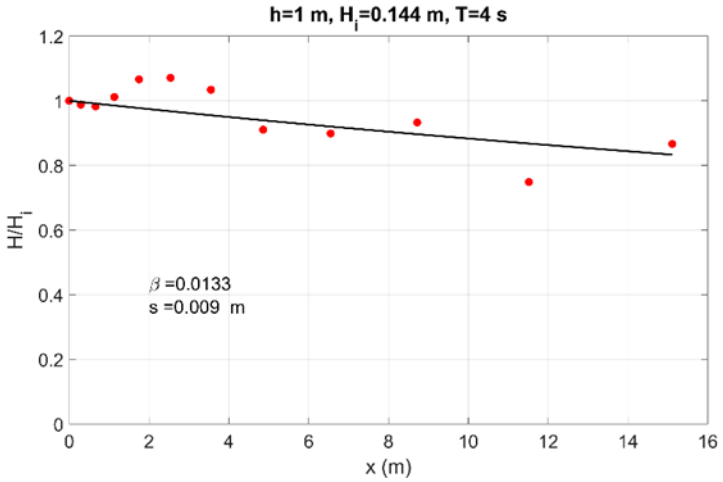
h=1 m, H$_i$=0.144 m, T=4 s
H/H$_i$
x (m)
β =0.0133
s =0.009 m

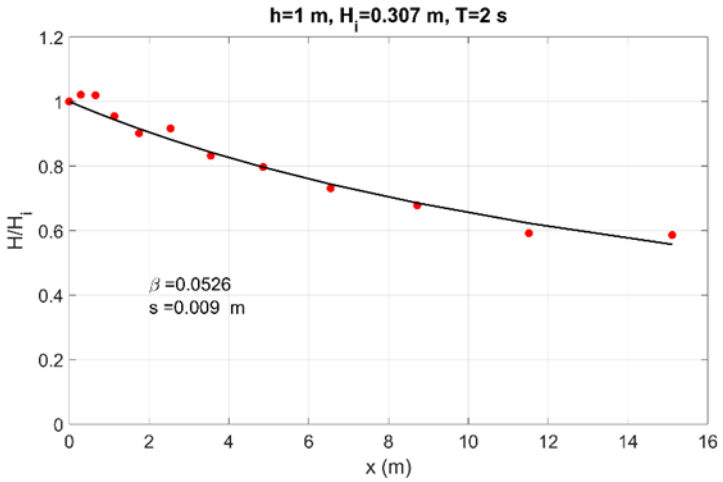
h=1 m, H$_i$=0.307 m, T=2 s
H/H$_i$
x (m)
β =0.0526
s =0.009 m

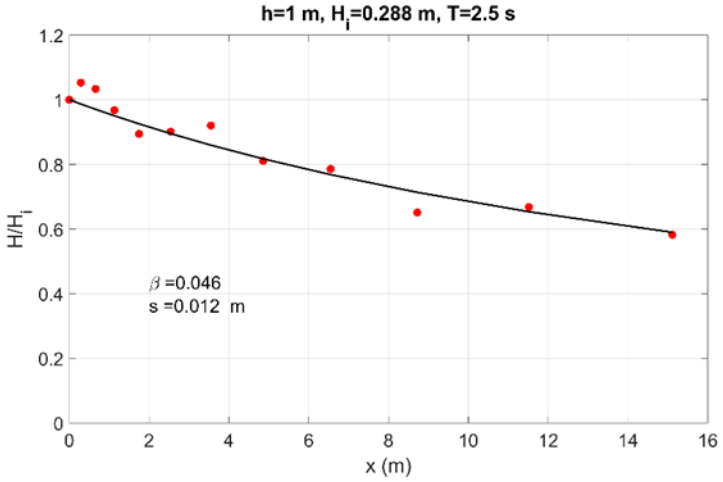
h=1 m, H$_i$=0.288 m, T=2.5 s
H/H$_i$
x (m)
β =0.046
s =0.012 m

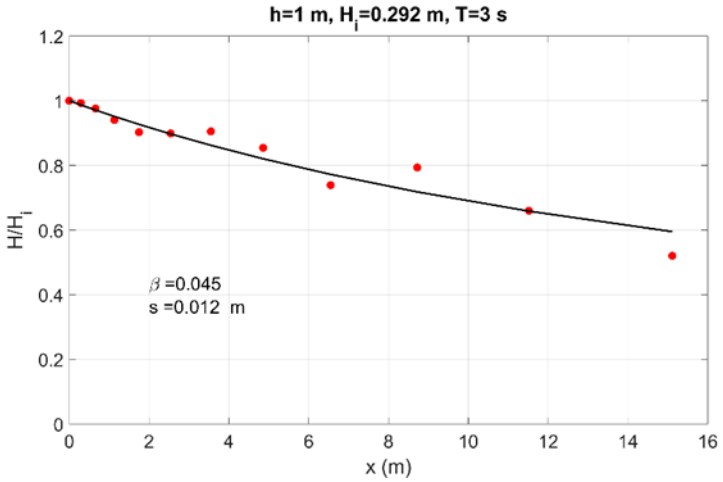
h=1 m, H$_i$=0.292 m, T=3 s
H/H$_i$
x (m)
β =0.045
s =0.012 m

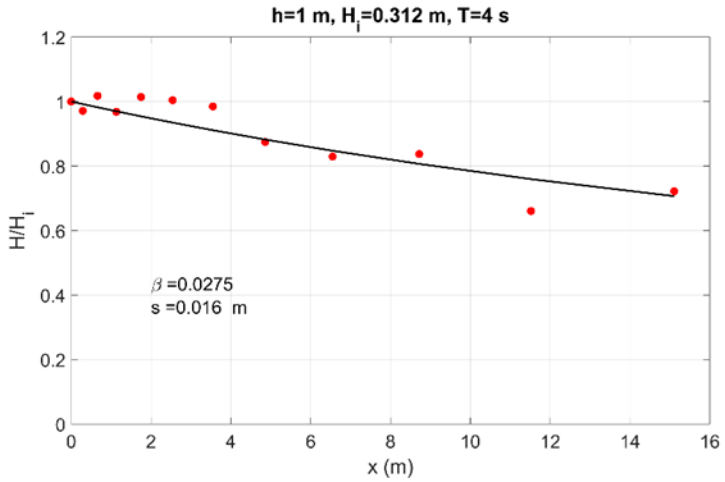
h=1 m, H$_i$=0.312 m, T=4 s
H/H$_i$
x (m)
β =0.0275
s =0.016 m
0
0.2
0.4
0.6
0.8
1
1.2
0
2
4
6
8
10
12
14
16

Appendix D: Drag Coefficients

Appendix D: Drag Coefficients shows the normalized wave height evolution with fitted drag coefficients (C_D) and standard error (s) for all tested wave conditions, both irregular (D.1) and regular (D.2). The label at the top of each figure corresponds with a wave condition listed in Table 1.

D.1 Irregular waves

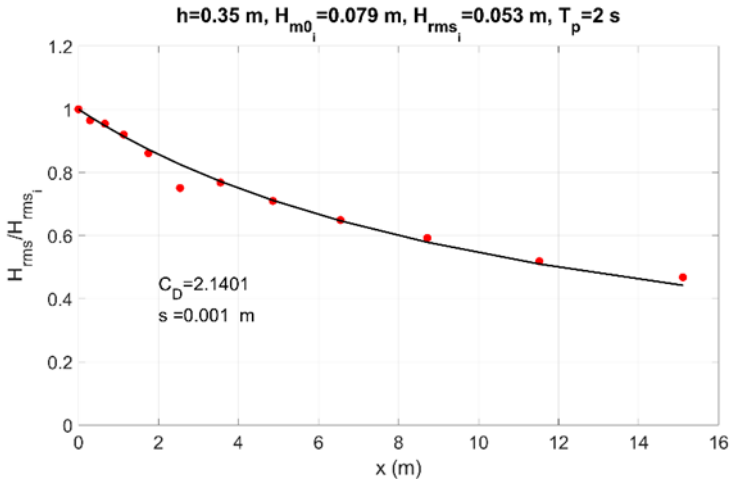

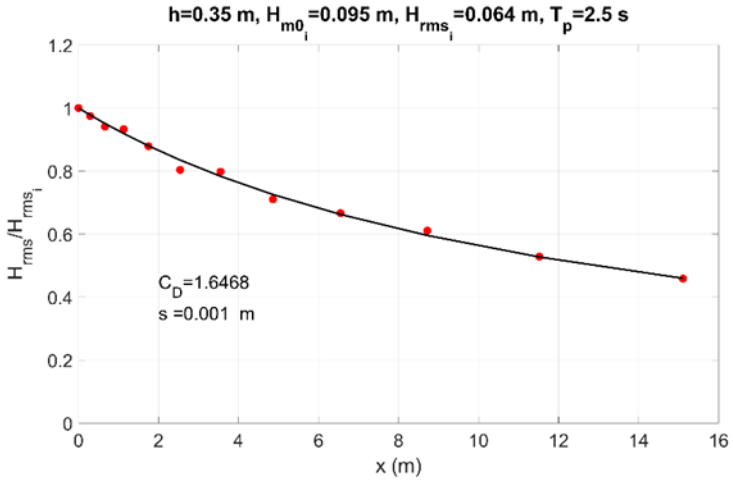

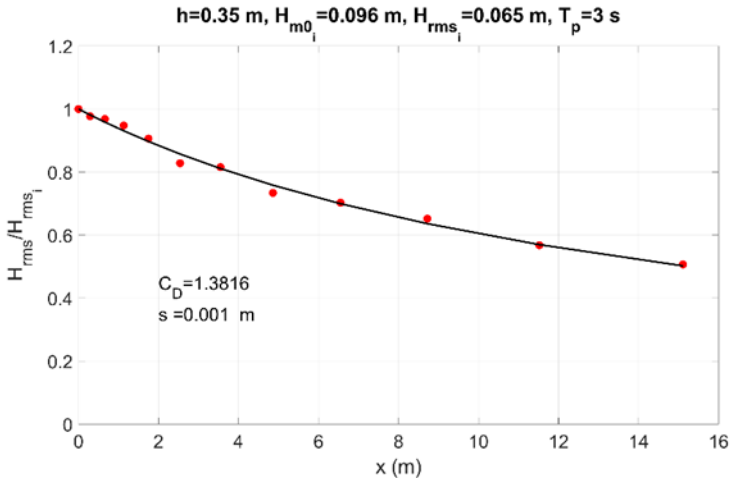
h=0.35 m, H$_{m0_i}$=0.096 m, H$_{rms_i}$=0.065 m, T$_p$=3 s
H$_{rms}$/H$_{rms_i}$
C$_D$=1.3816
s =0.001 m
x (m)

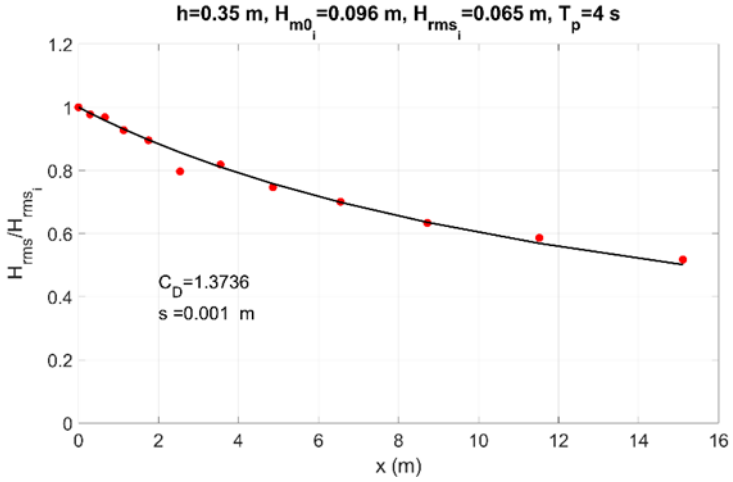
h=0.35 m, H$_{m0_i}$=0.096 m, H$_{rms_i}$=0.065 m, T$_p$=4 s
H$_{rms}$/H$_{rms_i}$
C$_D$=1.3736
s =0.001 m
x (m)

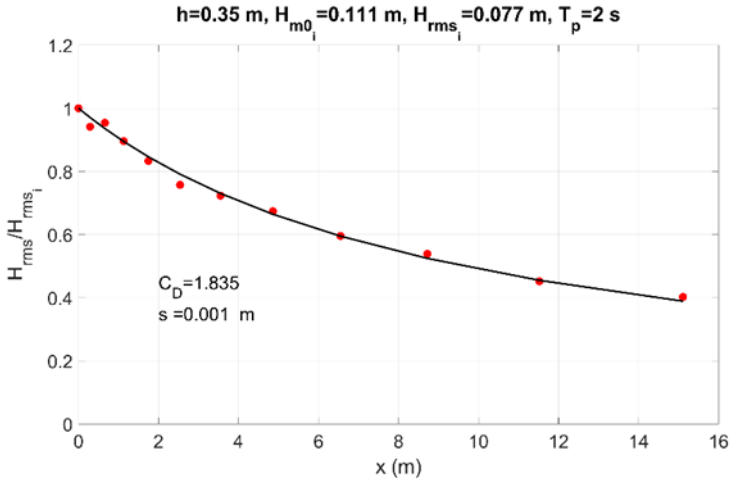
h=0.35 m, H$_{m0_i}$=0.111 m, H$_{rms_i}$=0.077 m, T$_p$=2 s
H$_{rms}$/H$_{rms_i}$
C$_D$=1.835
s =0.001 m
x (m)

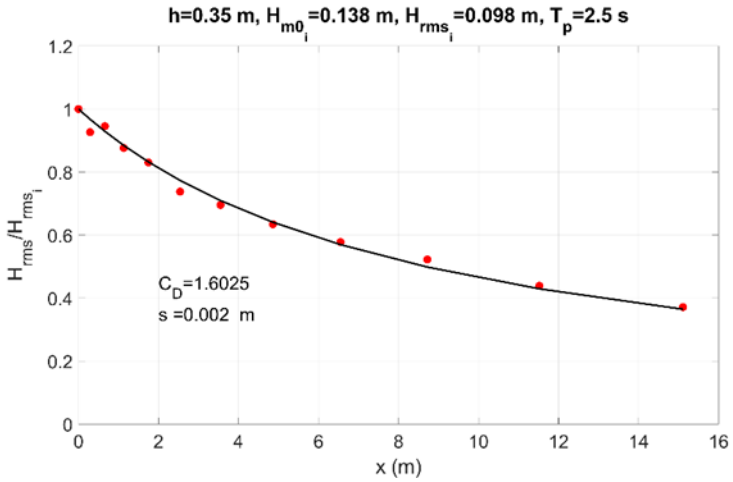
h=0.35 m, H$_{m0_i}$=0.138 m, H$_{rms_i}$=0.098 m, T$_p$=2.5 s
H$_{rms}$/H$_{rms_i}$
C$_D$=1.6025
s =0.002 m
x (m)

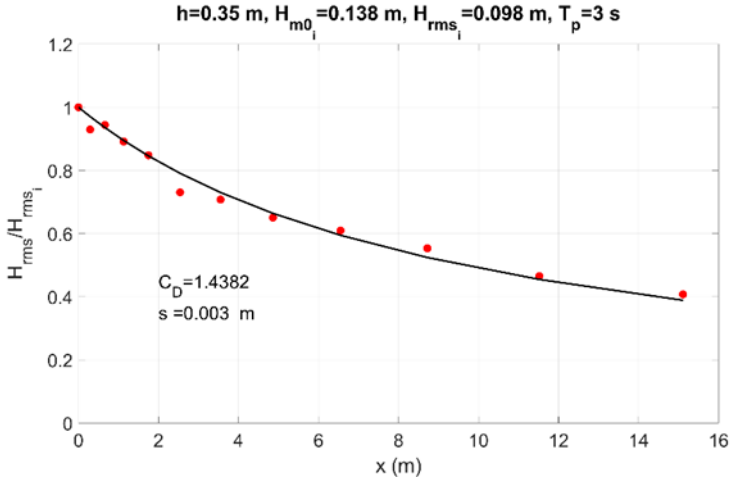
h=0.35 m, H$_{m0_i}$=0.138 m, H$_{rms_i}$=0.098 m, T$_p$=3 s
H$_{rms}$/H$_{rms_i}$
C$_D$=1.4382
s =0.003 m
x (m)

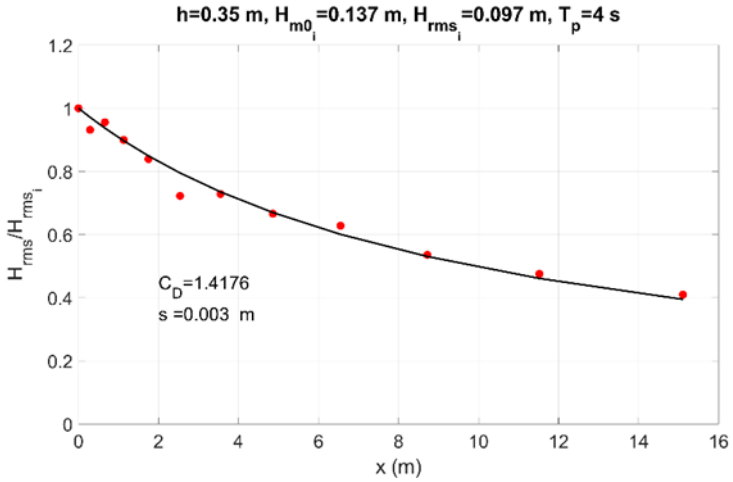
h=0.35 m, H$_{m0_i}$=0.137 m, H$_{rms_i}$=0.097 m, T$_p$=4 s
H$_{rms}$/H$_{rms_i}$
C$_D$=1.4176
s =0.003 m
x (m)

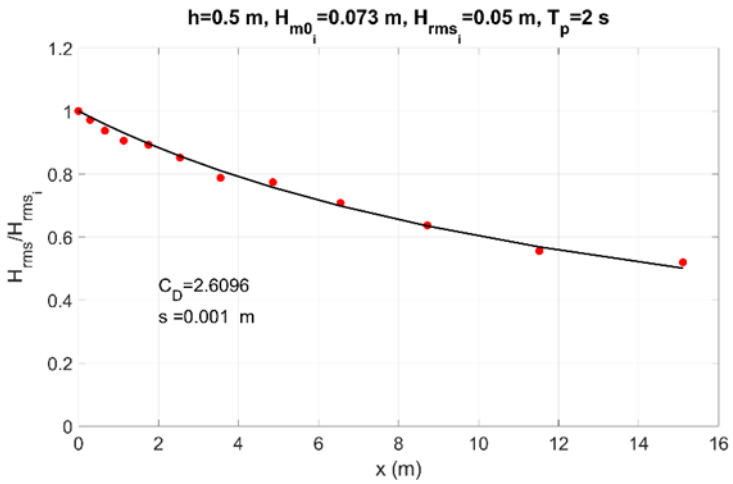
h=0.5 m, H$_{m0_i}$=0.073 m, H$_{rms_i}$=0.05 m, T$_p$=2 s
H$_{rms}$/H$_{rms_i}$
x (m)
C$_D$=2.6096
s =0.001 m

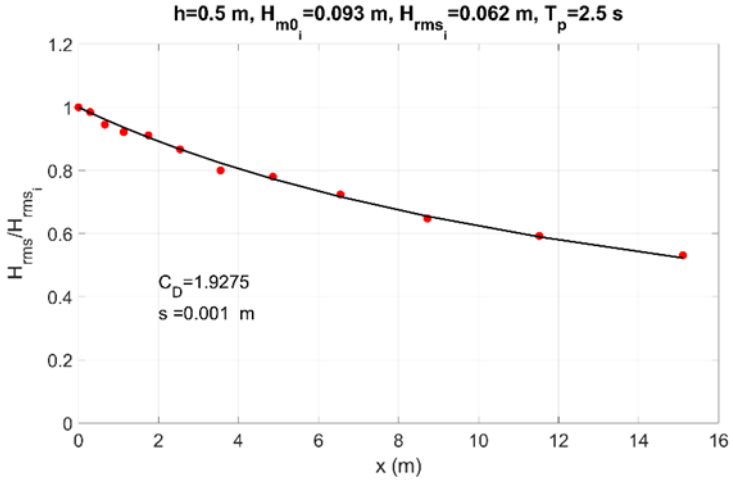
h=0.5 m, H$_{m0_i}$=0.093 m, H$_{rms_i}$=0.062 m, T$_p$=2.5 s
H$_{rms}$/H$_{rms_i}$
x (m)
C$_D$=1.9275
s =0.001 m

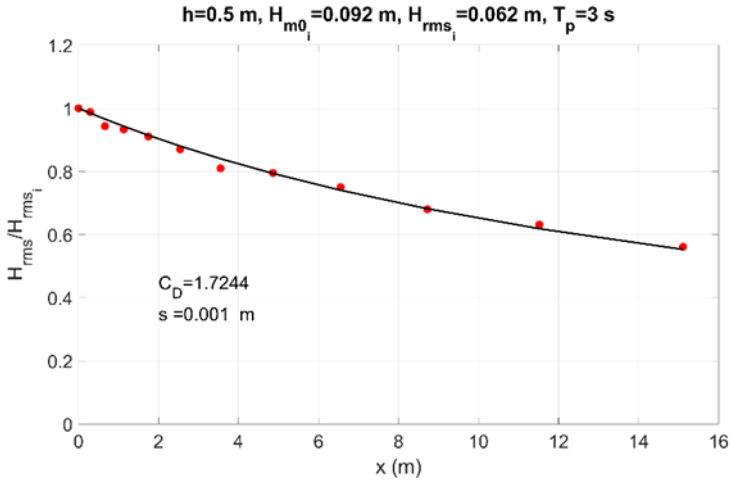
h=0.5 m, H$_{m0_i}$=0.092 m, H$_{rms_i}$=0.062 m, T$_p$=3 s
H$_{rms}$/H$_{rms_i}$
x (m)
C$_D$=1.7244
s =0.001 m

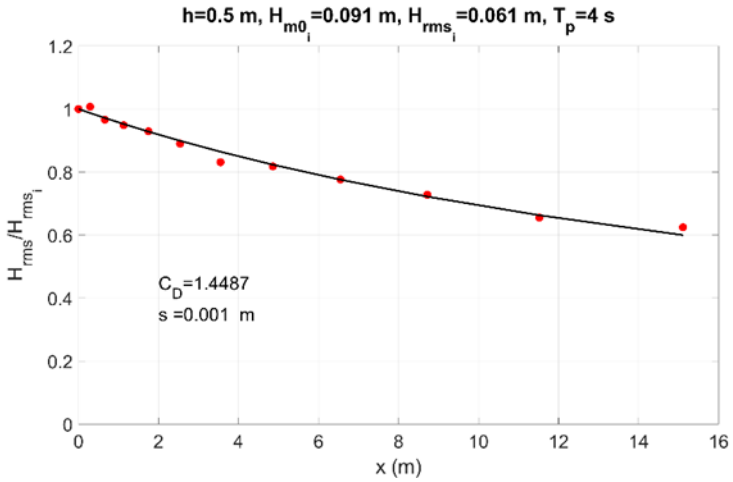
h=0.5 m, H$_{m0_i}$=0.091 m, H$_{rms_i}$=0.061 m, T$_p$=4 s
H$_{rms}$/H$_{rms_i}$
x (m)
C$_D$=1.4487
s =0.001 m

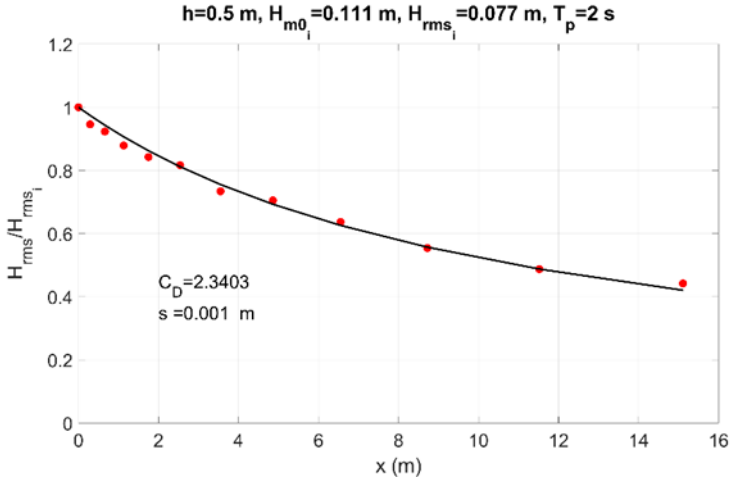
h=0.5 m, H$_{m0_i}$=0.111 m, H$_{rms_i}$=0.077 m, T$_p$=2 s
H$_{rms}$/H$_{rms_i}$
x (m)
C$_D$=2.3403
s =0.001 m

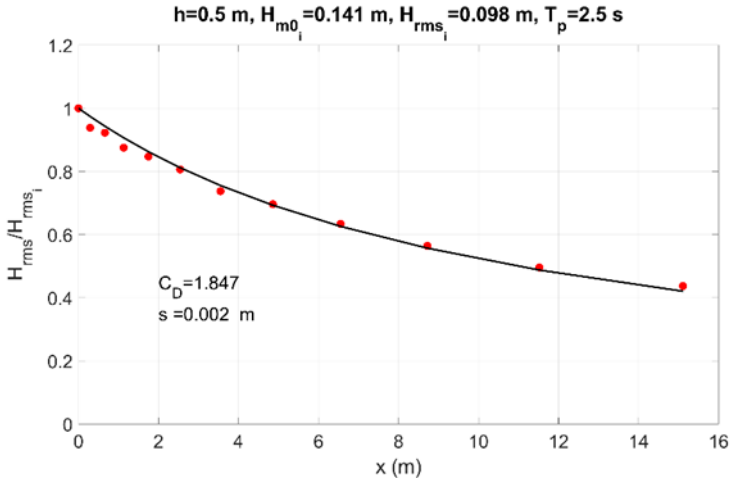
h=0.5 m, H$_{m0_i}$=0.141 m, H$_{rms_i}$=0.098 m, T$_p$=2.5 s
H$_{rms}$/H$_{rms_i}$
x (m)
C$_D$=1.847
s =0.002 m

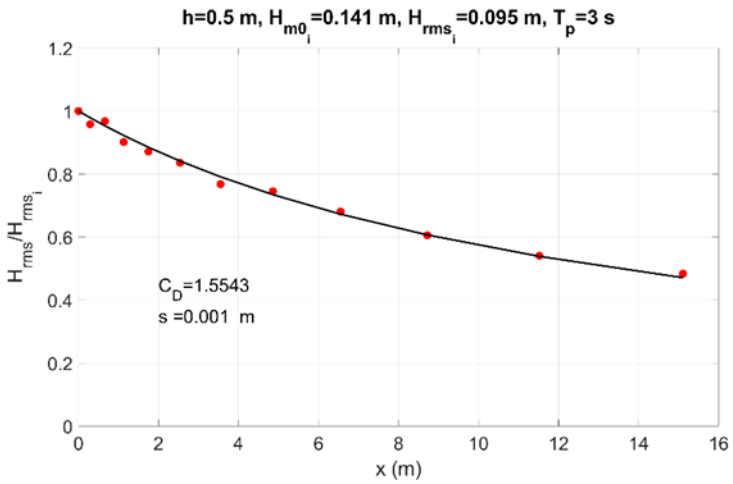
h=0.5 m, H$_{m0_i}$=0.141 m, H$_{rms_i}$=0.095 m, T$_p$=3 s
H$_{rms}$/H$_{rms_i}$
C$_D$=1.5543
s =0.001 m
x (m)

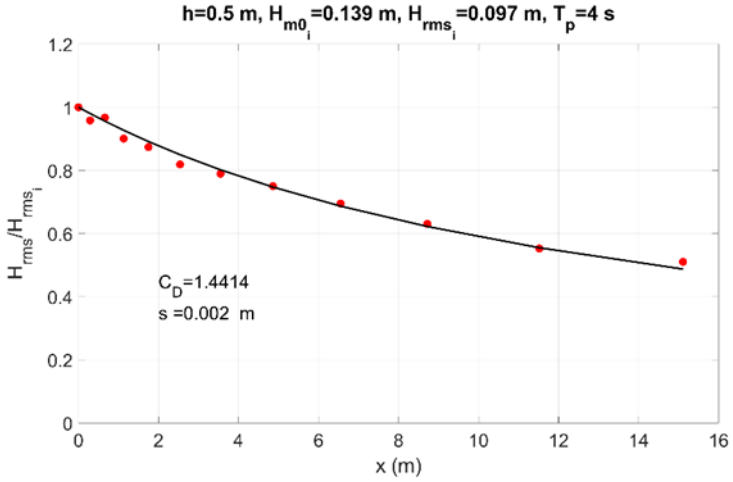
h=0.5 m, H$_{m0_i}$=0.139 m, H$_{rms_i}$=0.097 m, T$_p$=4 s
H$_{rms}$/H$_{rms_i}$
C$_D$=1.4414
s =0.002 m
x (m)

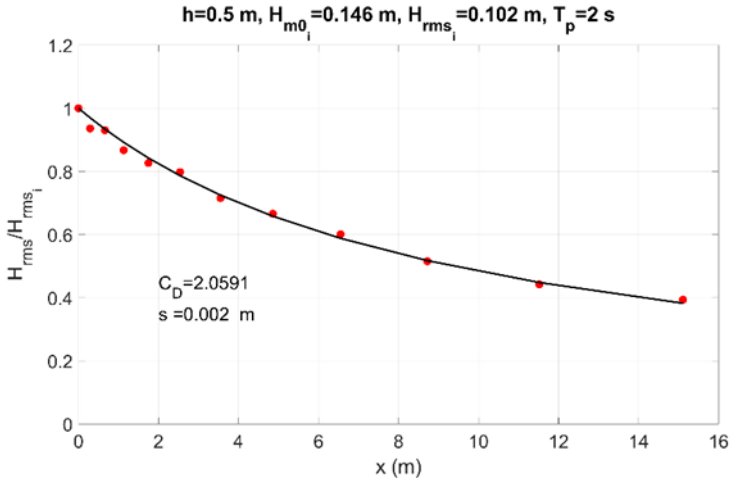
h=0.5 m, H$_{m0_i}$=0.146 m, H$_{rms_i}$=0.102 m, T$_p$=2 s
H$_{rms}$/H$_{rms_i}$
C$_D$=2.0591
s =0.002 m
x (m)

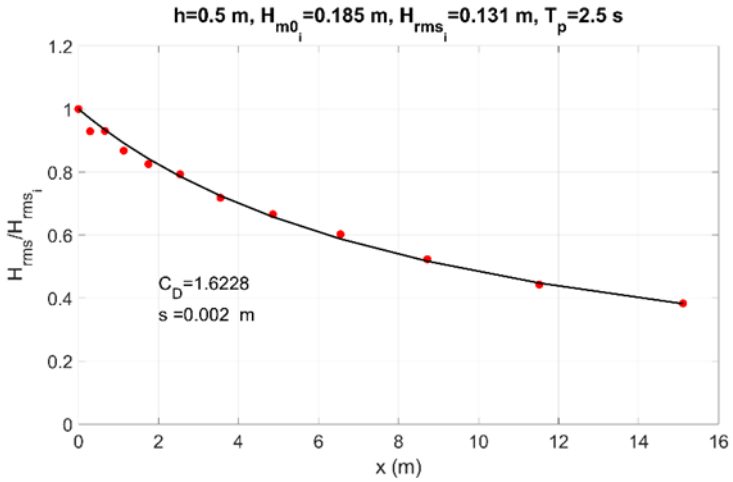
h=0.5 m, H$_{m0_i}$=0.185 m, H$_{rms_i}$=0.131 m, T$_p$=2.5 s
H$_{rms}$/H$_{rms_i}$
C$_D$=1.6228
s =0.002 m
x (m)

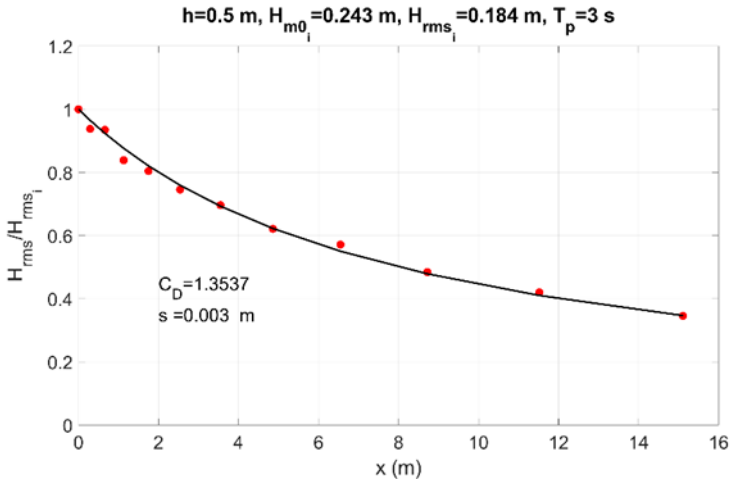
h=0.5 m, H$_{m0_i}$=0.243 m, H$_{rms_i}$=0.184 m, T$_p$=3 s
H$_{rms}$/H$_{rms_i}$
C$_D$=1.3537
s =0.003 m
x (m)

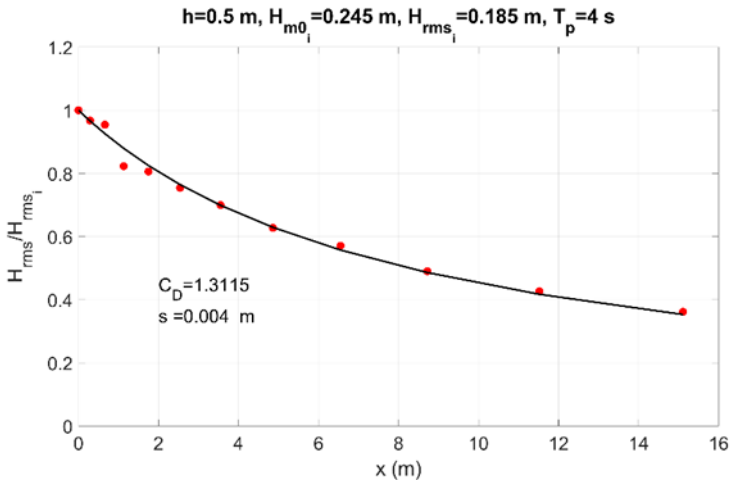
h=0.5 m, H$_{m0_i}$=0.245 m, H$_{rms_i}$=0.185 m, T$_p$=4 s
H$_{rms}$/H$_{rms_i}$
C$_D$=1.3115
s =0.004 m
x (m)

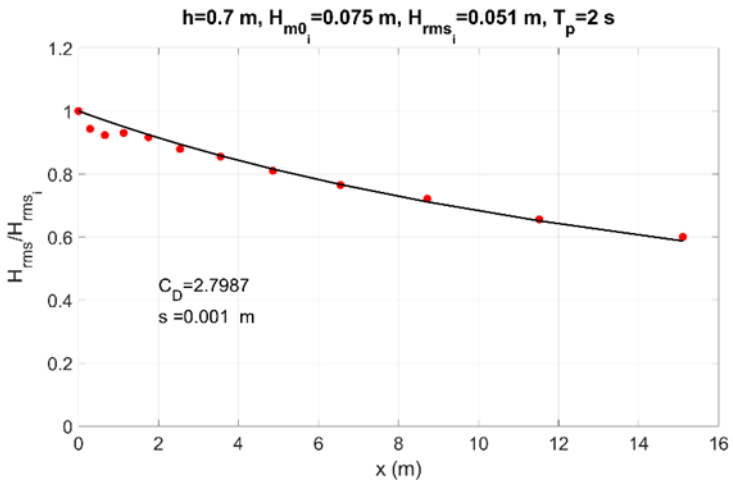
h=0.7 m, H$_{m0_i}$=0.075 m, H$_{rms_i}$=0.051 m, T$_p$=2 s
H$_{rms}$/H$_{rms_i}$
C$_D$=2.7987
s =0.001 m
x (m)

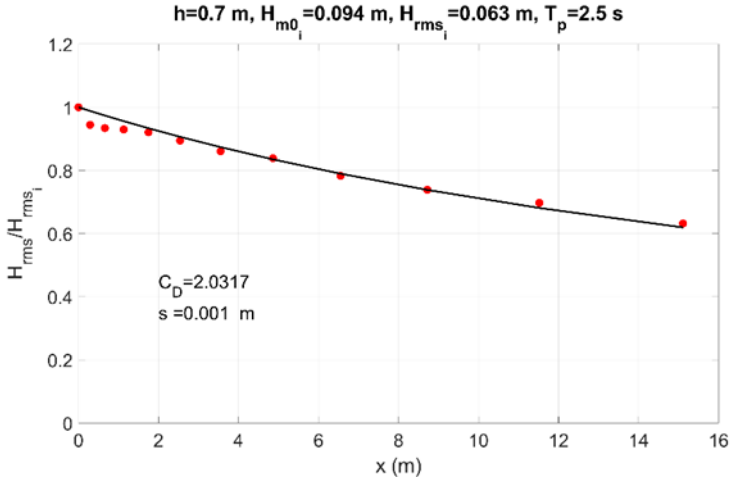
h=0.7 m, H$_{m0_i}$=0.094 m, H$_{rms_i}$=0.063 m, T$_p$=2.5 s
H$_{rms}$/H$_{rms_i}$
C$_D$=2.0317
s =0.001 m
x (m)

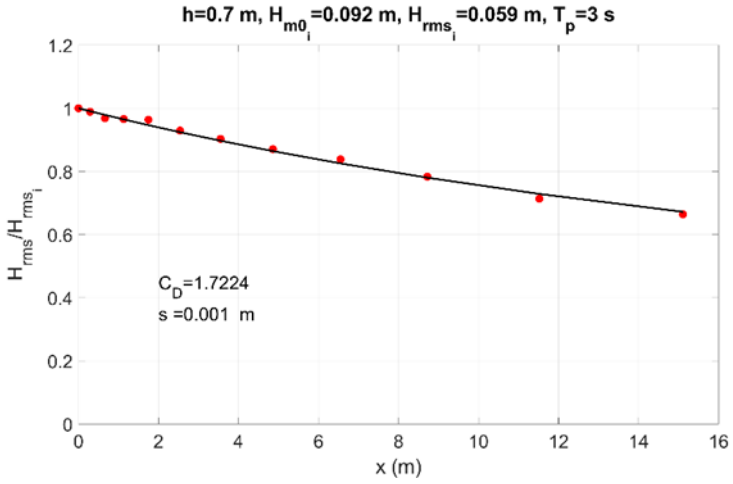
h=0.7 m, H$_{m0_i}$=0.092 m, H$_{rms_i}$=0.059 m, T$_p$=3 s
H$_{rms}$/H$_{rms_i}$
C$_D$=1.7224
s =0.001 m
x (m)

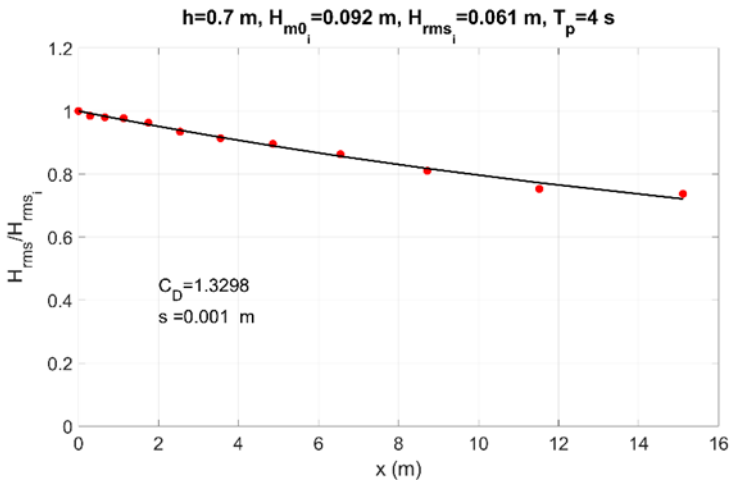
h=0.7 m, H$_{m0_i}$=0.092 m, H$_{rms_i}$=0.061 m, T$_p$=4 s
H$_{rms}$/H$_{rms_i}$
C$_D$=1.3298
s =0.001 m
x (m)

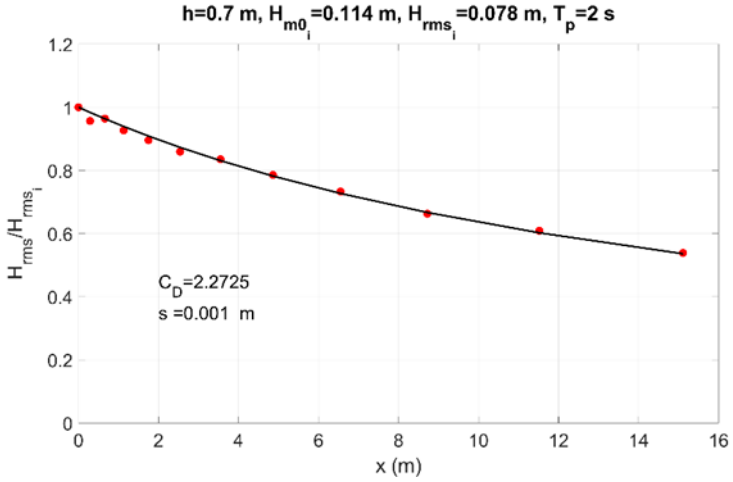
h=0.7 m, H$_{m0_i}$=0.114 m, H$_{rms_i}$=0.078 m, T$_p$=2 s
H$_{rms}$/H$_{rms_i}$
C$_D$=2.2725
s =0.001 m
x (m)

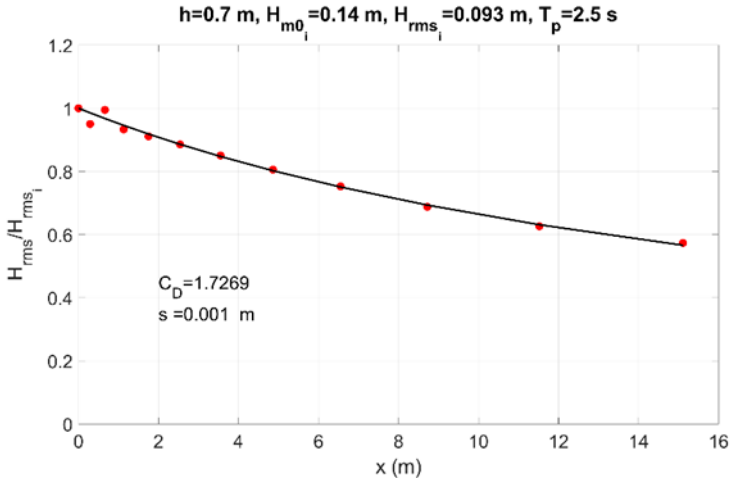
h=0.7 m, H$_{m0_i}$=0.14 m, H$_{rms_i}$=0.093 m, T$_p$=2.5 s
H$_{rms}$/H$_{rms_i}$
C$_D$=1.7269
s =0.001 m
x (m)

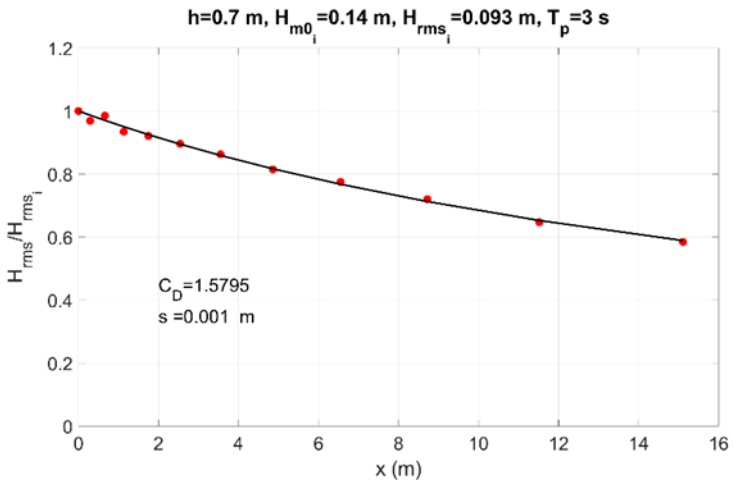
h=0.7 m, H$_{m0_i}$=0.14 m, H$_{rms_i}$=0.093 m, T$_p$=3 s
H$_{rms}$/H$_{rms_i}$
C$_D$=1.5795
s =0.001 m
x (m)

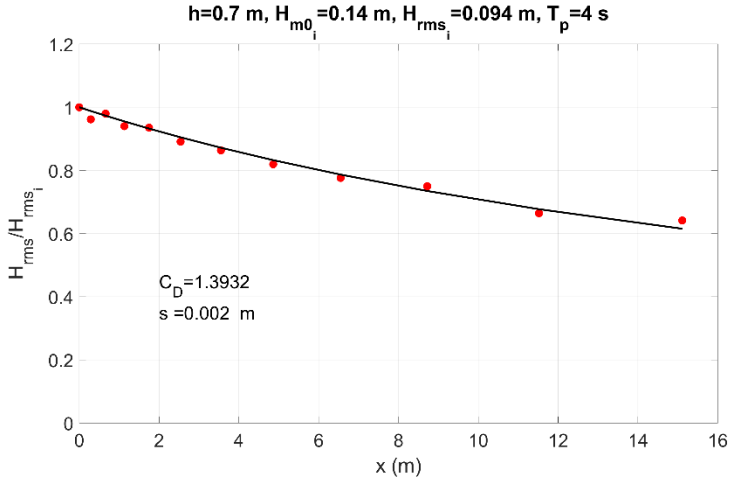
h=0.7 m, H$_{m0_i}$=0.14 m, H$_{rms_i}$=0.094 m, T$_p$=4 s
H$_{rms}$/H$_{rms_i}$
C$_D$=1.3932
s =0.002 m
x (m)

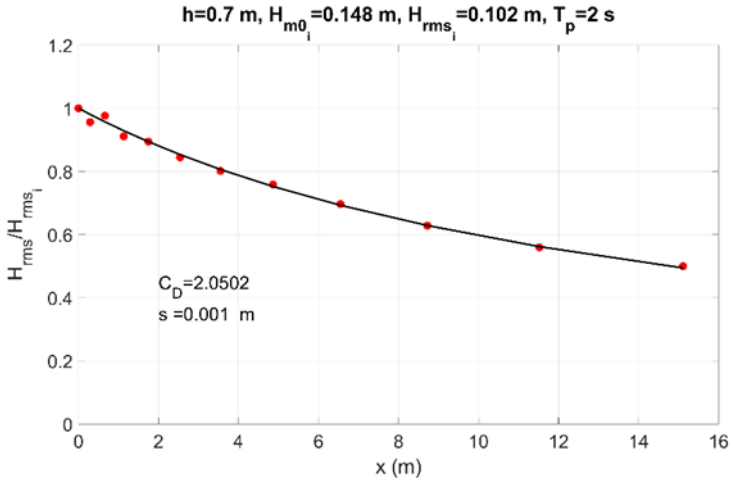
h=0.7 m, H$_{m0_i}$=0.148 m, H$_{rms_i}$=0.102 m, T$_p$=2 s
H$_{rms}$/H$_{rms_i}$
C$_D$=2.0502
s =0.001 m
x (m)

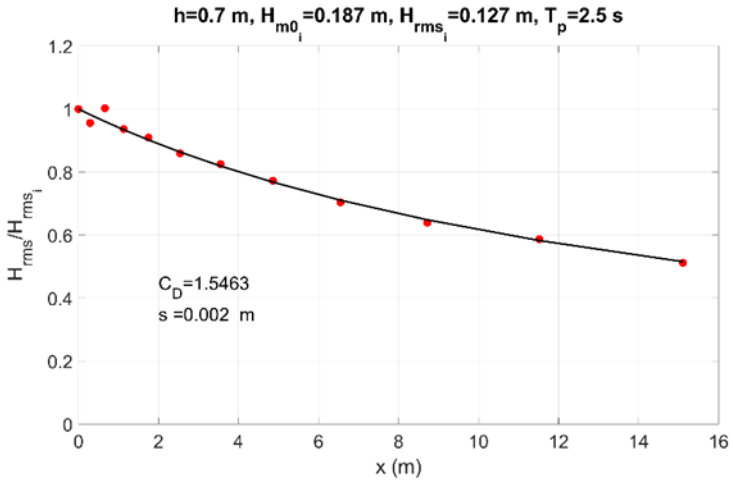
h=0.7 m, H$_{m0_i}$=0.187 m, H$_{rms_i}$=0.127 m, T$_p$=2.5 s
H$_{rms}$/H$_{rms_i}$
C$_D$=1.5463
s =0.002 m
x (m)

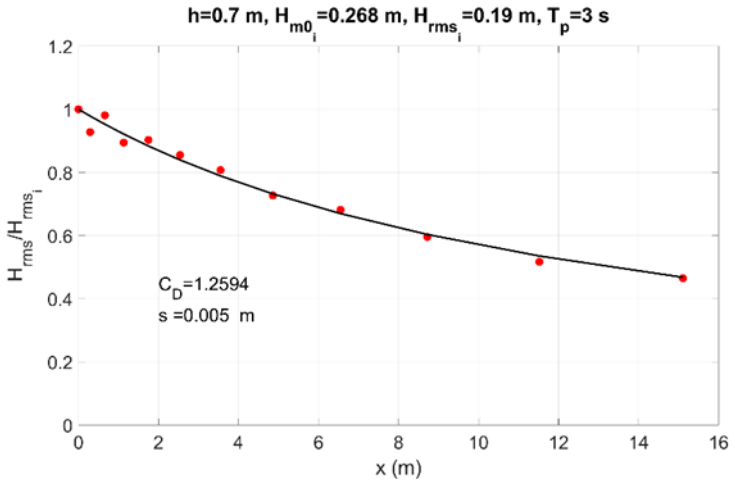
h=0.7 m, H$_{m0_i}$=0.268 m, H$_{rms_i}$=0.19 m, T$_p$=3 s
H$_{rms}$/H$_{rms_i}$
C$_D$=1.2594
s =0.005 m
x (m)

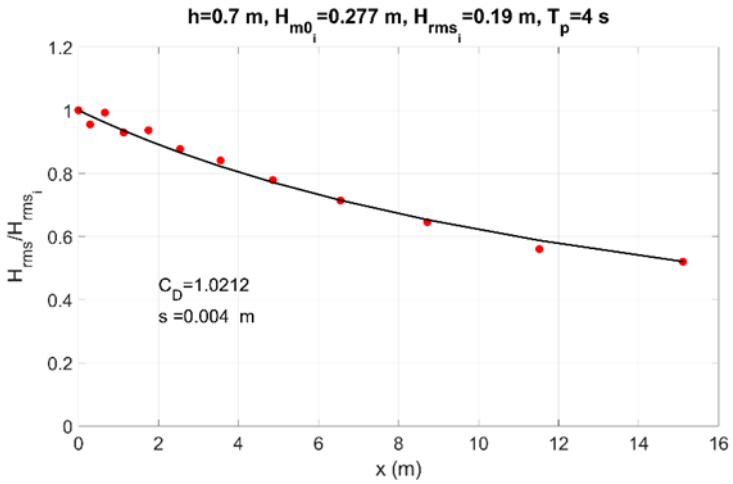
h=0.7 m, H$_{m0_i}$=0.277 m, H$_{rms_i}$=0.19 m, T$_p$=4 s
H$_{rms}$/H$_{rms_i}$
C$_D$=1.0212
s =0.004 m
x (m)

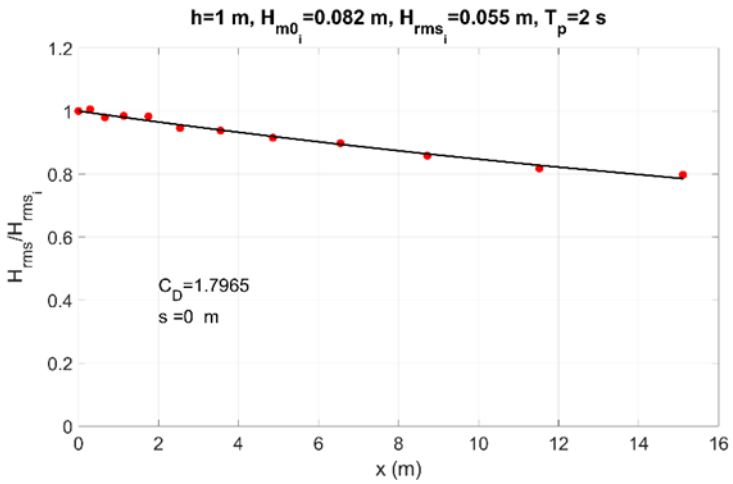
h=1 m, H$_{m0_i}$=0.082 m, H$_{rms_i}$=0.055 m, T$_p$=2 s
H$_{rms}$/H$_{rms_i}$
C$_D$=1.7965
s =0 m
x (m)

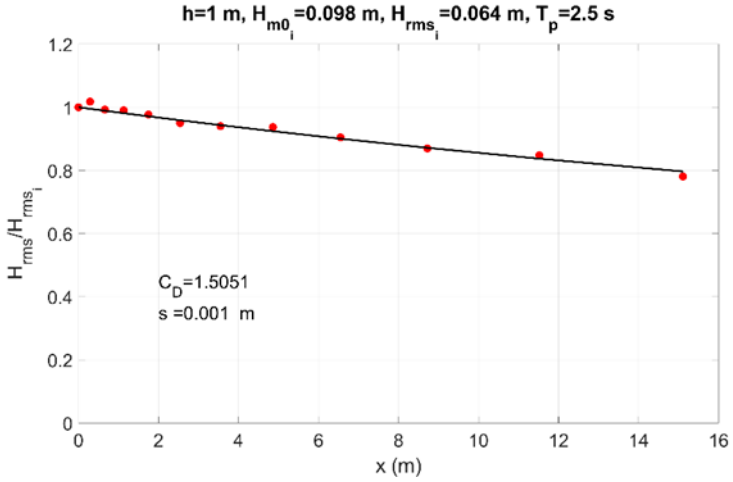
h=1 m, H$_{m0_i}$=0.098 m, H$_{rms_i}$=0.064 m, T$_p$=2.5 s
H$_{rms}$/H$_{rms_i}$
C$_D$=1.5051
s =0.001 m
x (m)

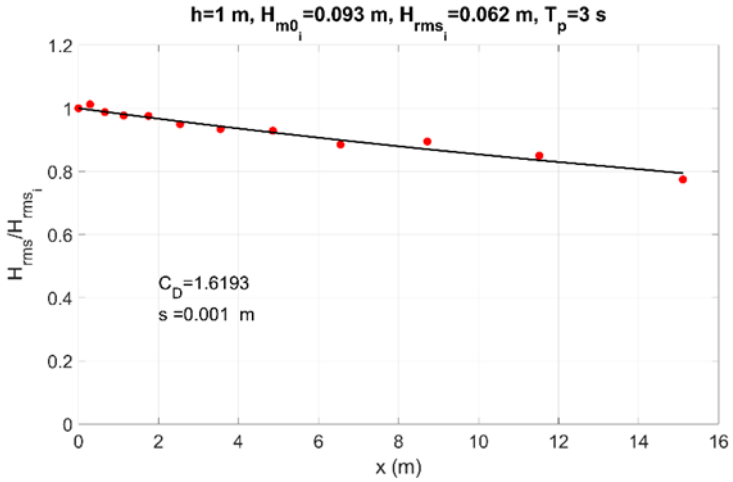
h=1 m, H$_{m0_i}$=0.093 m, H$_{rms_i}$=0.062 m, T$_p$=3 s
H$_{rms}$/H$_{rms_i}$
C$_D$=1.6193
s =0.001 m
x (m)

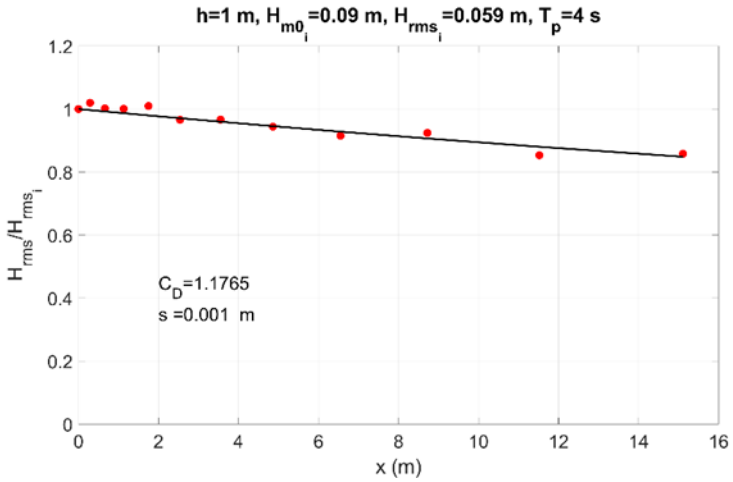
h=1 m, H$_{m0_i}$=0.09 m, H$_{rms_i}$=0.059 m, T$_p$=4 s
H$_{rms}$/H$_{rms_i}$
C$_D$=1.1765
s =0.001 m
x (m)

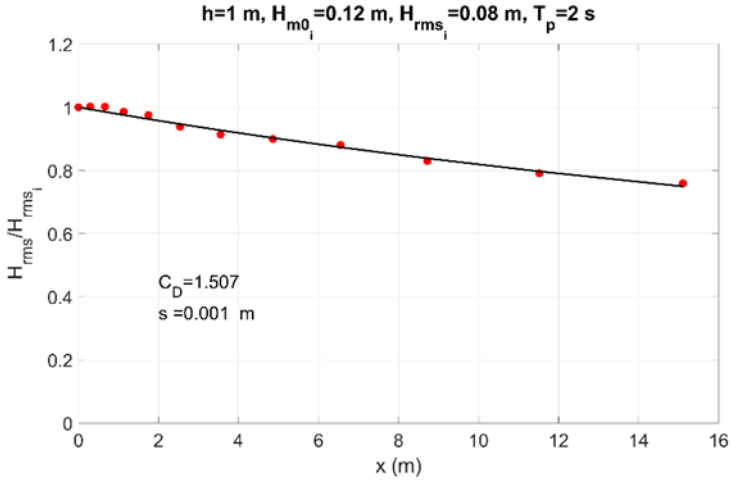
h=1 m, H$_{m0_i}$=0.12 m, H$_{rms_i}$=0.08 m, T$_p$=2 s
H$_{rms}$/H$_{rms_i}$
C$_D$=1.507
s =0.001 m
x (m)

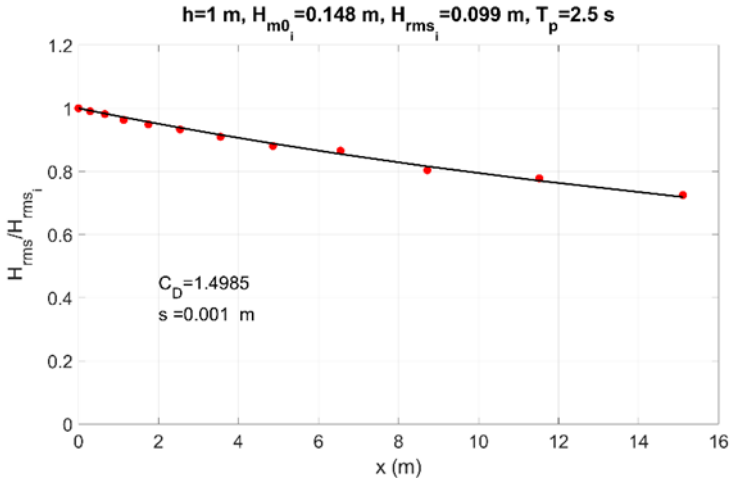
h=1 m, H$_{m0_i}$=0.148 m, H$_{rms_i}$=0.099 m, T$_p$=2.5 s
H$_{rms}$/H$_{rms_i}$
C$_D$=1.4985
s =0.001 m
x (m)

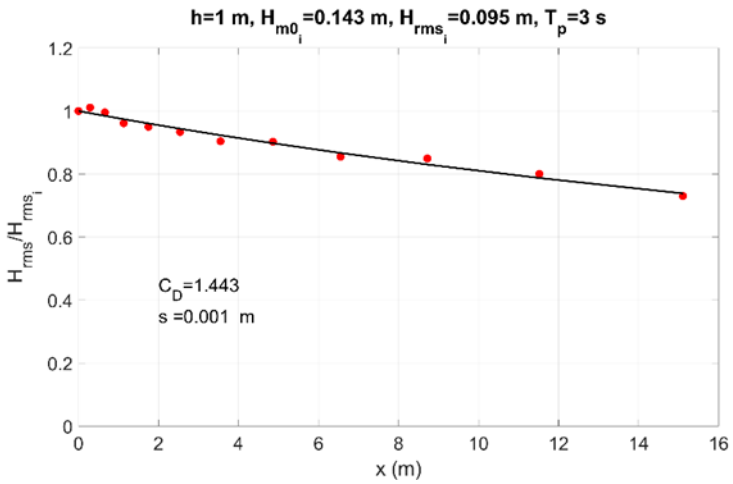
h=1 m, H$_{m0_i}$=0.143 m, H$_{rms_i}$=0.095 m, T$_p$=3 s
H$_{rms}$/H$_{rms_i}$
C$_D$=1.443
s =0.001 m
x (m)

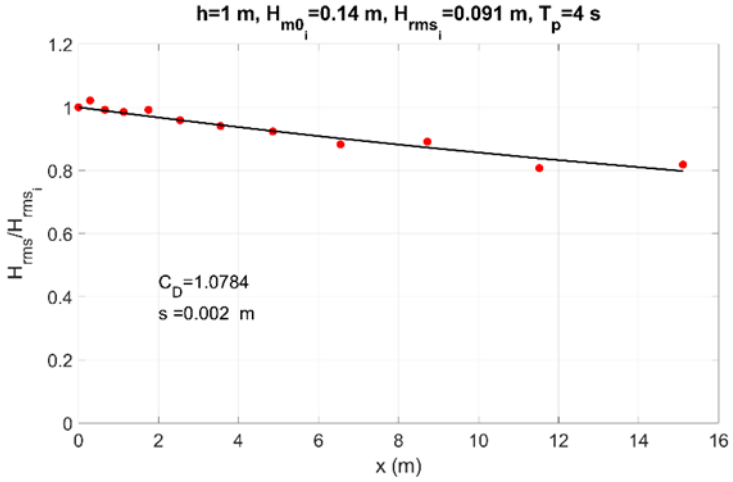
h=1 m, H$_{m0_i}$=0.14 m, H$_{rms_i}$=0.091 m, T$_p$=4 s
H$_{rms}$/H$_{rms_i}$
C$_D$=1.0784
s =0.002 m
x (m)

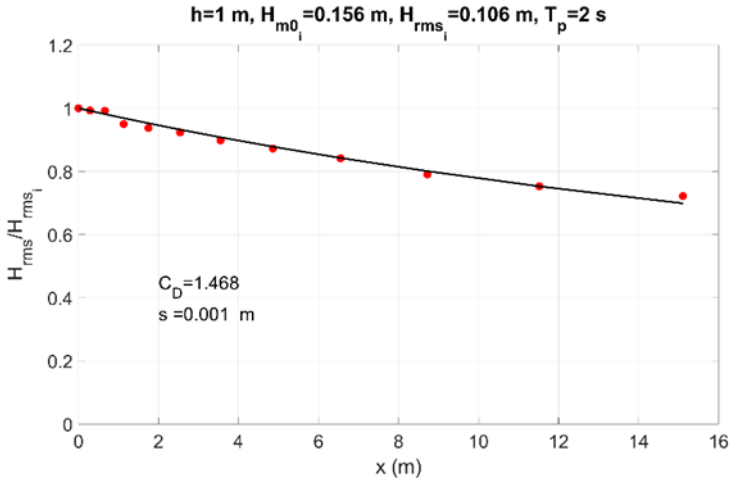
h=1 m, H$_{m0_i}$=0.156 m, H$_{rms_i}$=0.106 m, T$_p$=2 s
H$_{rms}$/H$_{rms_i}$
C$_D$=1.468
s =0.001 m
x (m)

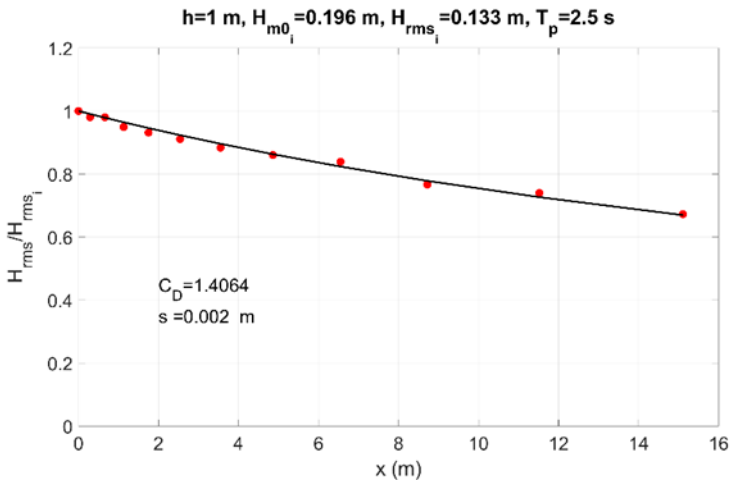
h=1 m, H$_{m0_i}$=0.196 m, H$_{rms_i}$=0.133 m, T$_p$=2.5 s
H$_{rms}$/H$_{rms_i}$
C$_D$=1.4064
s =0.002 m
x (m)

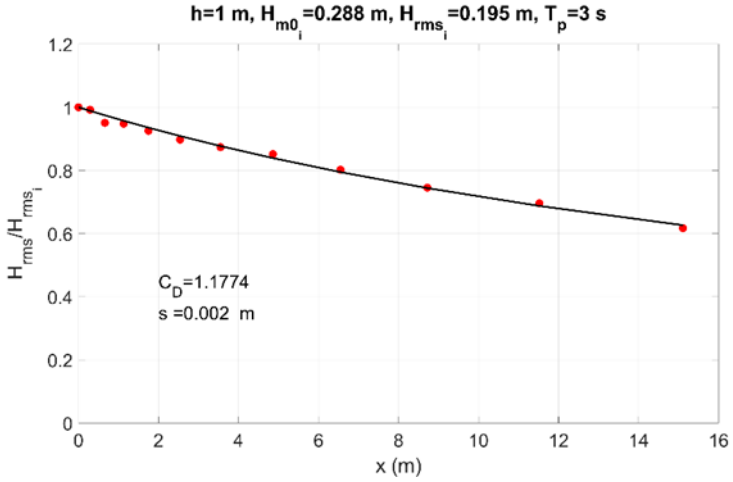
h=1 m, H$_{m0_i}$=0.288 m, H$_{rms_i}$=0.195 m, T$_p$=3 s
H$_{rms}$/H$_{rms_i}$
C$_D$=1.1774
s =0.002 m
x (m)

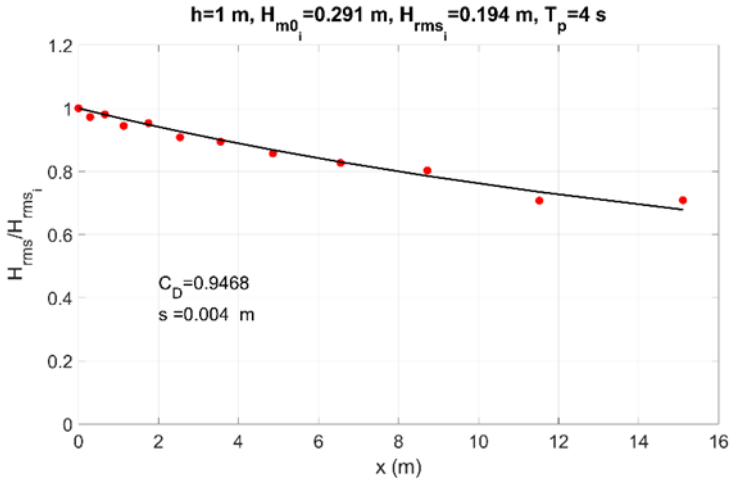
h=1 m, H$_{m0_i}$=0.291 m, H$_{rms_i}$=0.194 m, T$_p$=4 s
H$_{rms}$/H$_{rms_i}$
C$_D$=0.9468
s =0.004 m
x (m)

D.2 Regular waves

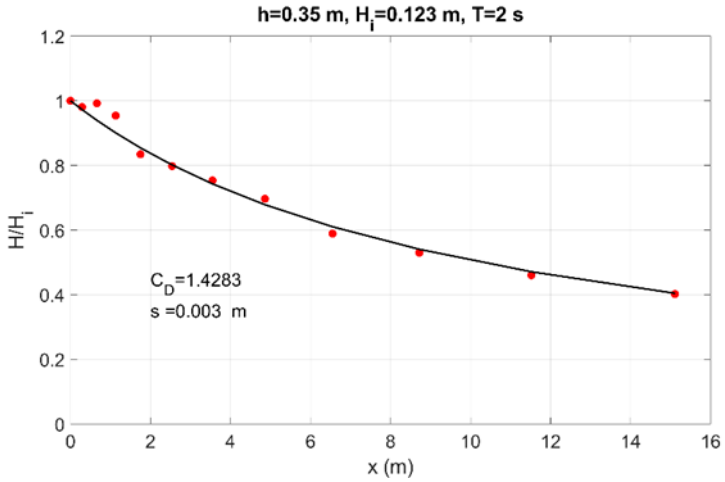

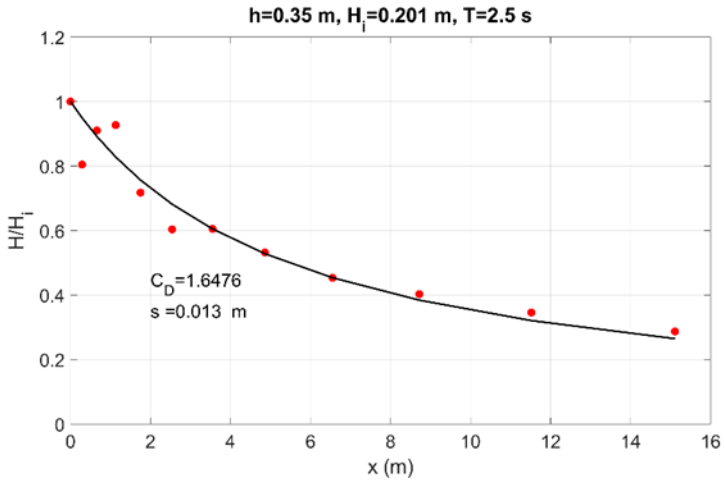

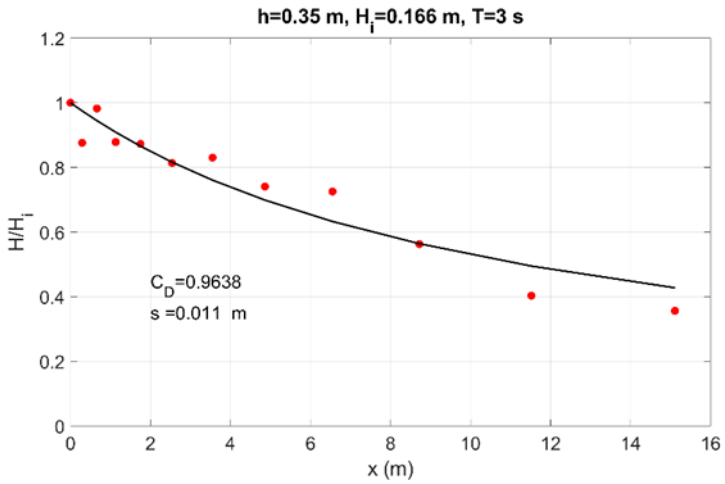

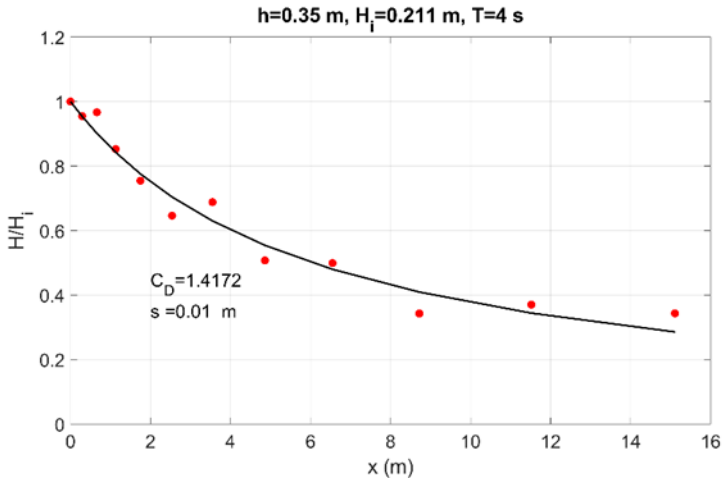
h=0.35 m, H$_i$=0.211 m, T=4 s
H/H$_i$
x (m)
C$_D$=1.4172
s =0.01 m

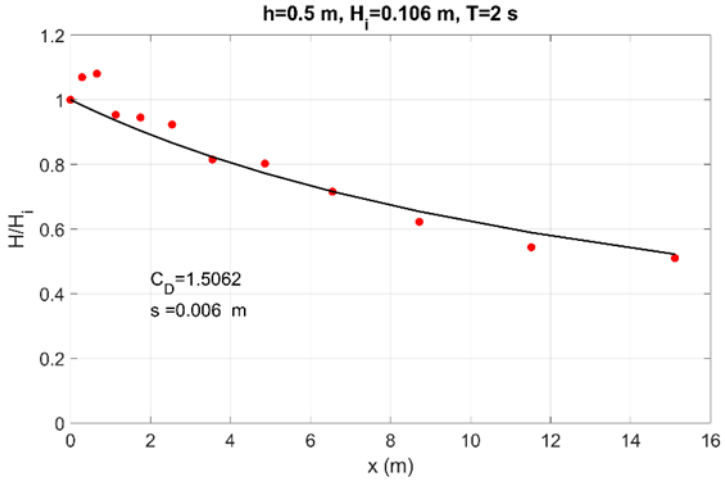
h=0.5 m, H$_i$=0.106 m, T=2 s
H/H$_i$
x (m)
C$_D$=1.5062
s =0.006 m

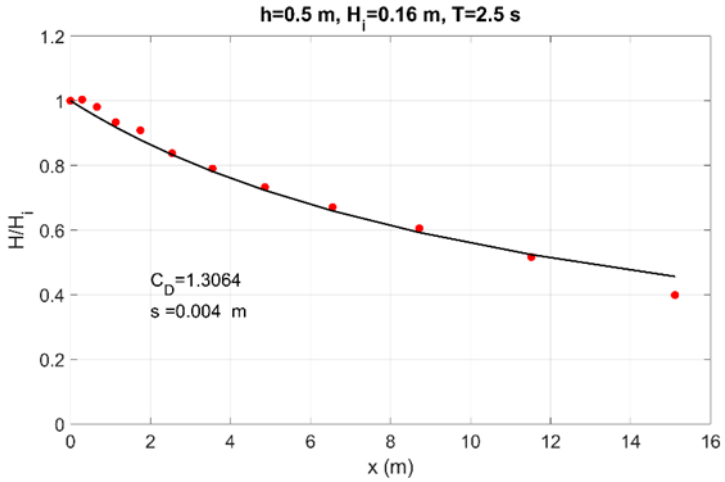
h=0.5 m, H$_i$=0.16 m, T=2.5 s
H/H$_i$
x (m)
C$_D$=1.3064
s =0.004 m

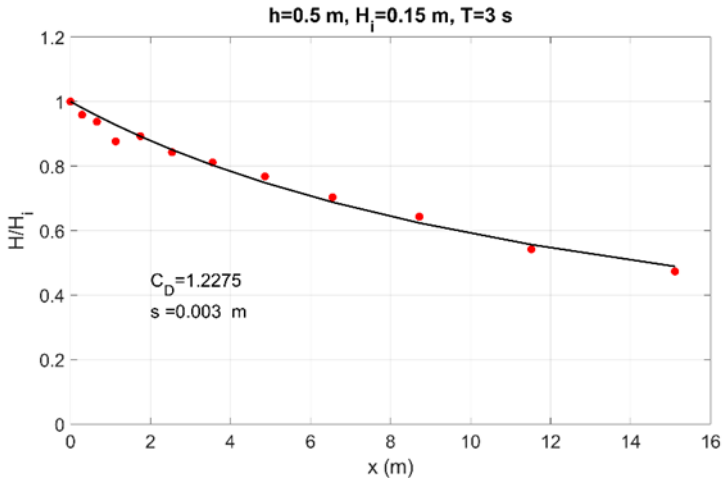
h=0.5 m, H$_i$=0.15 m, T=3 s
H/H$_i$
x (m)
C$_D$=1.2275
s =0.003 m

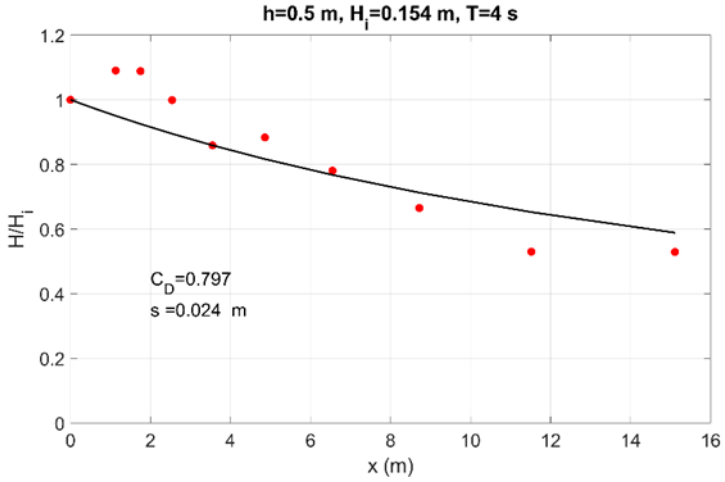
h=0.5 m, H$_i$=0.154 m, T=4 s
H/H$_i$
x (m)
C$_D$=0.797
s =0.024 m

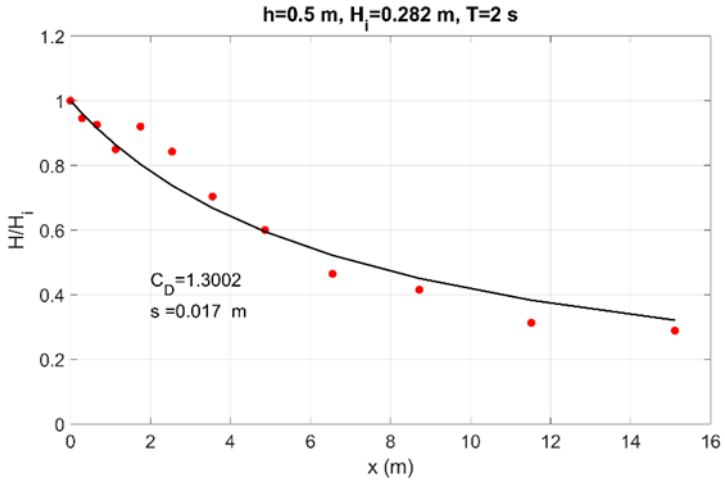
h=0.5 m, H$_i$=0.282 m, T=2 s
H/H$_i$
x (m)
C$_D$=1.3002
s =0.017 m

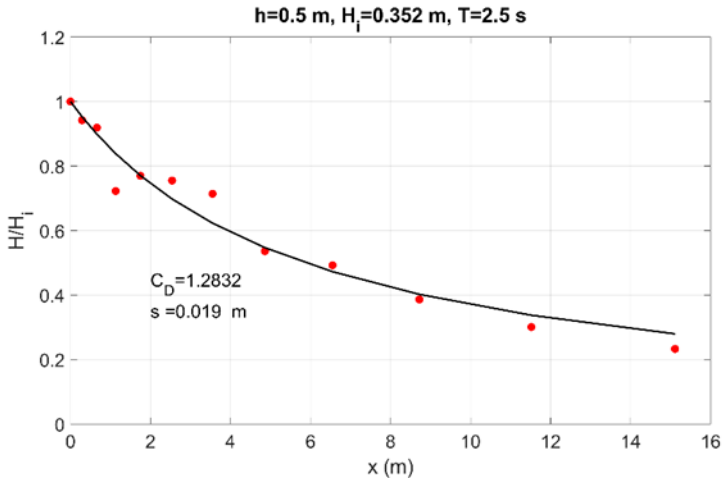
h=0.5 m, H$_i$=0.352 m, T=2.5 s
H/H$_i$
x (m)
C$_D$=1.2832
s =0.019 m

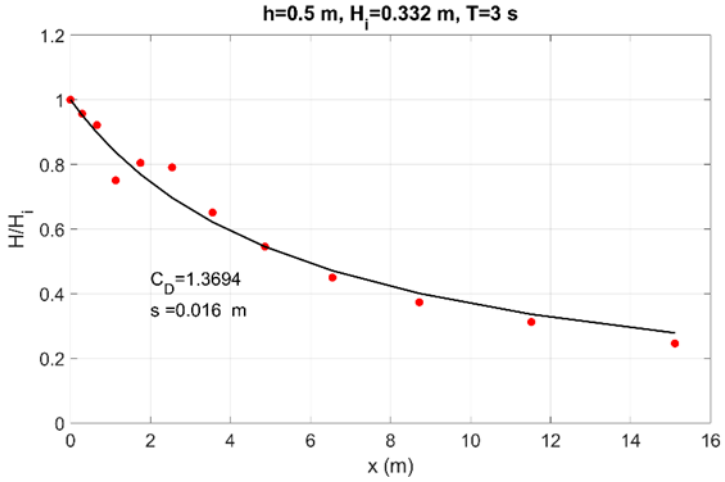
h=0.5 m, H$_i$=0.332 m, T=3 s
H/H$_i$
x (m)
C$_D$=1.3694
s =0.016 m

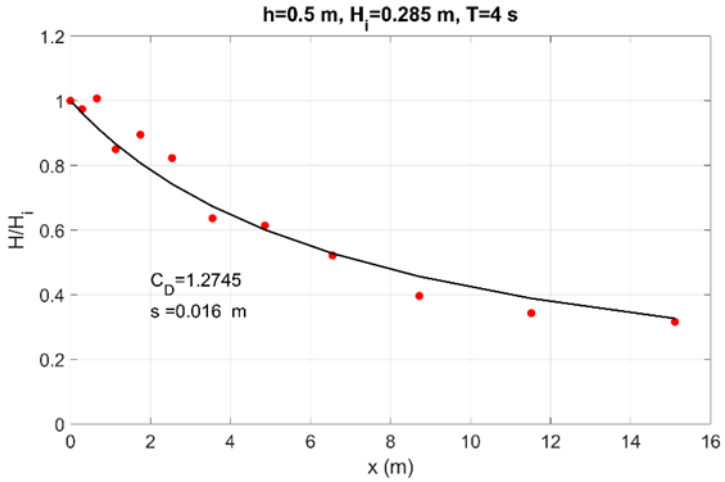
h=0.5 m, H$_i$=0.285 m, T=4 s
H/H$_i$
x (m)
C$_D$=1.2745
s =0.016 m

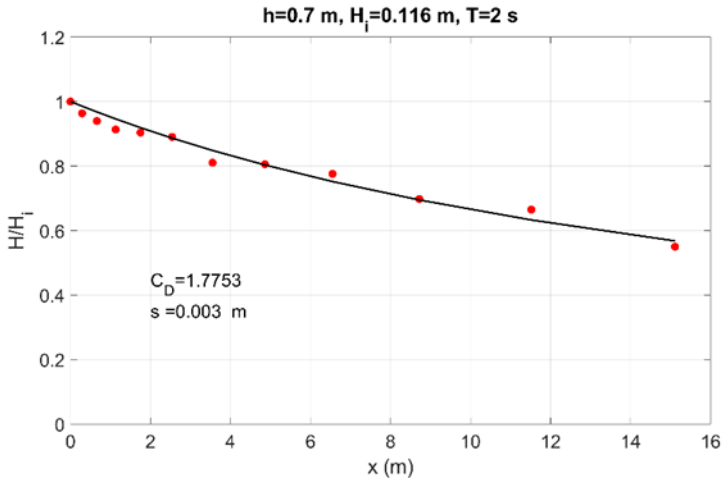
h=0.7 m, H$_i$=0.116 m, T=2 s
H/H$_i$
x (m)
C$_D$=1.7753
s =0.003 m

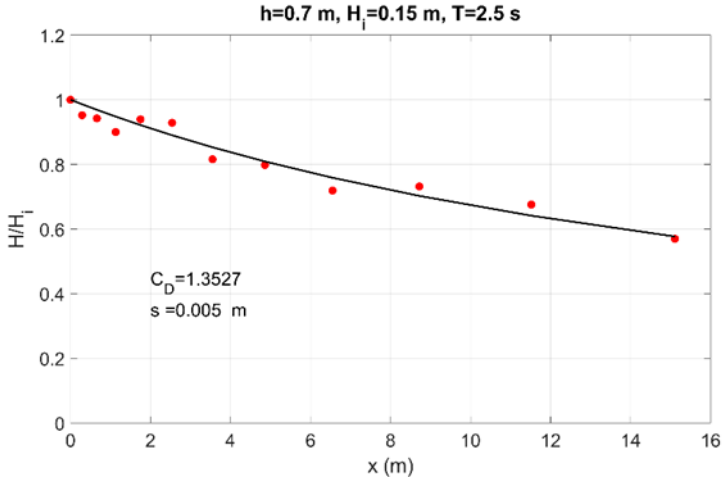
h=0.7 m, H$_i$=0.15 m, T=2.5 s
H/H$_i$
x (m)
C$_D$=1.3527
s =0.005 m

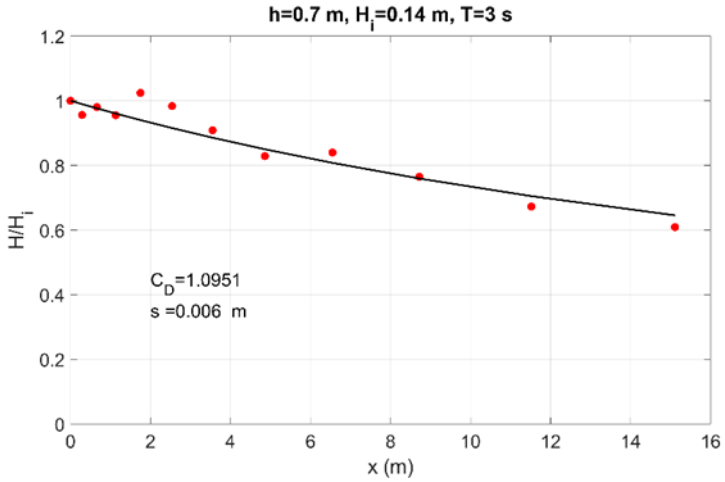
h=0.7 m, H$_i$=0.14 m, T=3 s
H/H$_i$
x (m)
C$_D$=1.0951
s =0.006 m

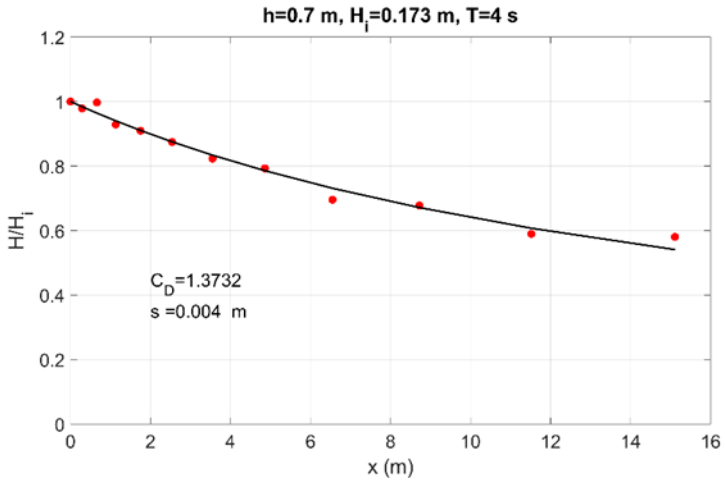
h=0.7 m, H$_i$=0.173 m, T=4 s
H/H$_i$
x (m)
C$_D$=1.3732
s =0.004 m

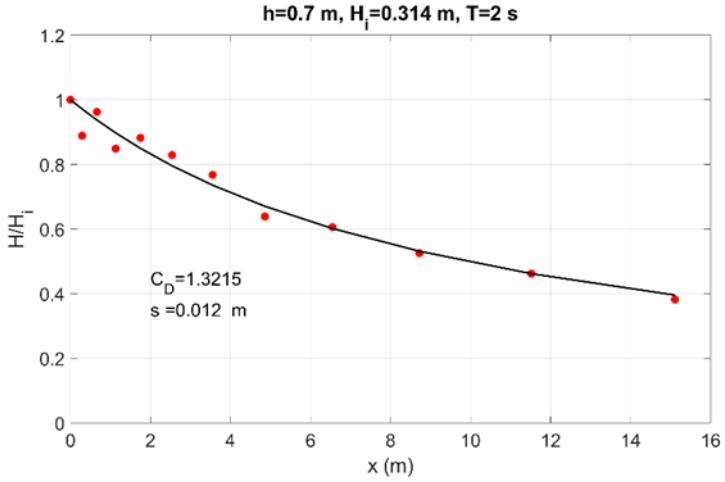
h=0.7 m, H$_i$=0.314 m, T=2 s
H/H$_i$
x (m)
C$_D$=1.3215
s =0.012 m

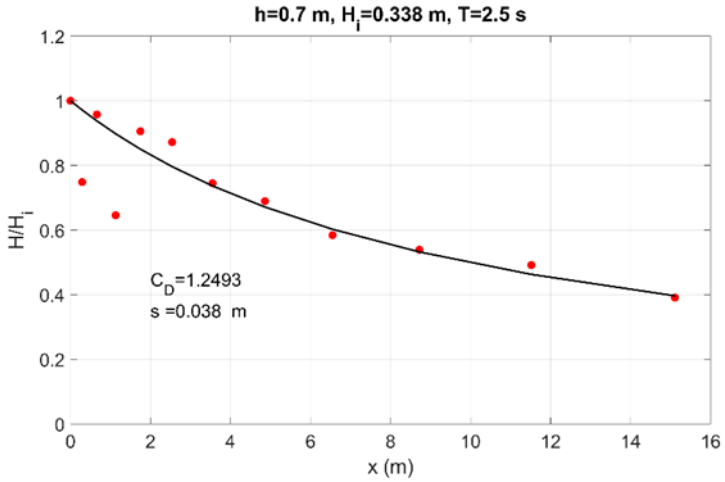
h=0.7 m, H$_i$=0.338 m, T=2.5 s
H/H$_i$
x (m)
C$_D$=1.2493
s =0.038 m

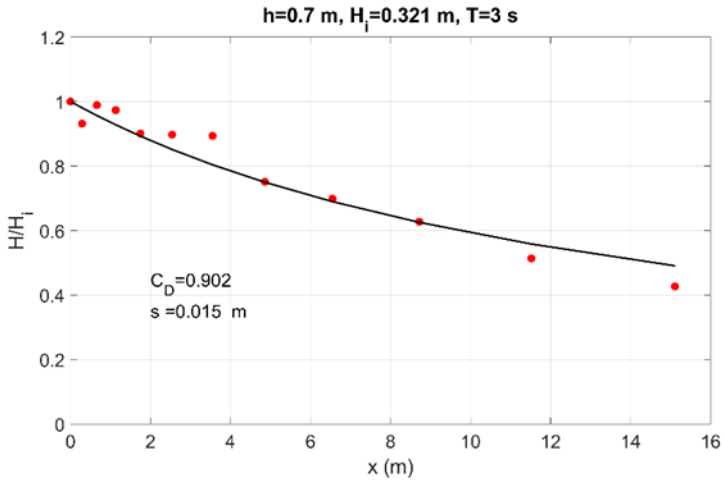
h=0.7 m, H$_i$=0.321 m, T=3 s
H/H$_i$
x (m)
C$_D$=0.902
s =0.015 m

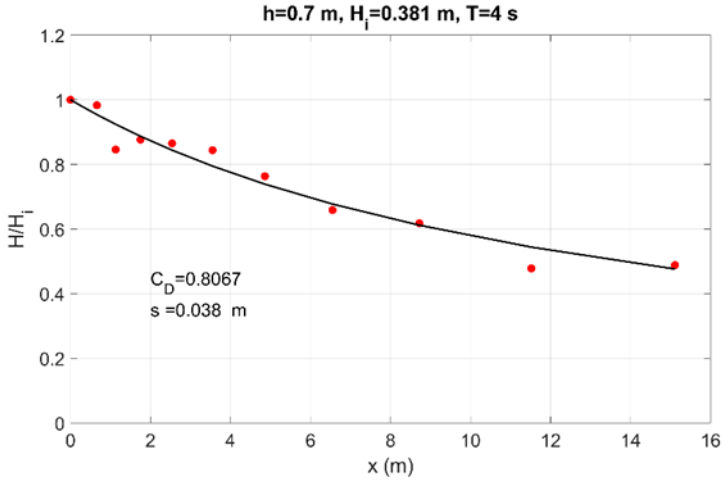
h=0.7 m, H$_i$=0.381 m, T=4 s
H/H$_i$
x (m)
C$_D$=0.8067
s =0.038 m

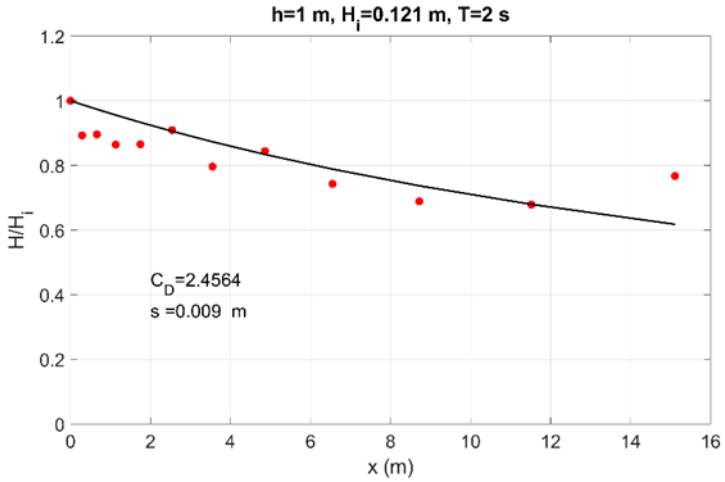
h=1 m, H$_i$=0.121 m, T=2 s
H/H$_i$
x (m)
C$_D$=2.4564
s =0.009 m

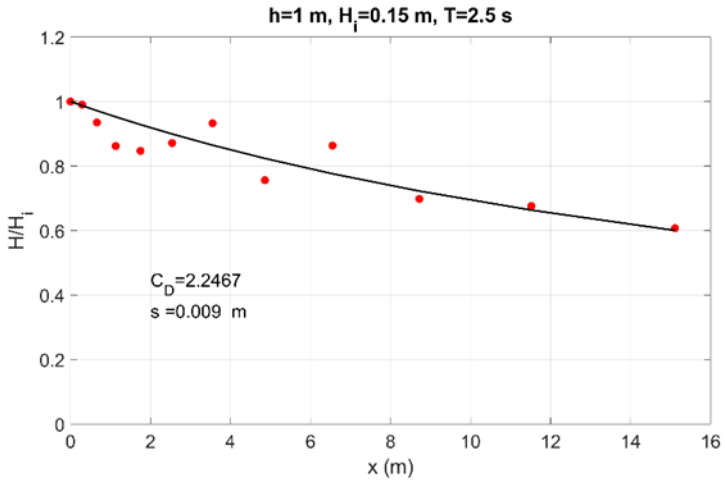
h=1 m, H$_i$=0.15 m, T=2.5 s
H/H$_i$
x (m)
C$_D$=2.2467
s =0.009 m

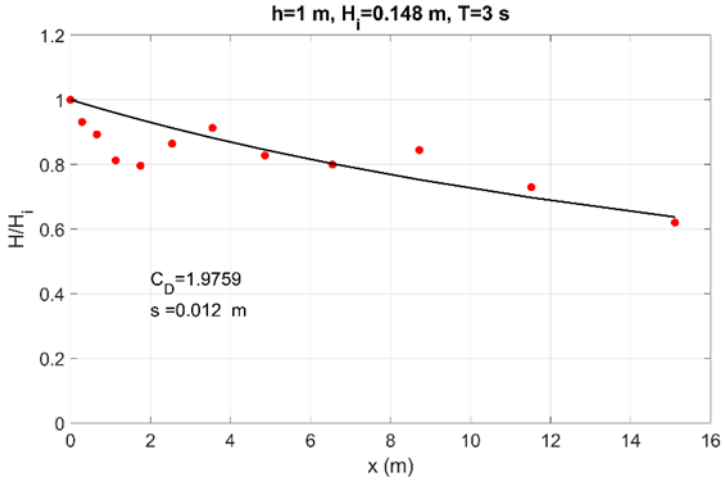
h=1 m, H$_i$=0.148 m, T=3 s
H/H$_i$
x (m)
C$_D$=1.9759
s =0.012 m

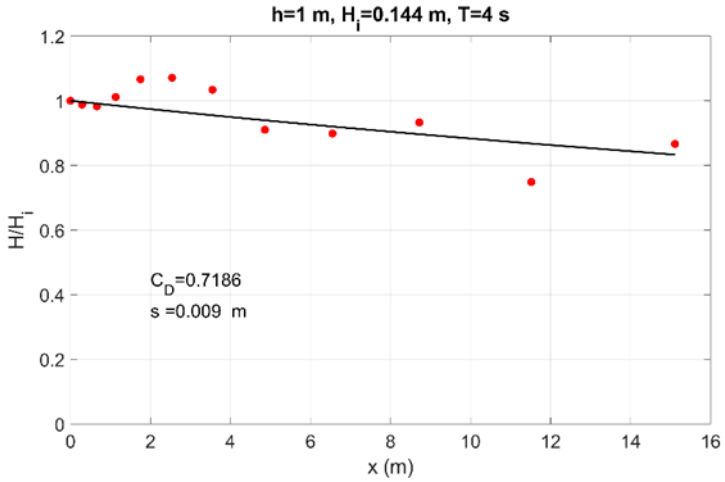
h=1 m, H$_i$=0.144 m, T=4 s
H/H$_i$
x (m)
C$_D$=0.7186
s =0.009 m

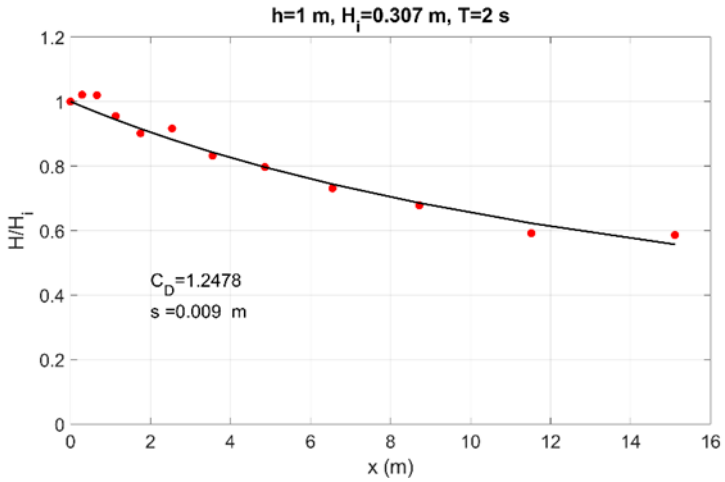
h=1 m, H$_i$=0.307 m, T=2 s
H/H$_i$
x (m)
C$_D$=1.2478
s =0.009 m

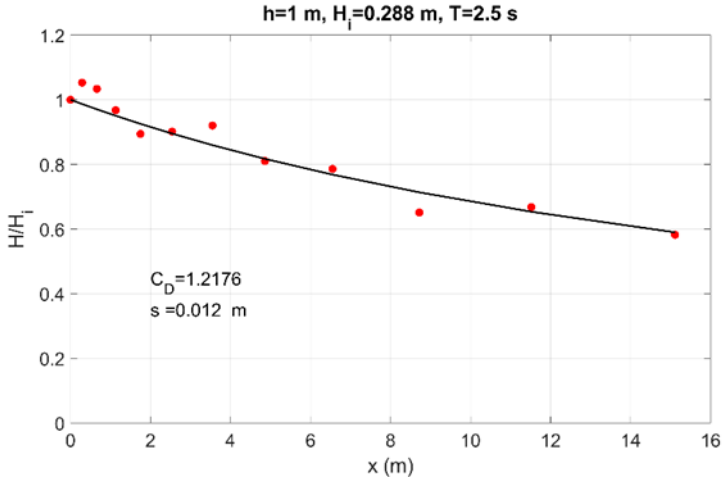
h=1 m, H$_i$=0.288 m, T=2.5 s
H/H$_i$
x (m)
C$_D$=1.2176
s =0.012 m

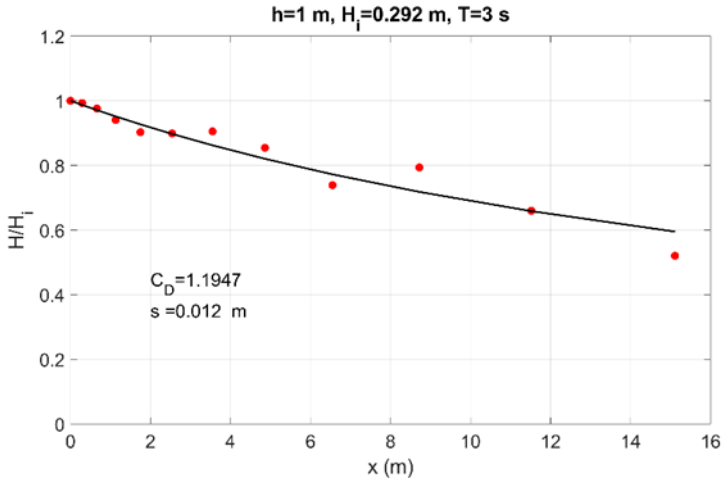
h=1 m, H$_i$=0.292 m, T=3 s
H/H$_i$
x (m)
C$_D$=1.1947
s =0.012 m

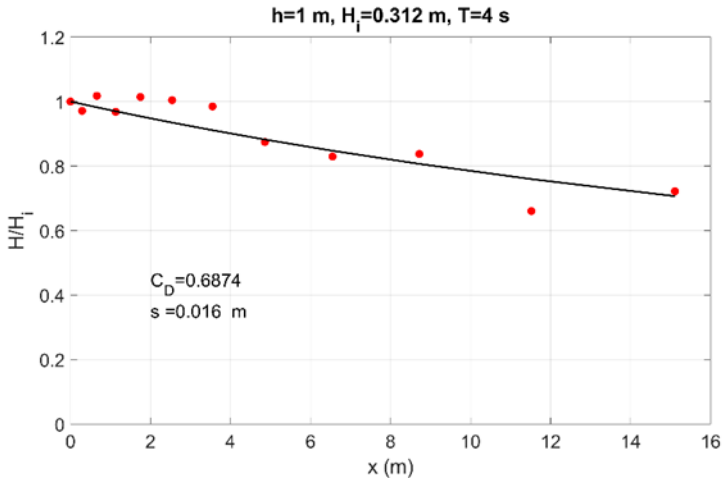
h=1 m, H_i=0.312 m, T=4 s
H/H_i
x (m)
C_D=0.6874
s =0.016 m
0
0.2
0.4
0.6
0.8
1
1.2
0
2
4
6
8
10
12
14
16

Appendix E: Manning's *n*

Appendix E: Manning's *n* shows the normalized wave height evolution with fitted Manning's *n* and standard error (*s*) for all irregular wave conditions. The label at the top of each figure corresponds with a wave condition listed in Table 1.

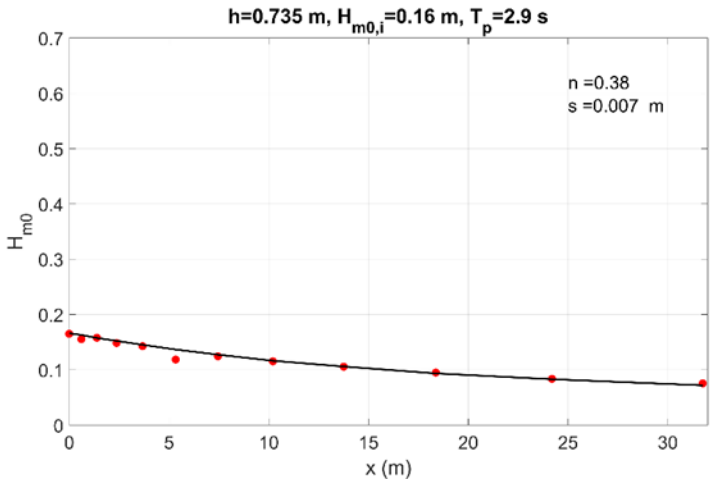

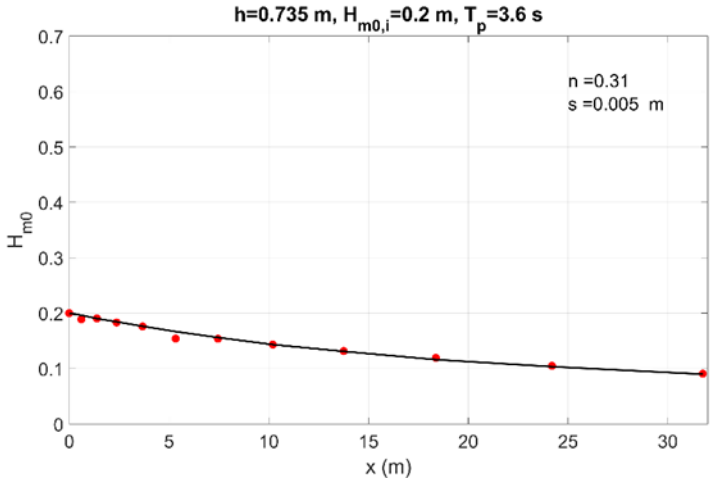

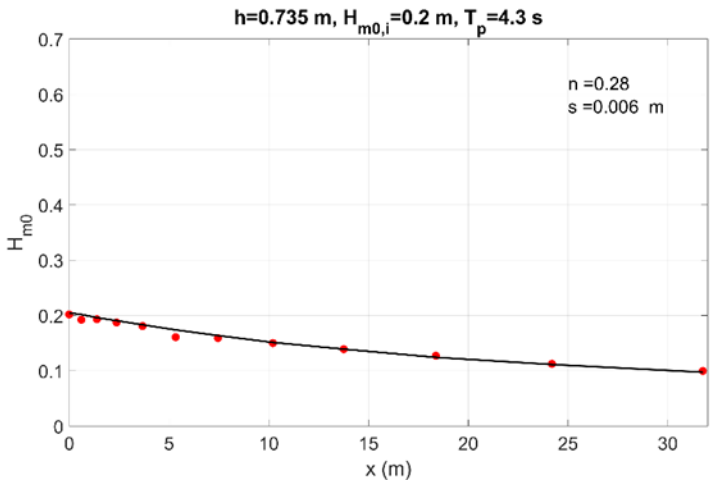
h=0.735 m, H$_{m0,i}$=0.2 m, T$_p$=4.3 s
n =0.28
s =0.006 m
H$_{m0}$
x (m)

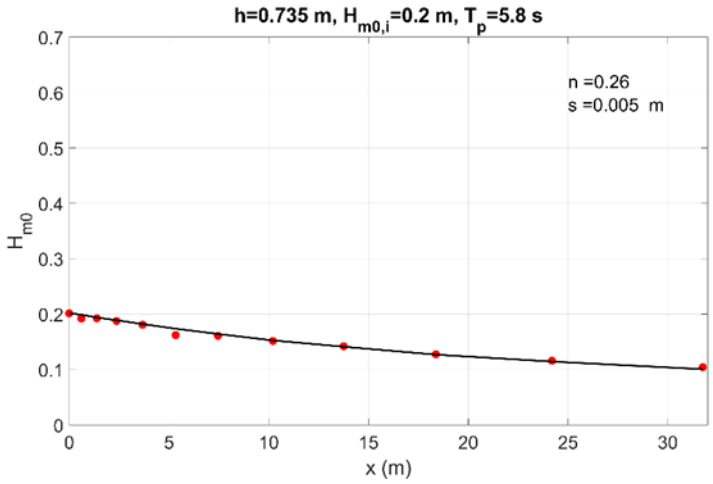
h=0.735 m, H$_{m0,i}$=0.2 m, T$_p$=5.8 s
n =0.26
s =0.005 m
H$_{m0}$
x (m)

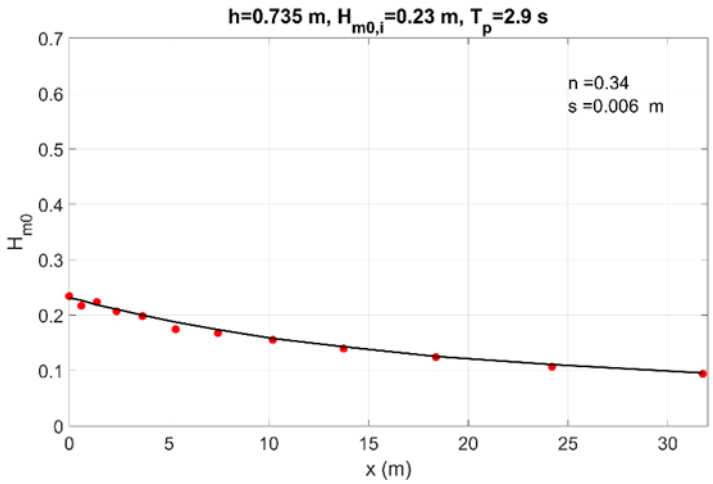
h=0.735 m, H$_{m0,i}$=0.23 m, T$_p$=2.9 s
n =0.34
s =0.006 m
H$_{m0}$
x (m)

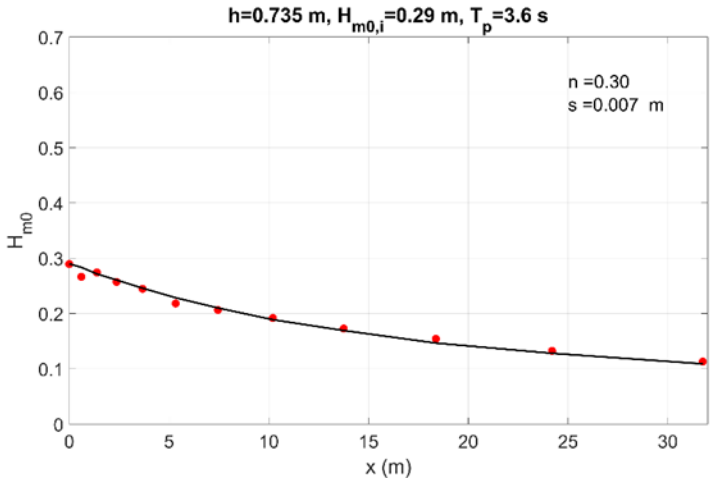
h=0.735 m, H$_{m0,i}$=0.29 m, T$_p$=3.6 s
n =0.30
s =0.007 m
H$_{m0}$
x (m)

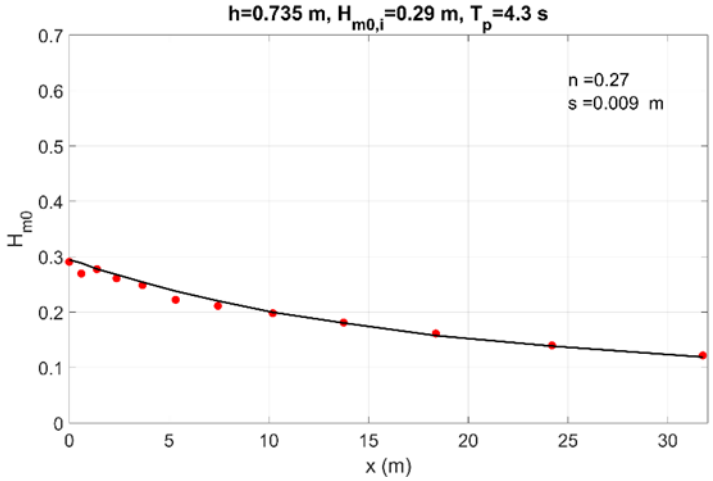
h=0.735 m, H$_{m0,i}$=0.29 m, T$_p$=4.3 s
n =0.27
s =0.009 m
H$_{m0}$
x (m)

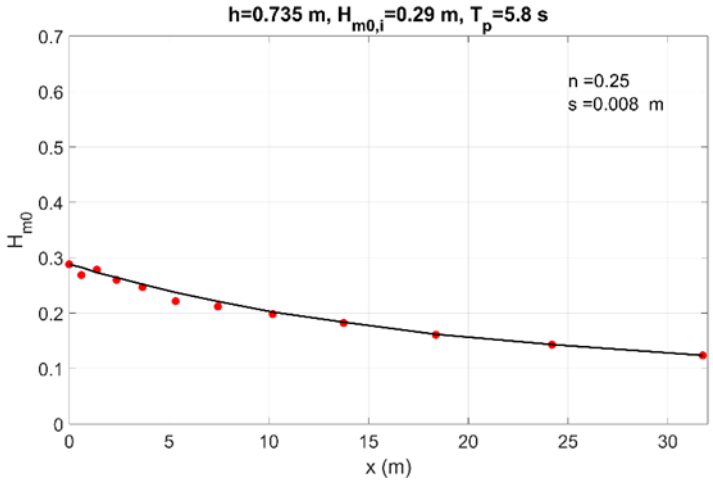
h=0.735 m, H$_{m0,i}$=0.29 m, T$_p$=5.8 s
n =0.25
s =0.008 m
H$_{m0}$
x (m)

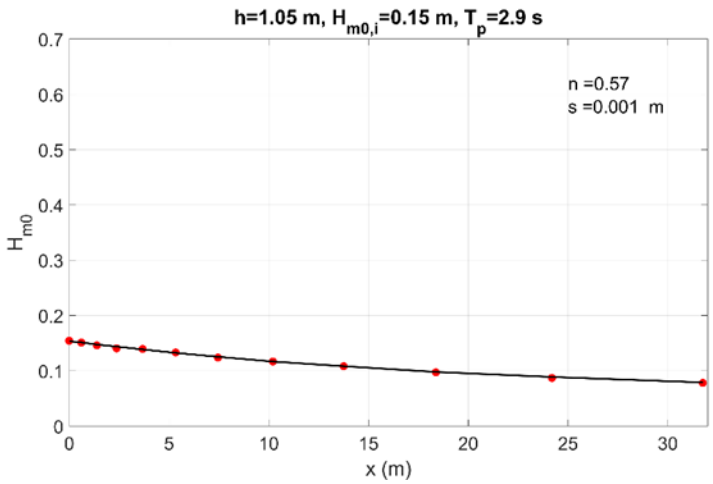
h=1.05 m, H$_{m0,i}$=0.15 m, T$_p$=2.9 s
n =0.57
s =0.001 m
H$_{m0}$
x (m)

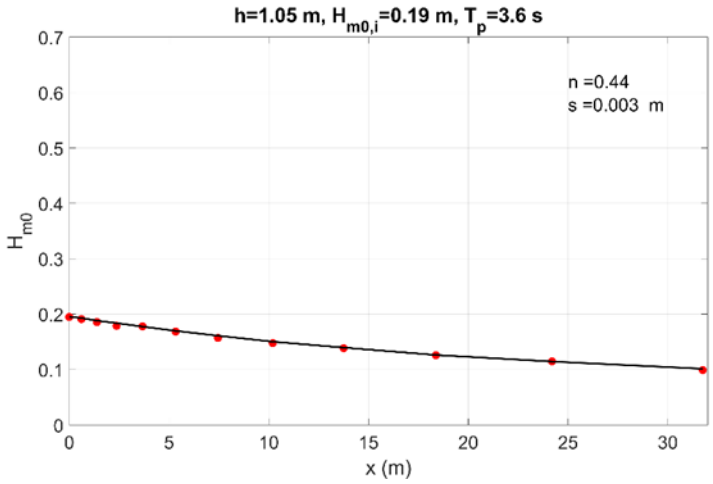
h=1.05 m, H$_{m0,i}$=0.19 m, T$_p$=3.6 s
n =0.44
s =0.003 m
H$_{m0}$
x (m)

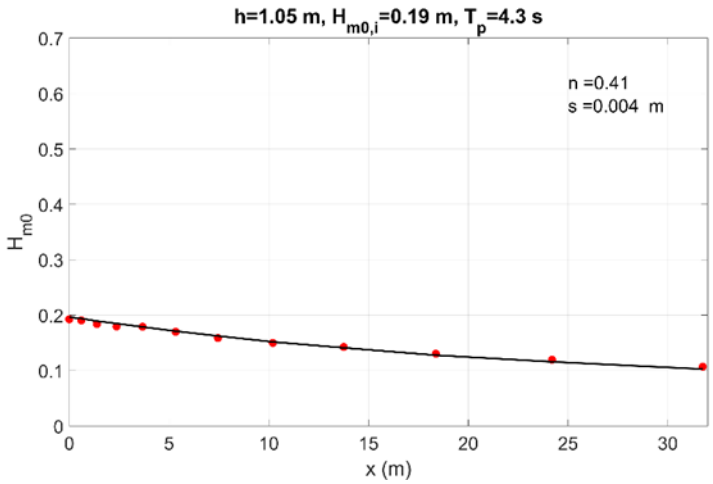
h=1.05 m, H$_{m0,i}$=0.19 m, T$_p$=4.3 s
n =0.41
s =0.004 m
H$_{m0}$
x (m)

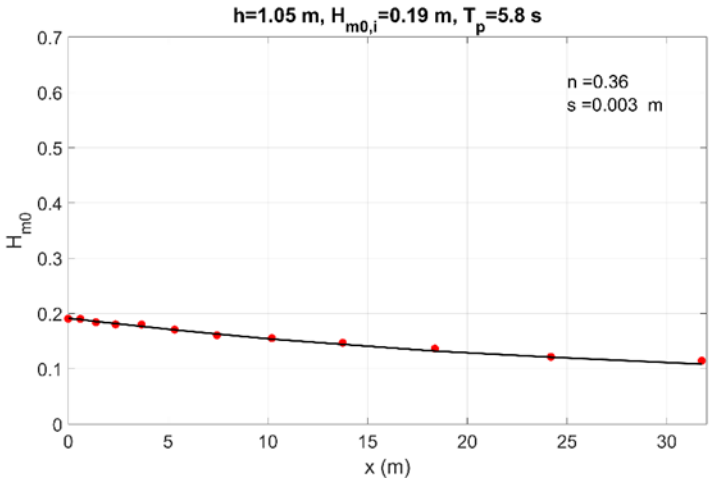
h=1.05 m, H$_{m0,i}$=0.19 m, T$_p$=5.8 s
n =0.36
s =0.003 m
H$_{m0}$
x (m)

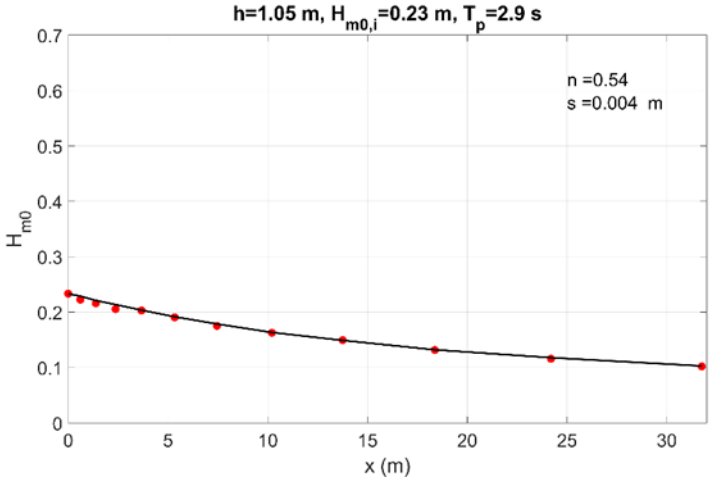
h=1.05 m, H$_{m0,i}$=0.23 m, T$_p$=2.9 s
n =0.54
s =0.004 m
H$_{m0}$
x (m)

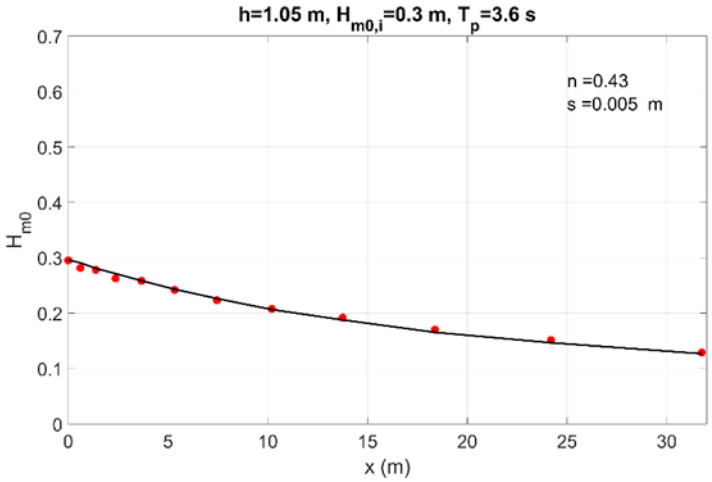
h=1.05 m, H$_{m0,i}$=0.3 m, T$_p$=3.6 s
n =0.43
s =0.005 m
H$_{m0}$
x (m)

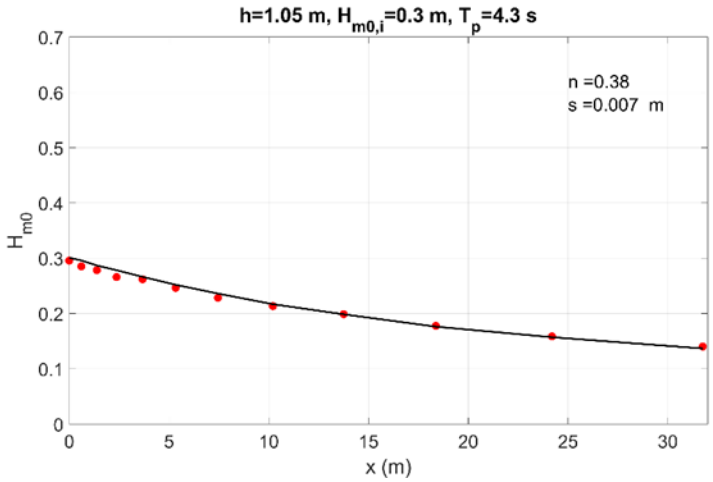
h=1.05 m, H$_{m0,i}$=0.3 m, T$_p$=4.3 s
n =0.38
s =0.007 m
H$_{m0}$
x (m)

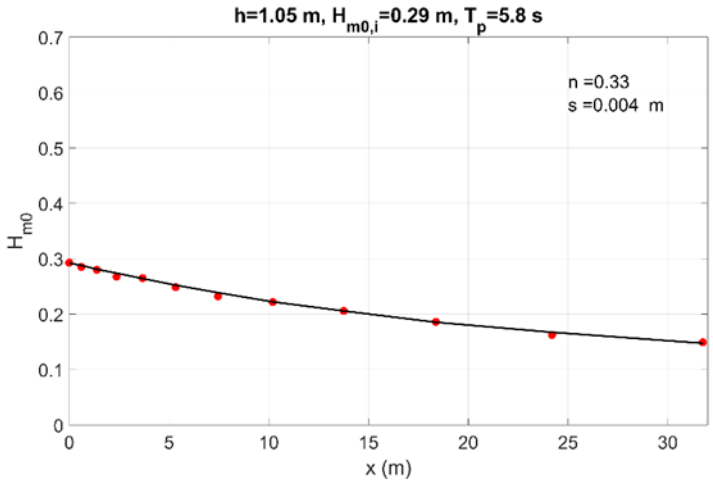
h=1.05 m, H$_{m0,i}$=0.29 m, T$_p$=5.8 s
n =0.33
s =0.004 m
H$_{m0}$
x (m)

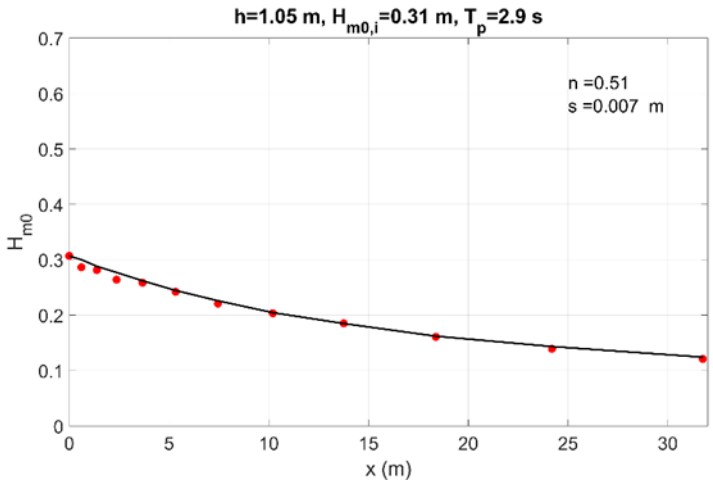
h=1.05 m, H$_{m0,i}$=0.31 m, T$_p$=2.9 s
n =0.51
s =0.007 m
H$_{m0}$
x (m)

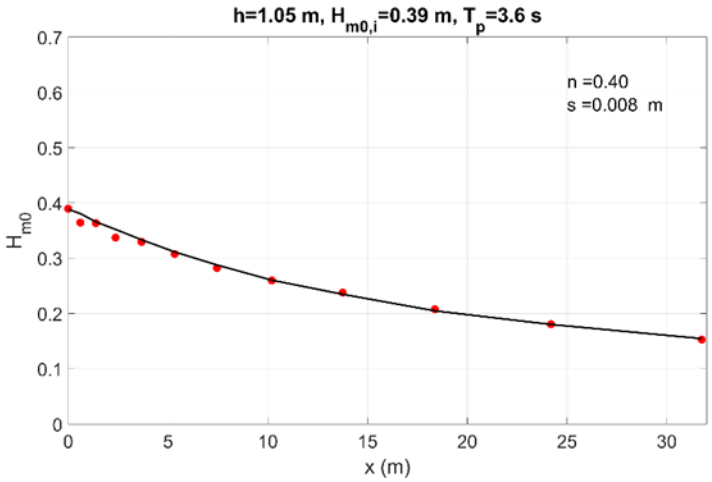
h=1.05 m, H$_{m0,i}$=0.39 m, T$_p$=3.6 s
n =0.40
s =0.008 m
H$_{m0}$
x (m)

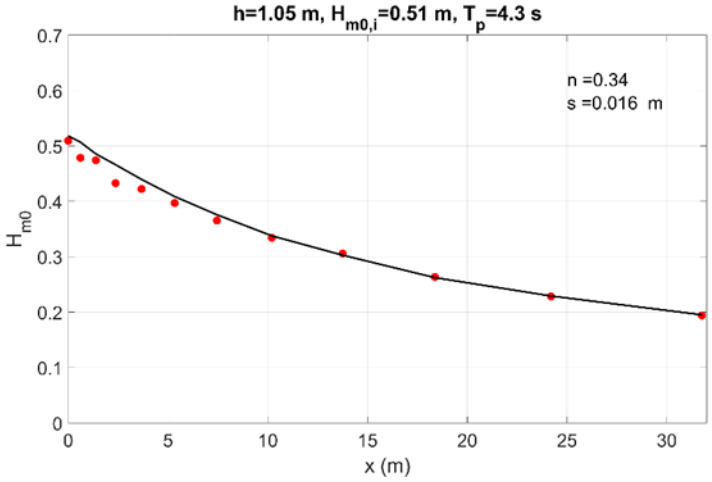
h=1.05 m, H$_{m0,i}$=0.51 m, T$_p$=4.3 s
n =0.34
s =0.016 m
H$_{m0}$
x (m)

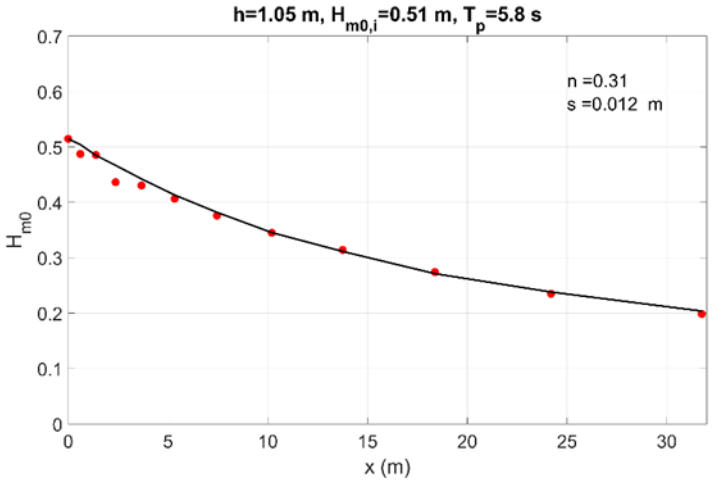
h=1.05 m, H$_{m0,i}$=0.51 m, T$_p$=5.8 s
n =0.31
s =0.012 m
H$_{m0}$
x (m)

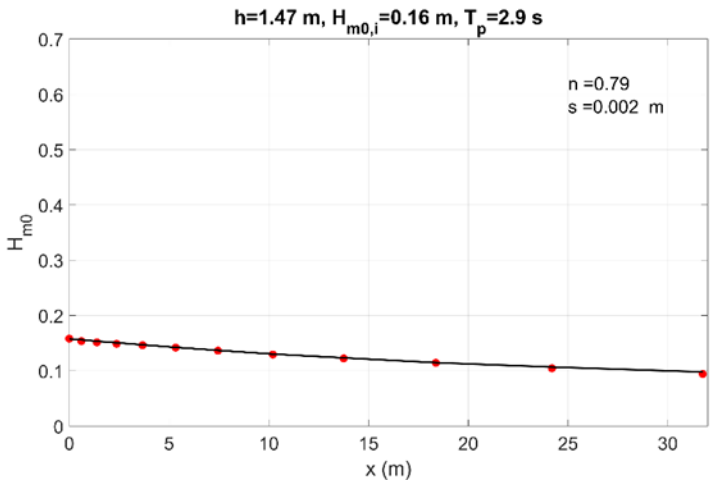
h=1.47 m, H$_{m0,i}$=0.16 m, T$_p$=2.9 s
n =0.79
s =0.002 m
H$_{m0}$
x (m)

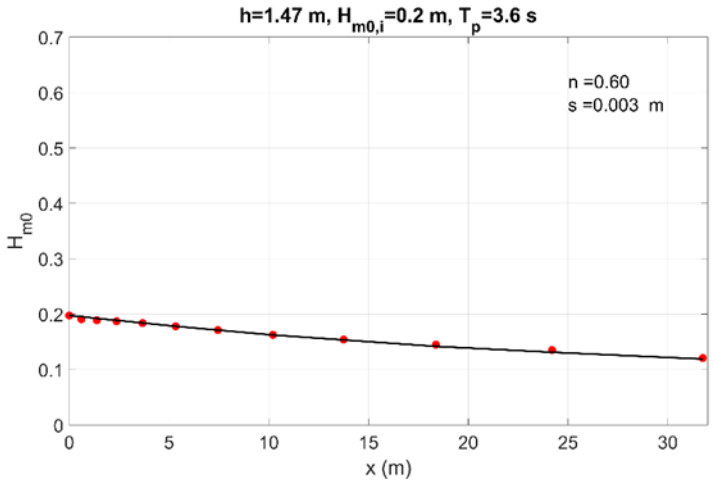
h=1.47 m, H$_{m0,i}$=0.2 m, T$_p$=3.6 s
n =0.60
s =0.003 m
H$_{m0}$
x (m)

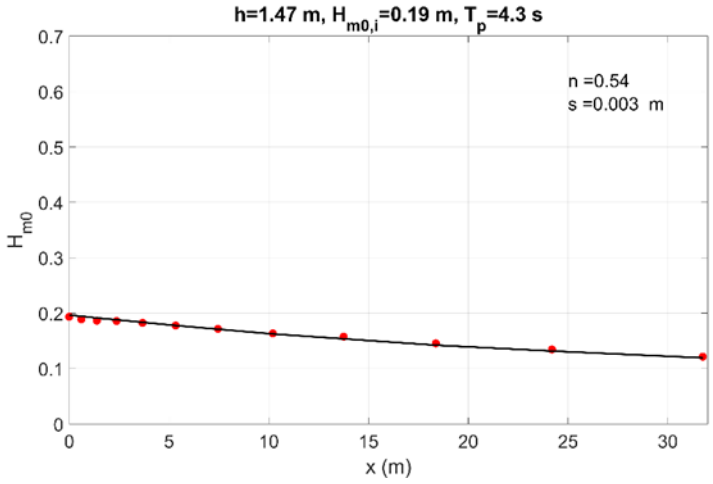
h=1.47 m, H$_{m0,i}$=0.19 m, T$_p$=4.3 s
n =0.54
s =0.003 m
H$_{m0}$
x (m)

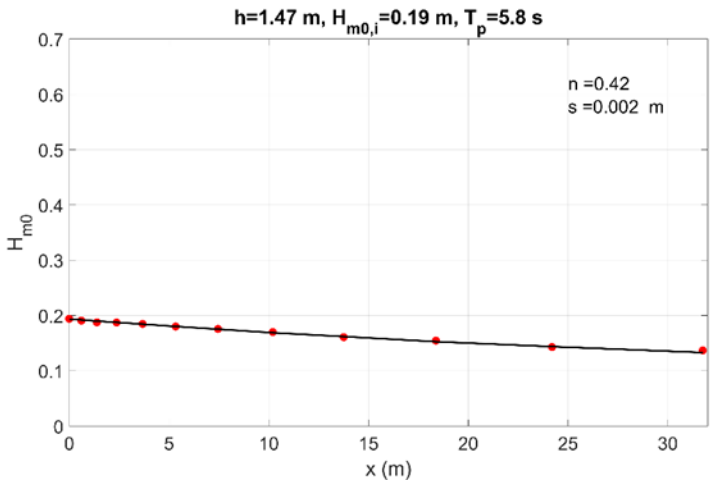
h=1.47 m, H$_{m0,i}$=0.19 m, T$_p$=5.8 s
n =0.42
s =0.002 m
H$_{m0}$
x (m)

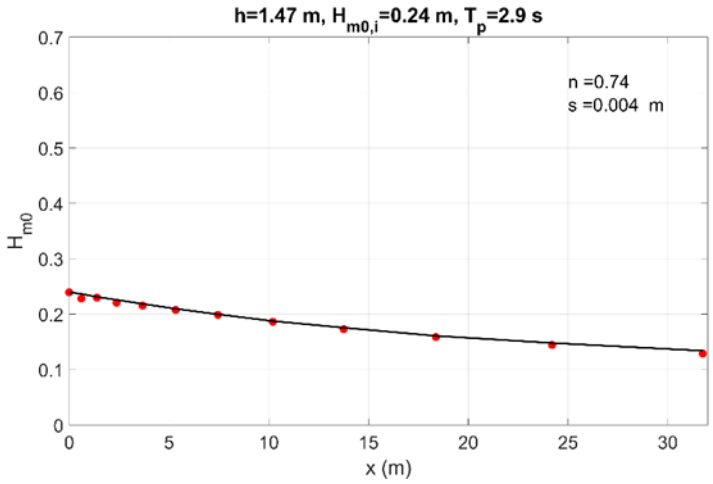
h=1.47 m, H$_{m0,i}$=0.24 m, T$_p$=2.9 s
n =0.74
s =0.004 m
H$_{m0}$
x (m)

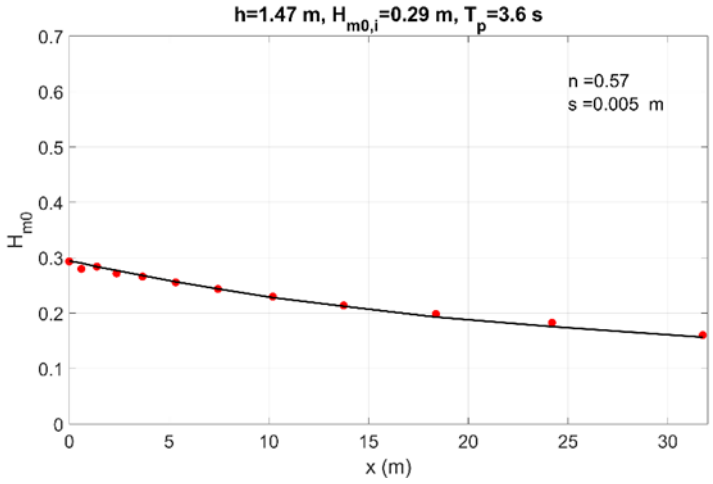
h=1.47 m, H$_{m0,i}$=0.29 m, T$_p$=3.6 s
n =0.57
s =0.005 m
H$_{m0}$
x (m)

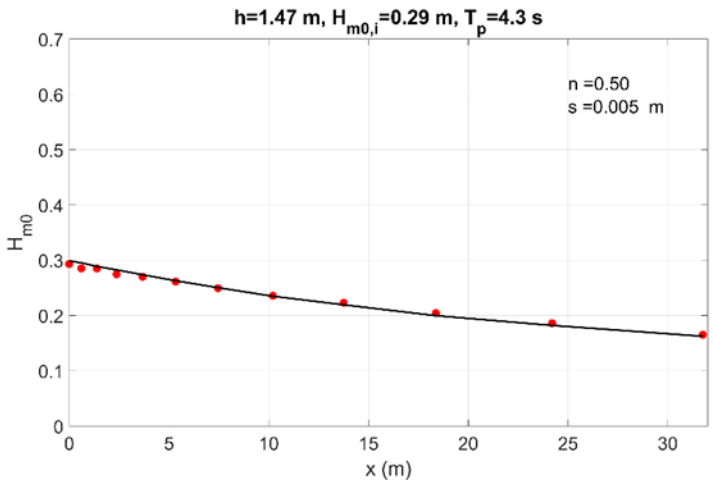
h=1.47 m, H$_{m0,i}$=0.29 m, T$_p$=4.3 s
n =0.50
s =0.005 m
H$_{m0}$
x (m)

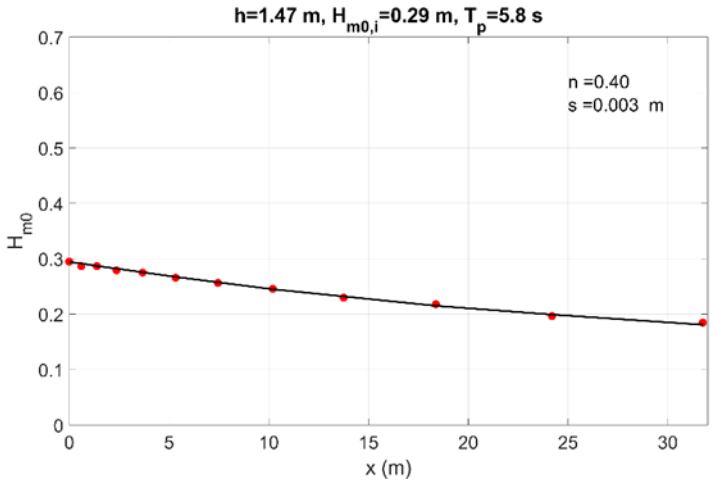
h=1.47 m, H$_{m0,i}$=0.29 m, T$_p$=5.8 s
n =0.40
s =0.003 m
H$_{m0}$
x (m)

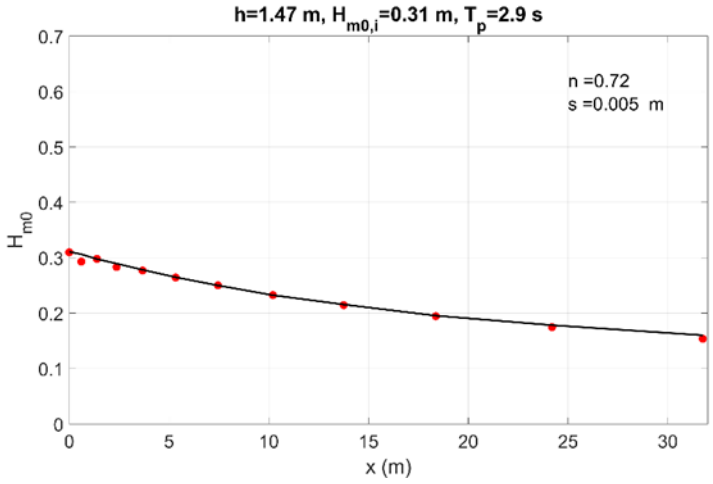
h=1.47 m, H$_{m0,i}$=0.31 m, T$_p$=2.9 s
n =0.72
s =0.005 m
H$_{m0}$
x (m)

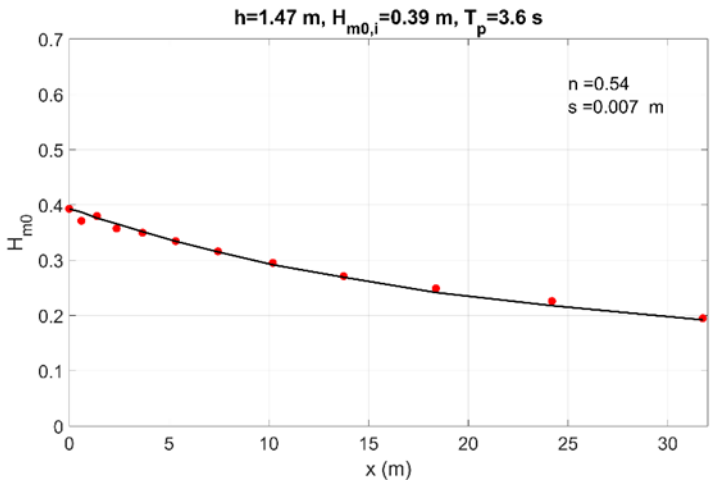
h=1.47 m, H$_{m0,i}$=0.39 m, T$_p$=3.6 s
n =0.54
s =0.007 m
H$_{m0}$
x (m)

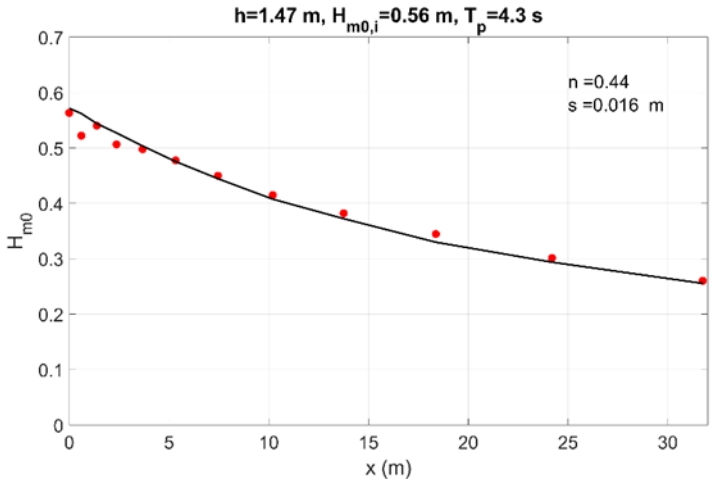
h=1.47 m, H$_{m0,i}$=0.56 m, T$_p$=4.3 s
n =0.44
s =0.016 m
H$_{m0}$
x (m)

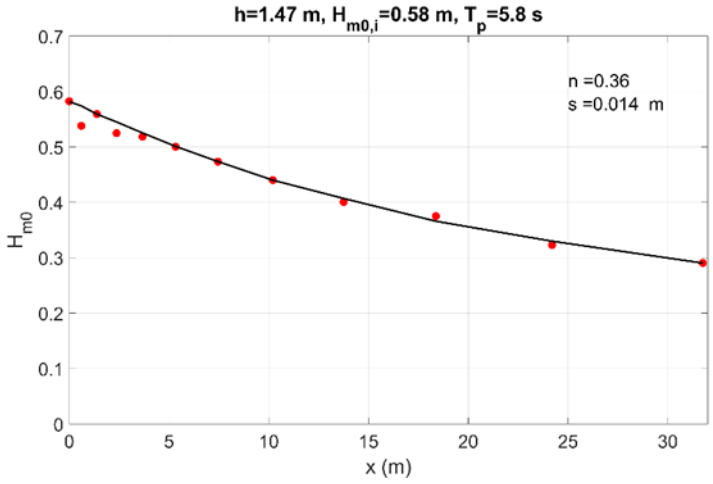
h=1.47 m, H$_{m0,i}$=0.58 m, T$_p$=5.8 s
n =0.36
s =0.014 m
H$_{m0}$
x (m)

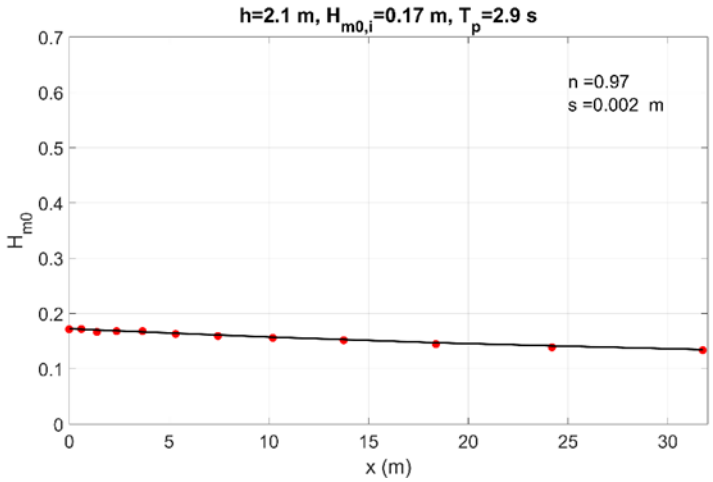
h=2.1 m, H$_{m0,i}$=0.17 m, T$_p$=2.9 s
n =0.97
s =0.002 m
H$_{m0}$
x (m)

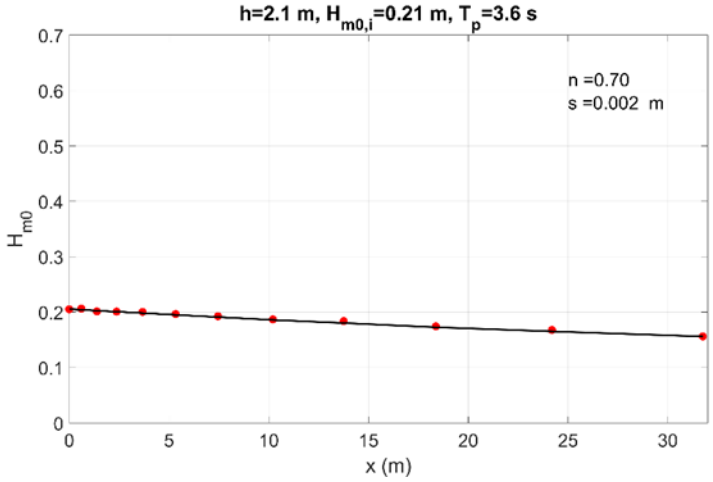
h=2.1 m, H$_{m0,i}$=0.21 m, T$_p$=3.6 s
n =0.70
s =0.002 m
H$_{m0}$
x (m)

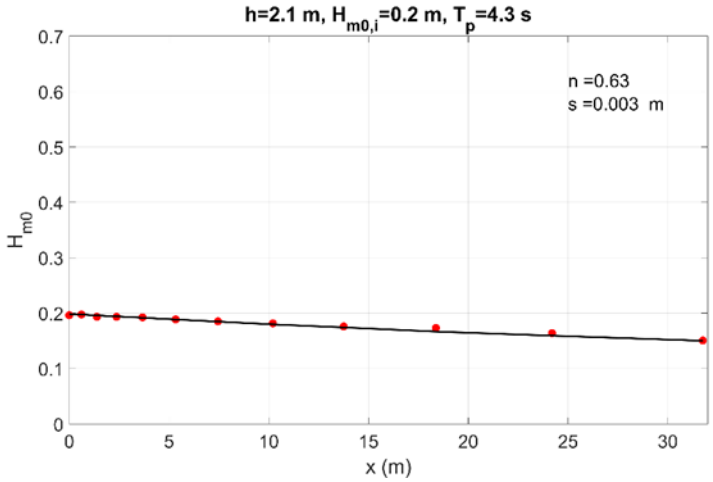
h=2.1 m, H$_{m0,i}$=0.2 m, T$_p$=4.3 s
n =0.63
s =0.003 m
H$_{m0}$
x (m)

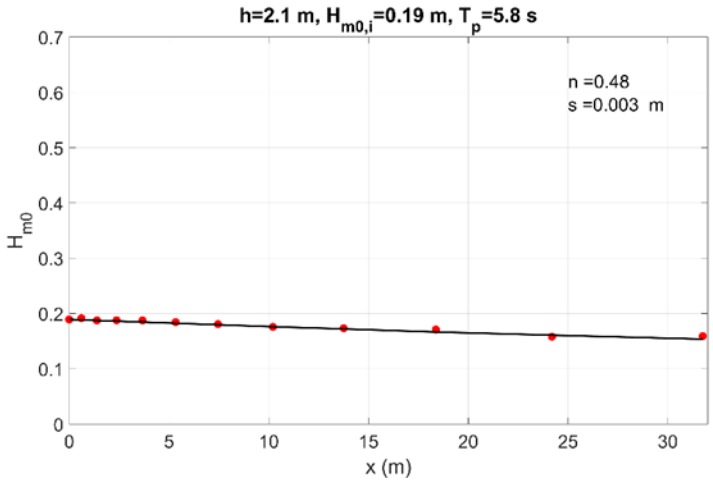
h=2.1 m, H$_{m0,i}$=0.19 m, T$_p$=5.8 s
n =0.48
s =0.003 m
H$_{m0}$
x (m)

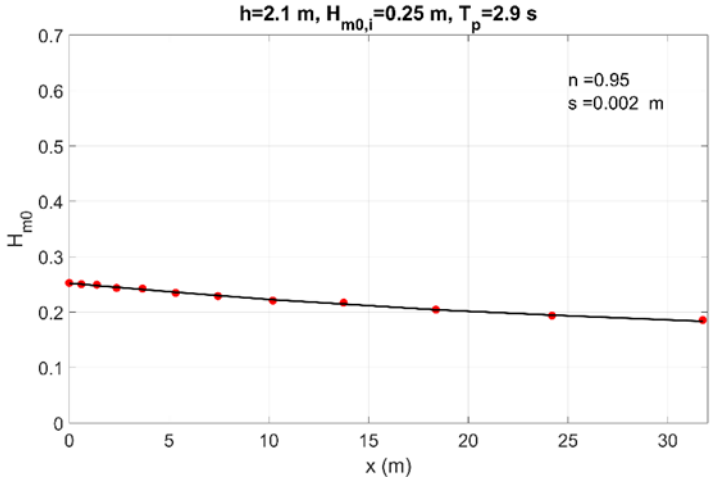
h=2.1 m, H$_{m0,i}$=0.25 m, T$_p$=2.9 s
n =0.95
s =0.002 m
H$_{m0}$
x (m)

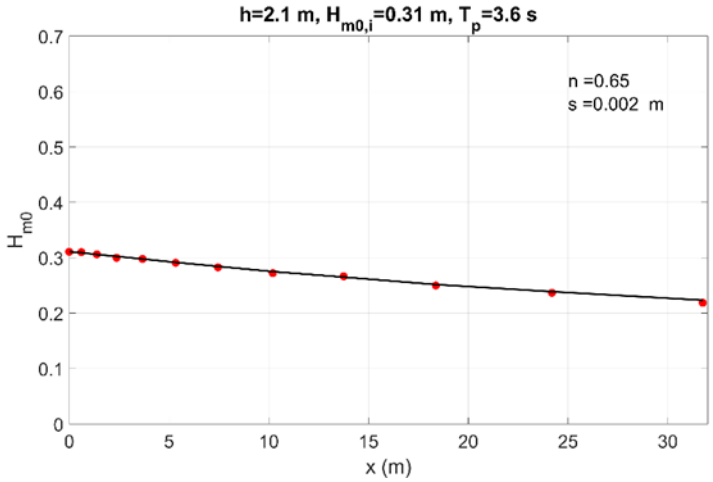
h=2.1 m, H$_{m0,i}$=0.31 m, T$_p$=3.6 s
n =0.65
s =0.002 m
H$_{m0}$
x (m)

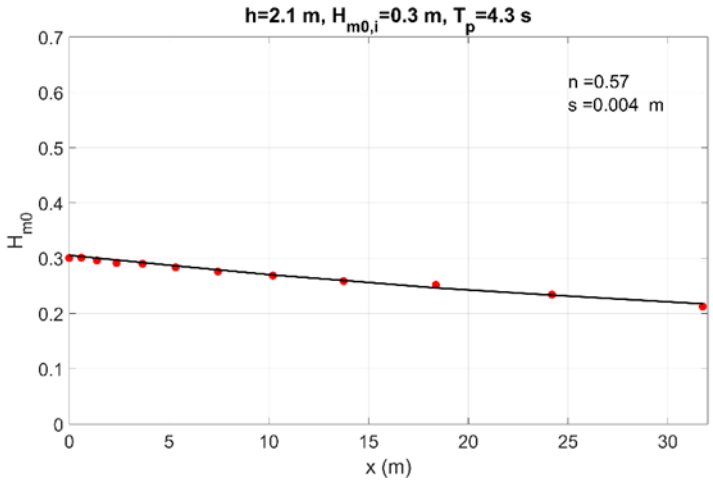
h=2.1 m, H$_{m0,i}$=0.3 m, T$_p$=4.3 s
n =0.57
s =0.004 m
H$_{m0}$
x (m)

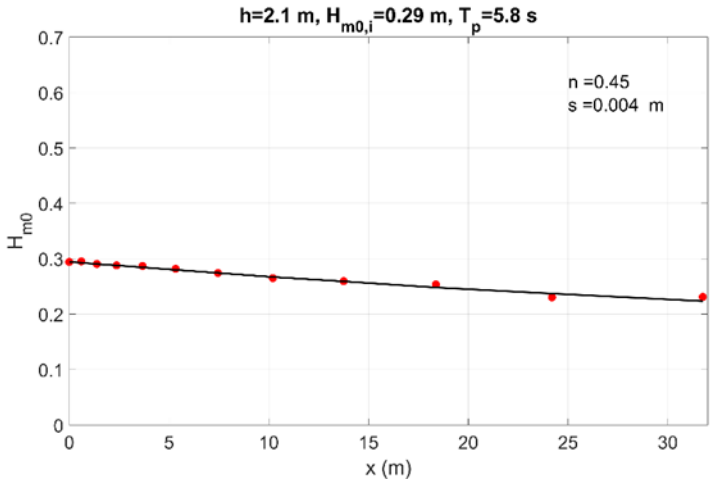
h=2.1 m, H$_{m0,i}$=0.29 m, T$_p$=5.8 s
n =0.45
s =0.004 m
H$_{m0}$
x (m)

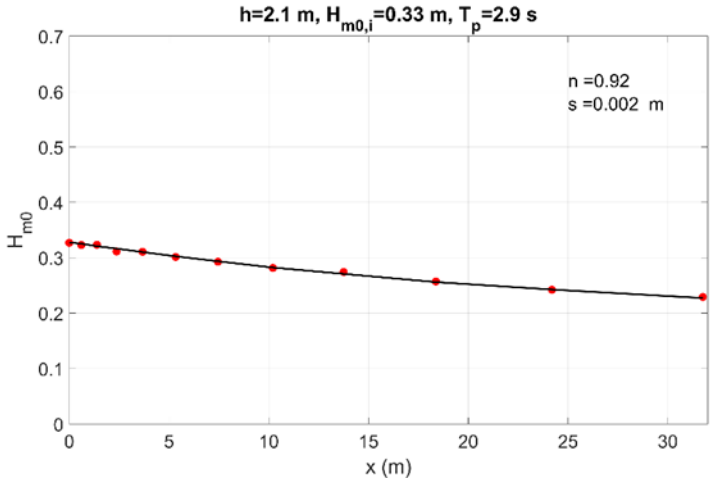
h=2.1 m, H$_{m0,i}$=0.33 m, T$_p$=2.9 s
n =0.92
s =0.002 m
H$_{m0}$
x (m)

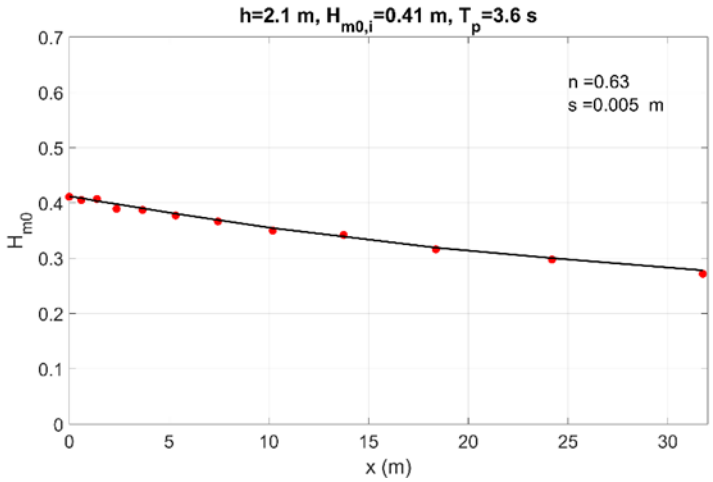
h=2.1 m, H$_{m0,i}$=0.41 m, T$_p$=3.6 s
n =0.63
s =0.005 m
H$_{m0}$
x (m)

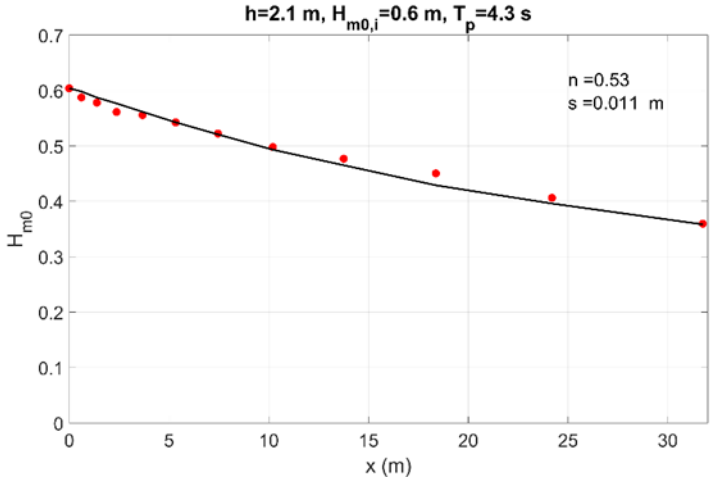
h=2.1 m, H$_{m0,i}$=0.6 m, T$_p$=4.3 s
n =0.53
s =0.011 m
H$_{m0}$
x (m)

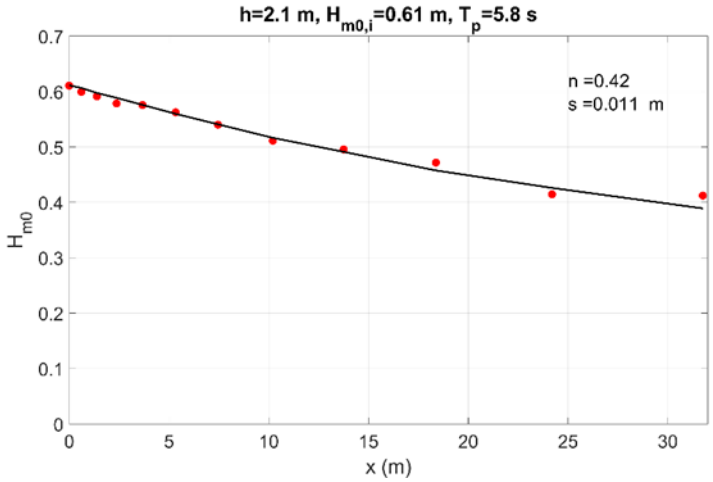
h=2.1 m, H$_{m0,i}$=0.61 m, T$_p$=5.8 s
n =0.42
s =0.011 m
H$_{m0}$
x (m)

Abbreviations

ADV	Acoustic doppler velocimeter
ERDC	Engineer Research and Development Center
DBH	Diameter at breast height
FFT	Fast Fourier transformation
NNBF	Natural and nature-based feature
PEX	Cross-linked polyethylene
SVF	Submerged volume fraction
TMA	Texel, Marson, and Arsole
USACE	US Army Corps of Engineers
WG	Wave gauge

REPORT DOCUMENTATION PAGE

Form Approved
OMB No. 0704-0188

1. REPORT DATE (DD-MM-YYYY)	2. REPORT TYPE	3. DATES COVERED (From - To)
September 2022	Final	

4. TITLE AND SUBTITLE
Wave Attenuation of Coastal Mangroves at a Near-Prototype Scale

5a. CONTRACT NUMBER

5b. GRANT NUMBER

5c. PROGRAM ELEMENT

6. AUTHOR(S)
Mary Anderson Bryant, Duncan B. Bryant, Leigh A. Provost, Nia Hurst, Maya McHugh, Anna Wargula, Tori Tomiczek

5d. PROJECT NUMBER

5e. TASK NUMBER

5f. WORK UNIT NUMBER

7. PERFORMING ORGANIZATION NAME(S) AND ADDRESS(ES)
US Army Engineer Research and Development Center (ERDC)
3909 Halls Ferry Road,
Vicksburg, MS 39180-6199

8. PERFORMING ORGANIZATION REPORT NUMBER
ERDC TR-22-17

9. SPONSORING / MONITORING AGENCY NAME(S) AND ADDRESS(ES)
US Army Corps of Engineers
441 G St. NW
Washington, DC 20314

10. SPONSOR/MONITOR'S ACRONYM(S)
USACE

11. SPONSOR/MONITOR'S REPORT NUMBER(S)

12. DISTRIBUTION / AVAILABILITY STATEMENT
Approved for public release; distribution is unlimited.

13. SUPPLEMENTARY NOTES
This study conducted under project 20-05 and 19-04, "Wave Attenuation of Coastal Mangroves during Extreme Water Levels at Near-Prototype Scales," funding account U4381627, AMSCO 089500.

14. ABSTRACT

A physical model study investigating the dissipation of wave energy by a 1:2.1 scale North American red mangrove forest was performed in a large-scale flume. The objectives were to measure the amount of wave attenuation afforded by mangroves, identify key hydrodynamic parameters influencing wave attenuation, and provide methodologies for application. Seventy-two hydrodynamic conditions, comprising irregular and regular waves, were tested. The analysis related the dissipation to three formulations that can provide estimates of wave attenuation for flood risk management projects considering mangroves: damping coefficient β, drag co-efficient CD, and Manning's roughness coefficient n.

The attenuation of the incident wave height through the 15.12 m long, 1:2.1 scale mangrove forest was exponential in form and varied from 13%–77%. Water depth and incident wave height strongly influenced the amount of wave attenuation. Accounting for differences in water depth using the submerged volume fraction resulted in a common fit of the damping coefficient as a function of relative wave height and wave steepness. The drag coefficient demonstrated a stronger relationship with the Keulegan–Carpenter number than the Reynolds number. The linear relationship between relative depth and Manning's *n* was stronger than that between Manning's *n* and either relative wave height or wave steepness.

15. SUBJECT TERMS
Flood control; Hydrodynamics; Mangrove plants; Shore protection; Water waves—Attenuation

16. SECURITY CLASSIFICATION OF:			17. LIMITATION OF ABSTRACT	18. NUMBER OF PAGES	19a. NAME OF RESPONSIBLE PERSON
a. REPORT	b. ABSTRACT	c. THIS PAGE			19b. TELEPHONE NUMBER (include area code)
Unclassified	Unclassified	Unclassified	SAR	126	